DOI: https://doi.org/10.2138/am-2020-6994

Journal

Invited contribution — *Special Issue* American Mineralogist on Halogens in Planetary Bodies (Editors Anita Cadoux; Keith Putirka)

Title

The distribution and abundance of halogens in eclogites: an in situ SIMS perspective of the Raspas Complex (Ecuador)

<u>Revision 2</u>

Authors

Benjamin M. Urann[1,2]*, Véronique Le Roux[2], Timm John[3], Grace M. Beaudoin[4], Jaime D. Barnes[4]

[1]MIT-WHOI Joint Program, Marine Geology and Geophysics, Woods Hole Oceanographic Institution, Woods Hole, MA 02543 USA

[2] Geology and Geophysics Department, Woods Hole Oceanographic Institution, Woods Hole, MA 02543 USA

[3] Institut für Geologische Wissenschaften, Freie Universität Berlin, Malteserstrasse 74-100, 12249 Berlin, Germany

[4] Department of Geological Sciences, University of Texas, Austin, TX 78712 USA

*email: burann@whoi.edu

Abstract

We present in situ secondary ion mass spectrometry (SIMS) and electron microprobe analyses of co-existing garnet, omphacite, phengite, amphibole, and apatite, combined with pyrohydrolysis bulk-rock analyses to constrain the distribution, abundance, and behavior of halogens (F and Cl) in six MORB-like eclogites from the Raspas Complex (Southern Ecuador). In all cases concerning lattice-hosted halogens, F compatibility decreases from apatite (1.47–3.25 wt %), to amphibole (563–4727 μg/g), phengite (610–1822 μg/g), omphacite (6.5–54.1 μg/g) and garnet (1.7–8.9 μg/g). The relative compatibility of Cl in the assemblage is greatest for apatite (192–515 μg/g), followed by amphibole (0.64–82.7 μg/g), phengite (1.2–2.1 μg/g), omphacite (<0.05–1.0 μg/g) and garnet (<0.05 μg/g). Congruence between SIMS-reconstructed F bulk abundances and yield-corrected bulk pyrohydrolysis analyses indicates that F is primarily hosted within the crystal lattice of eclogitic minerals. However, SIMS-reconstructed Cl abundances are a factor of five lower, on average, than pyrohydrolysis-derived bulk concentrations. This discrepancy results from the contribution of fluid inclusions, which may host at least 80% of the bulk rock Cl. The combination of SIMS and pyrohydrolysis is highly complementary. Whereas SIMS is well suited to determine bulk F abundances, pyrohydrolysis better quantifies bulk Cl concentrations, which include the contribution of fluid inclusion-hosted Cl. Raspas eclogites contain 145–258 μg/g F and at least 7–11 μg/g Cl. We estimate that ~95% of F is retained in the slab through eclogitization and returned to the upper mantle during subduction, whereas at least 95% of subducted Cl is removed from the rock by the time the slab equilibrates at eclogite facies conditions. Our calculations provide further evidence for the fractionation of F from Cl during high-pressure metamorphism in subduction zones. Although the HIMU mantle source (dehydrated oceanic crust) is often associated with enrichments in Cl/K and F/Nd, Raspas eclogites show relatively low halogen ratios identical within uncertainty to DMM. Thus, the observed halogen enrichments in HIMU ocean island basalts require either

further fractionation during mantle processing, or recycling of a halogen-enriched carrier lithology such as serpentinite into the mantle.

Keywords: eclogite, halogens, subduction, SIMS, nominally anhydrous minerals, HIMU

1. Introduction

Our understanding of the abundance and distribution of halogens in subducted slabs is limited. Hydrothermally altered oceanic crust (AOC) is thought to be a major halogen carrier during subduction, where F and Cl substitute into the hydroxyl sites of hydrous minerals such as amphibole and mica (Ito et al. 1983; Philippot et al. 1998; Van den Bleeken and Koga 2015; Barnes et al. 2018). Bulk estimates of pre-subduction AOC vary from 50–253 µg/g Cl and 216–400 µg/g F (Ito et al. 1983; Straub and Layne 2003; Barnes and Cisneros 2012; Van den Bleeken and Koga 2015; Chavrit et al. 2016). More recently, primary halogen measurements of altered oceanic crust from the East Pacific Rise (Penrose-type oceanic crust) and Atlantis Bank (SWIR, ultra-slow spreading) have shown extreme variability with both stratigraphic depth and lithology (Kendrick 2019a; 2019b). Bulk halogen measurements of blueschists and eclogites thought to represent high-pressure metamorphic AOC are also sparse. In a study of mélange rocks from Syros, Greece, Marschall et al. (2009) measured the bulk Cl content of eclogites (28–60 µg/g) and called into question previous estimates of eclogitized AOC Cl abundances, e.g. 100–200 µg/g Cl of Philippot et al. (1998), speculating that they may be overestimated. Pagé et al. (2016) analyzed a suite of blueschists from northwest Turkey; their results (8–22 µg/g Cl) also indicate that bulk eclogitized AOC could host less Cl than previously thought. Debret et al. (2016) reconstructed bulk halogen concentrations (57–79 µg/g Cl and 10–62 µg/g F) from in situ secondary ion mass spectrometry (SIMS) analyses for both blueschists and eclogites from the Western Alps, cautioning that typical bulk halogen measurements are not representative of prograde conditions due to potential retrogression during exhumation.

In situ halogen data in eclogitized AOC are also limited to a handful of studies, yet provide important first order observations. Debret et al. (2016) suggested that approximately 50% of F and 90% of Cl in the initial bulk-rock are lost to fluids during the first 80 km of subduction. Hughes et al. (2018) analyzed in situ halogen abundances of eclogites from the Western and Central Alps, and provided eclogitized AOC estimates of as low as 3 μg/g Cl. Finally, Pagé et al. (2016) reported low Cl and high F abundances in blueschist-hosted minerals, and concluded that Cl is primarily expelled at shallow depths, whereas F is retained to at least 80 km depth.

Estimates of halogen fluxes in subduction zones are typically derived from the difference between the trench inputs and extrusive products of arc magmatism (e.g. (Mather et al. 2006; Sadofsky et al. 2008; Pyle and Mather 2009; Freundt et al. 2014). Straub and Layne (2003) inferred a global arc recycling efficiency of 77–103% (Cl), and ~4–5% (F), implying near-total return of Cl to surface reservoirs whereas most F is returned to the mantle. John et al. (2011) reached similar conclusions based on Cl mass balance constraints regarding in- and out-fluxes from the subducted slab perspective. Barnes et al. (2018) also concluded that F is efficiently returned to the mantle, however their estimated Cl fluxes are more variable, indicating that some Cl could be delivered back into the mantle by serpentinites (John et al. 2011; Kendrick et al. 2017). In a recent study, Pagé et al. (2018) found that Himalayan antigorite serpentinites host significant quantities of F (50–650 μg/g) and are enriched in Cl (8.8–35 μg/g) with respect to depleted mantle (11.0 μg/g F and 0.51 μg/g Cl, Salters and Stracke (2004)). Taken together, these studies illustrate the challenge of estimating halogen input fluxes. A better understanding of the inherent variability within different lithologies used in flux calculations could help to refine such estimates.

In particular, the halogen content of eclogitized AOC remains largely unconstrained. Here we discuss the F and Cl abundances of Raspas Complex eclogites, a Cretaceous eclogite suite that we consider to be an ideal analog for subducted AOC. We combine in situ SIMS and EMP analyses of minerals with pyrohydrolysis-derived bulk halogen abundances and discuss the relative contribution of minerals, grain boundaries and fluid inclusions to the total budget of halogens in subducted eclogites. Finally, we present new constraints on slab halogen fluxes and discuss the implications for the signature of eclogitized AOC in the HIMU mantle source.

2. Geologic Context

An accreted parcel of oceanic lithosphere, the early Cretaceous Raspas Complex consists of blueschist- and eclogite-facies rocks (Feininger 1980; 1987; Maruyama et al. 1996). The high-pressure metamorphic suite is bound by the La Palma-El Guayabo Shear Zone to the north and lower grade greenschists and amphibolites to the south (Gabriele 2002). While no pillow structures or sheeted dikes were observed in the field, fluid-immobile REE and HFSE abundances, Nb/Zr and Hf/Yb systematics, TiO_2/Yb ratios, and Nd isotope systematics provide a well-reasoned rationale for inferred protoliths (John et al. 2010; Halama et al. 2011). Based on these characteristics, the blueschists and eclogites were derived from seamount-like basalt and normal mid-ocean ridge basalt (MORB) protoliths, respectively. Both underwent similar peak metamorphic conditions (based on major element thermobarometry) of ~600ºC to a maximum burial depth of approximately 60 km (John et al. 2010). Raspas eclogites show evidence for low-temperature seafloor alteration typical of basalts based on O isotopic compositions, and occur as two geochemically distinct groups: a MORB-type group (this study) with LREE depleted patterns, and a zoisite eclogite group characterized by significant incompatible trace-element enrichments which are interpreted to have been derived from serpentinite-derived dehydration fluids, and which also display a fluid component indicative of some minor sediment contribution (Halama et al. 2011; Herms et al. 2012). Thus, the Raspas MORB-type group provides an excellent analog to study the in situ distribution of halogens in eclogitized AOC processed through subduction systems globally.

3. Sample Description

We chose a set of six minimally retrogressed MORB-type eclogites which have been previously described by John et al. (2010). Samples consist of omphacite + garnet + rutile + apatite ± amphibole ± phengite ± quartz with minor secondary titanite. Subhedral to euhedral garnet porphyroblasts vary in size from <100 μm to 4mm, often hosting inclusions of rutile and quartz. Some samples exhibit weakly deformed fabrics characterized by lineated omphacite. A single sample, SEC42-06, shows a strongly foliated texture with alternating layers of nearly monomineralic garnet and omphacite domains. Modal mineralogy varies significantly between samples, from nearly bimineralic garnet + omphacite to ~30% modal amphibole; such variability at similar P-T conditions is likely the result of bulk chemical compositional effects (Beinlich et al. 2010; John et al. 2010; Rebay et al. 2010). Representative photomicrographs of sample textures are presented in Fig. 1 and S1. Petrographic observations reveal near-ubiquitous fluid inclusions (FI). All samples contain variable quantities of FI hosted in omphacite and garnet, typically located in mineral cores (Fig. 1; see also Herms et al. (2012)). In SEC46-02, monomineralic amphibole veinlets crosscut eclogite textures and contain secondary titanite overgrowths rimming rutile. Directly adjacent to these veinlets, FI-rich omphacite appears opaque in thin section (Fig. 1), which is unique to this sample and appears to reflect fluid infiltration.

4. Methods

4.1 SIMS

SIMS analyses were conducted at the Northeast National Ion Microprobe Facility (NENIMF) at the Woods Hole Oceanographic Institution using a Cameca IMS 1280. We follow the methods outlined in Urann et al. (2017), adding OH and S measurements to the protocol. 150μm polished thick-sections were used for all analyses. Samples were cleaned with ethanol and deionized water to remove surface contamination, then placed in a vacuum oven to dry. Samples were gold coated to ~160 nm thickness and placed into a vacuum chamber for storage until analysis. Samples were loaded into the instrument sample chamber at least 12 hours prior to analysis, to allow adequate pump down time and achieve chamber pressures of no more than ~5×10^{-9} torr. Each spot location was chosen to avoid surface cracks, which are known to influence analyses (Urann et al. 2017). A primary Cs^+ beam of 5.0–7.5 nA was sputtered through the sample surface with a 30 x 30 μm^2 raster and a 400 μm field aperture, allowing only transmission of ions from the innermost 5 x 5 μm^2 of the beam crater. Secondary magnet mass calibration was done before each measurement with mass resolving power of > 6000 ($m/\Delta m$ at 10 % peak height). We measured $^{19}F/^{30}Si$, $^{16}O^1H/^{30}Si$, $^{32}S/^{30}Si$, and $^{35}Cl/^{30}Si$ ratios in glass reference materials D51-3, D52-5, ALV519-4-1, 46D, 1649-3, 1654-3 6001, and AII107-D20 to produce a calibration slope for each one-week analytical session (Fig. S2). Calibration slopes (m) were obtained by plotting measured isotope ratios (x) against known reference material concentrations (y) of the form $y = mx$ for each element of interest. Sample unknowns were then calculated by multiplying measured ratios by *m*. Calibration slope uncertainties were assessed utilizing a bootstrapping technique (5000 iterations) to derive confidence intervals. Measurements where the internal precision (one standard deviation) was greater than 20% were screened and excluded from the data set; these low precision measurements (less than ten in total) were associated with elevated C (not reported) and Cl concentrations, and are likely the result of analyses conducted on micro-fractures. After screening, analytical uncertainties over five counting cycles (internal precision: typical standard error ~1 % OH, <1.5 % F, <3% Cl) were combined with calibration slope uncertainties (accuracy: typical uncertainty 6% OH, 5% F, <10% Cl, 95% confidence intervals) to yield no more than 8%, 6% and 16% total uncertainty (2SE, 95% confidence intervals) for OH, F and Cl measurements, respectively. Since mineral-specific calibrations are not well constrained and/or not available for halogens in most eclogitic phases, we used a basaltic glass calibration to present a unified dataset that is self-consistent. This may introduce crystal-specific matrix effects, although preliminary calibrations of F in pyroxene and glass (Kumamoto et al. 2017) show slopes indistinguishable within uncertainty. Continuous measurements of ALV519-4-1 were used throughout the session to monitor instrument drift, which was found to be negligible. The OH, F, and Cl concentrations of Suprasil and Herasil 102, both optical-quality glasses, along with Synthetic Forsterite, were measured regularly in each session. There are no published values for the OH, F, and Cl content of Suprasil, Herasil 102 and Synthetic Forsterite, but those samples are believed to have very low OH, F, and Cl concentrations (less than 0.1 μg/g), respectively (E. Hauri, *pers. comm.*). To quantify our maximum backgrounds, we assume that Suprasil contains no OH, Herasil contains no F, and Synthetic Forsterite contains no Cl. Background OH, F, and Cl values were less than 7.3 μg/g, 0.19 μg/g, and 0.15 μg/g, respectively, for all sessions. Individual mineral analyses were not corrected for background when background values were less than propagated 2SE uncertainty; otherwise, measurements are corrected to remove backgrounds (Table 1). Cl measurement uncertainties on omphacite, garnet, and phengite are near parity with Synthetic Forsterite Cl values. We therefore subtracted our background Cl values from measured values for all bulk calculations.

4.2 EPMA

All mineral phases were analyzed using JEOL JXA–8200 electron microprobe (EMP) at the Massachusetts Institute of Technology. A 1nA beam current and 15kV accelerating potential were used for all analyses except apatite which utilized a 10 nA beam current. Beam diameter was <1 micron for garnet and omphacite, and 10 μm for amphibole and phengite. Data reduction was done using CITZAF software (Armstrong 1995). The counting times used for phase analysis was 40s on peak, and 20s on background. With respect to halogen abundances in amphibole and phengite, detection limits based on counting statistics were ~470 μg/g for F and ~60 μg/g for Cl. For apatite, care was taken to address known issues pertaining to fluorine excitation by electron microprobe analysis (Stormer and Pierson 1993). Peak searches were conducted only on the standard, and background was only measured on the first point for each grain. In addition, the LDE1 (W/Si) crystal was used for F measurements, which suppresses elemental interferences. Counting times for F were abbreviated to 10s on peak and 40 s for P, Ca, and Cl while background counts were 5s for F and 20s for Ca, P, and Cl. Analytical uncertainties including background for F and Cl in apatite based on counting statistics were 3.4–4.4% and 7.2–11.6% (1σ), respectively, at concentrations of 1.47–3.25 wt % F and 192–515 μg/g Cl.

4.3 Bulk halogen measurements

Sample powders were washed in ultra-pure (18MΩ) deionized water and oven-dried overnight to avoid surficial Cl contamination by adsorption. This may have removed a portion of halogens along grain boundaries or in fluid inclusions; therefore we report Cl concentrations as minimums. We note that fluid inclusion dimensions (~1µm to 10 µm, on average) are smaller than estimated powder grain size (<100 µm), and were likely retained, as demonstrated in a subsequent section. Halogens were extracted from approximately 2 grams of sample powder by pyrohydrolysis, in which a stream of water vapor captures volatiles as they are released from the sample during fusion by a gas torch. The vapor is condensed to produce an aqueous solution (Schnetger and Muramatsu 1996). From this solution, F and Cl concentrations are measured via ion chromatography (IC) using a Dionex Integrion HPIC System at the University of Texas at Austin. Detection limits of the analyzed solution are 0.05 µg/g for both F and Cl. The halogen content of the whole rock is then calculated using solution concentration, solution volume, and the mass of the powder melted. Using the JB-2 basalt reference material (98.5 µg/g F and 281 µg/g Cl (Imai et al. 1995)), F and Cl yields are 75–83% and 68–95% (n = 5), respectively. Samples were analyzed with triple replicates in two batches. Since JB-2 yields are constrained within each contemporaneous batch, concentrations were yield-corrected by batch to the JB-2 reference material to more rigorously quantify absolute halogen concentrations. The yield correction assumes that standard yields and sample yields are similar. Although not perfect, this correction likely provides more accurate values. Both uncorrected and yield-corrected values are presented in this study for comparison. Reproducibility for each sample (precision) was combined with batch-specific JB-2 yield uncertainty (accuracy) to derive 1σ uncertainties. Replicate measurements of JB-2 and uncertainties are given in Table S9.

4.4 Modal mineralogy

We calculated the modal abundances of each phase by inverting the bulk-rock major element data of John et al. (2010) with EMP analyses of individual phases (Tables S1-S6). Although EMPA indicates zonation in some phases (e.g. TiO_2 and MnO), changes in modal proportions were negligible (often <1% difference) when varying mineral compositions were used. We performed our calculations by taking the mean composition for each phase. SiO_2, TiO_2, Al_2O_3, FeO, MnO, MgO, CaO, Na_2O, K_2O, and P_2O_5 were used in the minimization. P_2O_5 was assumed to reside entirely within apatite. Calculated modes agree well with independently estimated mineral modes based on optical microscopy. Calculated mineral modes and uncertainties are shown in Table 2.

All eclogite samples contain >35 modal % garnet. Omphacite modal proportions range from 23–53 vol.%, whereas phengite, when present, makes up 2–4 vol% of the bulk-rock modally. Samples contain varying modal proportions of amphibole, from 0.5 vol% to ~30 vol%. Quartz, when present, is up to 8 vol% of the bulk rock whereas rutile (1–2 vol%) and apatite (0.25–1.6 vol%) are omnipresent.

5. Results

5.1 Major element variability by EMPA

Major element profiles show garnet zonation with respect to end member components almandine, pyrope, grossular, and spessartine (Table S1). Garnet porphyroblast cores are often elevated in the spessartine component as well as TiO_2, with a gradual decrease towards the rim consistent with prograde garnet growth.

Omphacite (Cpx) Mg# (molar Mg/(Mg+Fe)) varies from 0.68 to 0.79 (Table S2) and correlates negatively with Cpx abundances, reflecting the influence of bulk-rock chemistry on mineral modes. Omphacite EMPA profiles show some intra-mineral zonation; in particular, SEC42-06 and SEC43-01 show increasing Si concentrations from core to rim, while SEC43-03 Si content decreases from core to rim. Mg# remain uniform within single grains.

Phengite was analyzed in samples SEC42-06, SEC43-01, and SEC47-01 (Table S5). SEC42-06 is relatively homogeneous, with slight Na enrichment approaching the rim. A full rim-to-rim profile in SEC43-01 shows strong zonation with increases in Na and Al from core to rim, and decreases in Si, K, Fe and Mg (Fig. S3). SEC47-01 shows slight Si, K, and Mg rim depletions. Both phengite profiles are consistent with continued grain growth or partial recrystallization during decompression due to decreasing Si from core to rim (Massonne and Schreyer 1987).

Amphibole occurs as several different species which likely reflect bulk compositional variations; analyses are presented in Table S4, along with IMA 2012 recommended nomenclature calculated using the routine of Locock (2014). SEC42-06, SEC43-01, and SEC43-03 are Na-Ca subgroup katophorite, SEC46-01 and SEC46-02 are Ca subgroup pargasite, and SEC47-01 is classified as a Na-Ca subgroup winchite. Nearly all EMP analyses show Cl abundances at or below the detection limit of ~60 μg/g. However, F concentrations show significant intra-grain variability, differing by as much as a factor of two from core to rim (e.g. SEC42-06, 869–1834 μg/g).

Apatite halogen contents range from 1.47–3.25% wt% F and 0.019–0.051 wt% Cl (Table S5). The hydroxyl content of the apatite are taken as the oxide sum subtracted from one hundred, which classifies apatite in samples SEC43-03, SEC46-01, SEC46-02, and SEC47-01 as hydroxylapatite and apatite in sample SEC43-01 and SEC42-06 as fluoroapatite. Apatite halogen abundances are similar to apatite from other blueschist and eclogite metamorphic terranes with low Cl abundances (Pagé et al. 2016; Hughes et al. 2018) whereas some HP terranes developed from oceanic protoliths also contain Cl-rich apatite (John and Schenk 2003). Typical MORB (0.164 wt% P_2O_5, Gale et al. (2013)) must undergo significant fractional crystallization (>70%) before reaching apatite saturation (~0.7 wt% P_2O_5); indeed, apatite-saturated MORB are few (Anderson and Greenland 1969; Watson 1979). Based on the bulk rock chemistry of Raspas provided by John et al. (2010) these conditions are unlikely to have been met. Therefore interstitial grains most likely formed as new growth during progressive metamorphism.

5.2. Halogen and water variability

Bulk rock pyrohydrolysis analyses are presented in Table 3. As noted previously, we report both yield-corrected and uncorrected halogen abundances. Yield-corrected F and Cl concentrations for all samples were 115—199 µg/g and 6.7—19.9 µg/g, respectively. In situ halogen measurements are presented in Tables 1 and S5. Resolvable intra- and inter-grain heterogeneity is observed for F and OH in all phases both in single-grain SIMS profiles (Table S7) and in multiple grains from the same sample.

Halogen variability is notable in nominally anhydrous minerals (NAMs), particularly garnet with both inter- and intra-grain heterogeneity observed (Figure S4, Tables 1 and S7). Grain-averaged sample values range from 1.7 to 8.9 µg/g F and 60 to 201 µg/g OH, while Cl is always at or near detection limits. Intra-sample garnet F and OH variability is up to 93% and 67%, respectively (1σ, Table 1). Variations from core to rim were not systematic, nor can they be attributed to analytical uncertainty; in some cases cores were enriched in F or OH relative to rims, while in other grains the case was reversed. Core and rim measurements for OH and F are presented in Fig. 2, illustrating that while some intragrain variability is present, most grains plot on or near 1:1 lines within uncertainty.

Omphacite has highly variable F abundances (6.5–54.1 μg/g) while OH range from 445 to 773 μg/g. Similar to garnet, Cl abundances are less than 0.1 μg/g for five of the six samples. However, SEC46-02 yields significantly higher mean Cl abundances of 1.05 μg/g. F and OH variability within a single sample was less than 24% and 14%, respectively. A profile of Cpx from SEC43-01 exemplifies core to rim variations, with F and OH concentrations of 42.1–69.7 μg/g and 362–557 μg/g, respectively (Fig. S5). While these variations are discernable, heterogeneity in this grain is 15% or less for all three species; core to rim variations are modest and typically plot along a 1:1 line, within uncertainty (Fig. 2).

Amphibole occurs as both interstitial grains and monomineralic veinlets, with veins only occurring in SEC46-02. Interstitial amphibole yields F and Cl abundances of 747–4727 μg/g and 0.56–82.6 μg/g, respectively. Pargasite veins from SEC46-02 contain on average 563 μg/g F and 11.7 μg/g Cl. Single sample averaging produces variability of no more than 18% for F and 37% for Cl (1σ).

Phengite from three samples contains 610–1822 μg/g F and 1.01–1.98 μg/g Cl. Two of the three grains analyzed show no systematic core to rim halogen variations. Phengite is relatively homogeneous in terms of F and Cl, with 1σ sample variations of less than 20%. However, in a rim to rim transect of SEC43-01 phengite (Fig. S6), intra-grain variability is evident. F concentrations show a systematic decrease from core to rim, paralleling major element trends of decreasing K_2O, SiO_2, and MgO. Cl is enriched near grain boundaries by approximately 40% with respect to cores, following Al_2O_3 and Na_2O rim enrichments (Fig. S3 and S6). Finally, a single secondary titanite in SEC46-02 contains 1394 μg/g F, <0.1 μg/g Cl, and 4010 μg/g OH.

6. Discussion

6.1. Halogen redistribution during eclogitization

Halogen distribution during prograde metamorphism depends to a large extent on bulk-rock chemistry, which dictates the equilibrium mineral assemblage and phase proportions at any given pressure and temperature. Raspas eclogites show a strong positive correlation between the proportion of omphacite in the bulk-rock and the F content of omphacite (Fig. S7), suggesting that F is repartitioned during eclogitization and progressive omphacite growth. In addition, we compare the modal proportion of nominally anhydrous minerals (omphacite + garnet + quartz) to the volatile content of analyzed phases (Fig. S8). As the proportion of NAMs in the bulk assemblage increases, the F content of each phase shows a commensurate increase. Indeed, modal abundances of amphibole are negatively correlated with F concentrations in both omphacite and apatite, again suggesting effective redistribution of F during prograde metamorphism. Further, apatite Cl abundances increase as amphibole modes decrease and the mineral assemblage becomes dominated by garnet and omphacite. In all cases concerning lattice-hosted halogens, F is accommodated primarily in apatite (1.47–3.25 wt %), amphibole (563–4727 μg/g), and phengite (610–1822 μg/g) with lesser amounts in omphacite (6.5–54.1 μg/g) and garnet (1.7–8.9 μg/g). In addition, Cl is primarily hosted in apatite (192–515 μg/g), with lesser amounts in amphibole (0.64–82.7 μg/g), phengite (1.2–2.1 μg/g), omphacite (<0.05–1 μg/g) and garnet (<0.05 μg/g).

Our in situ measurements permit the calculation of distribution coefficients between various phases of interest (Figs. 3 and 4, Table S8). Given the scarcity of data, these new values provide important constraints on the distribution of F and Cl in eclogitic phases. A number of observations can made from the above distribution coefficients. First, F partitioning between mineral pairs defines a narrow range and appears to be insensitive to concentrations, which in some cases span nearly an order of magnitude. Second, as expected apatite will preferentially host crystal lattice-bound F and Cl when present in eclogitic assemblages, similar to apatite's halogen affinity in the presence of aqueous fluids (Kusebauch et al. 2015). Finally, F and Cl are preferentially partitioned into amphibole over phengite in all samples by a factor of 2.4 and 20, respectively. Interestingly, this observation is in contrast to blueschists studied by Pagé et al. (2016) who found $D_F^{Amph-Phen}$ was always less than unity whereas $D_{Cl}^{Amph-Phen}$ was approximately equal to one within error. Hence, blueschist to eclogite phase transformations may elicit changes in the relative compatibilities of halogens between coexisting phases, likely as a function of changing modal proportions, mineral compositions (e.g. glaucophane to katophorite), and P-T conditions.

6.2. Comparison between measured and reconstructed bulk halogen abundances

Using mineral modes, in situ SIMS data, and EPMA halogen concentrations, we calculate a reconstructed bulk-rock F and Cl content for each eclogite sample, which can then be compared to bulk values measured by pyrohydrolysis (Table 3, Fig. 5). Both raw (not corrected for yield) and yield-corrected pyrohydrolysis halogen abundances are given in Table 3. We use yield-corrected concentrations in subsequent discussions.

Reconstructed concentrations and pyrohydrolysis measurements yield F concentrations of 168–415 µg/g and 115–199 µg/g, respectively. Reconstructed F abundances are broadly concordant with measured values; three of the six samples agree within uncertainty, whereas three samples display higher reconstructed values (Fig. 6; Table 3). The relative congruence between reconstructed and measured F values implies that F may be entirely hosted within the crystal lattice of eclogitic phase assemblages. The discrepancy observed for three of the six samples may be due to a combination of factors including uncertainties in pyrohydrolysis yields (Table S9) that are typically larger than SIMS analyses, inter-grain halogen heterogeneity, or uncertainties in the calculated modal proportions (Table 2). We note that calculated modal proportions as derived from whole rock analysis were assessed, but found to be minor.

Bulk reconstructed and measured Cl concentrations for all samples are 0.8–8.2 µg/g and 6.7–19.9 µg/g, respectively. Unlike F, Cl shows very large and systematic discrepancies between reconstructed and measured values, with reconstructed values representing only 12–41% of the pyrohydrolysis-derived bulk values. We discuss these drastic differences below, in terms of uncertainties and possible means of reconciliation between the two methods. We consider three possible processes to explain the difference: retrograde alteration, grain boundary hosted Cl, and Cl-bearing fluid inclusions.

Bulk halogen analyses rely on the assumption that samples are perfectly preserved and have not been retrogressed along their exhumation path. Even minute amounts of alteration (e.g. chlorite or titanite) can drastically affect such bulk measurements (Debret et al. 2016). Most Raspas eclogites appear to be pristine with little to no visible alteration or retrogression, with the exception of SEC46-02 that contains titanite-on-rutile overgrowths and monomineralic amphibole veinlets adjacent to FI-rich omphacite, indicating possible fluid assimilation. This sample also displays elevated reconstructed (8.2 μg/g) and bulk (19.9 μg/g) Cl compared to the rest of the suite. In light of this suspected fluid assimilation, and the large F incongruity (~100%) between the two methods, we exclude this sample from subsequent bulk rock calculations. Minor retrogression may have contributed to the discrepancy for SEC46-02, however all other samples still show at least a factor of three difference between reconstructed and measured bulk Cl concentrations. Therefore, a factor other than late alteration is likely at play.

To further explore this discrepancy, we conducted additional SIMS analyses on grain boundaries of FI-free amphibole and garnet (Fig. S9). Both profiles across grain boundaries display pronounced spikes in $^{35}Cl/^{30}Si$ signals within the immediate grain boundary at near-constant ^{30}Si counts. These grain boundary measurements are equivalent to 7–18 μg/g Cl. Yet, the grain boundaries themselves are far smaller than the dimensions of our analysis spot (3.8x3.8 μm) and depending on their size, could contain > 1 wt% Cl assuming a grain boundary thickness of 5 nm or less. As grain boundary porosity values in eclogites are poorly constrained, we used equation 9.6 of Turcotte and Schubert (2002) to calculate grain boundary porosity values based on a simplified grain geometry over a range of grain boundary thicknesses (1–25 nm) with realistic grain sizes (500 μm) to yield values of $9x10^{-12}$ to $6x10^{-9}$ (Table S10). The Cl contribution from grain boundaries alone (<0.1 μg/g Cl in all cases, or <2% contribution compared to pyrohydrolysis Cl abundances), given the above parameters, is unable to reconcile the reconstructed versus measured Cl abundances.

Finally, we consider the possible role of fluid inclusions, as they could represent an important host for Cl (Philippot and Selverstone 1991; Herms et al. 2012; Kendrick 2018). FI

(~1 μm to 10 μm on average) are found ubiquitously hosted in garnet (Fig. S1C) and omphacite cores, both of which appear in textural equilibrium with adjacent phases and occur in all samples. FI are far more abundant in SEC46-02, in particular where omphacite is in contact with monomineralic pargasitic amphibole veinlets (Fig. 1B). FI appear cloudy in thin section owing to their prolific abundance. These features likely reflect crystallization in the presence of fluids, possibly during prograde conditions (e.g. John et al (2010) and Herms et al. (2012)); such features have also been noted elsewhere in previous studies (e.g. Massonne et al. (2012), Zack et al. (2001)). Although we cannot directly analyze fluid inclusions by SIMS, heterogeneous Cl enrichments in SEC46-02 FI–rich omphacite (44–94 μg/g Cl) indicate that each SIMS analysis may incorporate some Cl-rich FI material. FI-free (optically clear) omphacite from the same sample also contains an order of magnitude more Cl (1.05 μg/g) compared to omphacite from all other samples (<0.1 μg/g), which is consistent with assimilation of pervasive fluids during crystallization (Herms et al. 2012). FI may host significant quantities of Cl from hundreds of μg/g to >10 wt% NaCl equivalent (Philippot and Selverstone 1991; Philippot et al. 1998; Scambelluri and Philippot 2001; Svensen et al. 2001; Kendrick et al. 2015; Kendrick 2018). Herms et al. (2012) have shown that omphacite and garnet hosted FIs from Raspas contain ~2 wt% NaCl, congruent with the salinity of dehydration-related FI found in rocks that have undergone blueschist-to-eclogite conversion (Gao and Klemd 2001). Assuming that FI contain ~2 wt% NaCl and represent 0.05–0.1% of the total sample volume, one may reconcile the discrepancy between in situ and bulk Cl abundances. Thus, pyrohydrolysis appears to incorporate fluid inclusion contributions, whereas SIMS analyses do not. Our calculations imply that FI host the majority (at least 80%) of Cl in Raspas eclogites; whether these fluid inclusions are all primary in nature, and therefore should be considered in the halogen budget of recycled eclogites, remains to be determined.

Combining SIMS and pyrohydrolysis techniques affords unique insights on the distribution and abundance of halogens in subducted slabs. SIMS provides detailed constraints on crystal lattice hosted halogen abundances, and is well suited to determine bulk F concentrations, given the uncertainty that can be associated with pyrohydrolysis yields. Minimally retrogressed Raspas eclogites analyzed by SIMS contain between 145 and 258 μg/g F; F may be entirely hosted within the crystal lattice of eclogites, whereas only ~20% of Cl (at most), on average, is crystallographically hosted when FI are present. However, SIMS cannot accurately account for Cl abundances if primary fluid inclusions are present in the sample, which dominate the Cl budget of eclogites. Assuming that fluid inclusions observed here are primary features, pyrohydrolysis is the preferred method to measure the bulk Cl content of pristine FI-bearing rocks; minimally retrogressed Raspas eclogites analyzed by pyrohydrolysis contain between 6.7 and 11.3 μg/g Cl.

7. Implications

Previous studies have suggested that amphibole is the primary carrier of halogens to the upper mantle (Debret et al. 2016; Barnes et al. 2018). Our results suggest a more nuanced view when one takes into account the contributions from coexisting phases and FI; amphibole's contribution to mineral-hosted bulk F and Cl abundances range from 6–84% and 4–85%, respectively (Fig. 6, S7). When amphibole modes are below ~5% (three of six samples), apatite is the most important carrier for mineral-hosted halogens, containing >80% of mineral–hosted Cl and 38–71% of mineral–hosted F. Apatite is thought to be stable to 7.5 GPa at 950º (Konzett and

Frost 2009), and will act as an important halogen carrier in eclogitized ocean crust. The remaining F is distributed between amphibole (4–53%), phengite (6–32%), omphacite (4–16%), and garnet (up to 2.2%). The above calculations consider only crystal matrix hosted halogen abundances; our results further indicate that FI host the majority of Cl in the bulk rock (at least 80%, on average). The ultimate fate of Cl will be dictated by the redistribution of free fluid phases during subsequent phase transformations, diffusive re-equilibration, and dynamic recrystallization at higher pressures and temperatures.

Raspas reconstructed bulk F concentrations (145–258 μg/g) are similar to previous pre-subduction AOC estimates of 216 μg/g (Straub and Layne 2003), blueschist (457 ± 159 μg/g F) and eclogite-facies (283 ± 146 μg/g F) AOC (Pagé et al. 2016; Hughes et al. 2018), as well as mean N–MORB values of 183 ± 107 μg/g calculated from recent work from Le Voyer et al. (2018) (Fig. 7A). Therefore, F concentrations remain relatively unchanged during the progression from nascent MORB, to AOC, and finally eclogitized AOC. Our results indicate that F is efficiently returned (~95%, derived from SIMS) to the upper mantle during subduction (Straub and Layne 2003; John et al. 2011; Pagé et al. 2016). Conversely, bulk pyrohydrolysis Cl measurements (6.7–11.3 μg/g) are at least an order of magnitude lower than pre-subduction AOC estimates (e.g. 207 μg/g (Barnes and Cisneros 2012)). Yet, observed Raspas concentrations are quite similar to recent blueschist and eclogite-facies AOC estimates by Hughes et al. (2018) of 3–23 μg/g Cl and Pagé et al. (2018) of 12 μg/g Cl, and well within the range observed in MORB (excluding Cl/K >0.1 after Shimizu and Saal (2016) and references therein) (Fig. 7A). Progression from initial MORB generation to seafloor alteration leads to an increase in Cl content, while subsequent eclogitization leads to a decrease in Cl abundances, returning to values similar to MORB. Using the pre-subduction AOC Cl bulk-rock estimate of Barnes and Cisneros

(2012) of 207 µg/g Cl and data presented here, we calculate that the vast majority (>95%, derived from bulk pyrohydrolysis) of subducted Cl is expelled from the slab by the time the AOC parcel equilibrates at eclogite-facies conditions (Table 3), in agreement with previous workers (Straub and Layne 2003; John et al. 2011; Kendrick et al. 2014; Pagé et al. 2016). What little Cl remains will reside primarily in FI (at least 80%, on average). Thus, while most F is retained in the subducting slab at eclogite-facies conditions, most Cl previously added through hydrothermal alteration is expelled, fractionating F from Cl in eclogitized AOC. Yet, halogen abundances in Raspas are similar to unaltered MORB (Fig. 7A), while ratios of F and Cl with elements of similar compatibility during melting, Cl/K (0.0066 ± 0.0043), Cl/Nb (3.9 ± 1.0) and F/Nd (15.5 ± 4.8), are indistinguishable within uncertainty from DMM ratios of Salters and Stracke (2004) (Fig. 7B).

The HIMU (high U/Pb) mantle source is thought to contain ancient altered oceanic crust based on Pb isotope systematics (and more recently Tl, see Shu et al. (2019)), yielding enrichments in F/Nd, $^{35}Cl/^{37}Cl$, and often Cl/K and Cl/Nb ratios (Chase 1981; Hofmann and White 1982; Zindler et al. 1982; Stroncik and Haase 2004; John et al. 2011; Cabral et al. 2014; Jackson et al. 2015; Le Voyer et al. 2015; Kendrick et al. 2017; Rose-Koga et al. 2017; Hanyu et al. 2019). Our data indicate that halogen enrichments, and elevated F/Nd and Cl/K ratios, in the HIMU source cannot be produced by simple addition of recycled eclogitized AOC (Fig. 7B), but rather require delivery by an additional lithology, e.g. serpentinite as proposed by Kendrick et al. (2017), or an efficient fractionation mechanism to elevate halogen ratios during subsequent processing (e.g. Niu and O'Hara (2003)). The broad spectrum of F/Nd and Cl/K ratios observed in HIMU melts may then reflect variable contributions from subducted serpentinite (green line, Fig. 7B). However, antigorite serpentinite breakdown by the reaction: antigorite = olivine +

orthopyroxene + H_2O requires geochemical transfer of halogens, likely into a fluid phase as both F and Cl are highly incompatible in olivine and orthopyroxene (Dalou et al. 2014; Joachim et al. 2015; Beyer et al. 2016); their ultimate host within the upper mantle remains unknown. Direct phase transformation from antigorite serpentinite to the dense hydrous magnesium silicate Phase A may occur along cold geothermal gradients (Schmidt and Poli 1998), or halogens may become more compatible in K-rich clinopyroxene at increasing pressures as K solubility in clinopyroxene increases to ~1 wt. % K_2O at 100 kbar (Schmidt and Poli 1998). Thus, subduction proceeds in returning to the upper mantle an eclogitized AOC parcel with halogen ratios quite similar to the MORB from which it was derived.

Figures

See attached folder

Figure Captions

Figure 1. Representative photomicrographs of Raspas eclogite textures. A. SEC43-03 contains garnet porphyroblasts within a matrix of omphacite and lesser quartz. B. Amphibole veinlet in sample SEC46-02. Adjacent omphacite shows abundant fluid inclusions (yellow arrow). C. SEC43-03 Megacrystic, inclusion-rich garnet showing sector zoning.

Figure 2. Core and rim measurements for OH (A. and B.) and F (C. and D.) in garnet and omphacite. The majority of samples show core and rim values that fall on a 1:1 line, within uncertainty, allowing a high degree of confidence in bulk rock calculations based on in situ measurements. Error bars are 2SE.

Figure 3. Inter-mineral F partitioning between A. omphacite and garnet, B. omphacite and apatite, C. omphacite and amphibole, and D. omphacite and phengite. White triangles are literature data from Debret et al. (2016). Solid lines show constant inter-mineral partition coefficients (labeled), while mean partition coefficients for each mineral pair are presented in the bottom right panel corner.

Figure 4. Inter-mineral Cl partitioning between A. phengite and apatite, B. apatite and amphibole, C. phengite and amphibole, and D. apatite Cl and garnet F concentrations. White triangles are literature data from Debret (2016), green diamonds from Hughes et al. (2018) and

blue upside down triangles from Pagé et al. (2016). Solid lines denote constant inter-mineral partition coefficients as in Fig. 3.

Figure 5. Bulk reconstructed and bulk measured (yield corrected) halogen abundances for F (A.) and Cl (B.). Y error bars show analytical reproducibility propagated with yield precision. Yield-uncorrected pyrohydrolysis values are shown in panels C and D, where positive Y error bars incorporate yield uncertainty. Red dots denote SEC46-02, which was not included in bulk calculations; see text for more information. Solid lines represent 1:1 lines; dashed lines plot various slopes, labeled accordingly.

Figure 6. Pie diagrams show modal abundances (A. and B.), as well as the percent contribution from each phase to mineral-hosted halogen abundances as derived from SIMS analyses for F (C. and D.) and Cl (E. and F.) in two representative, yet mineralogically distinct, samples.

Figure 7. A. F and Cl abundances from this study in comparison to literature values for MORB glasses from Le Voyer et al. (2018), HIMU OIB (Cabral et al. 2014; Jackson et al. 2015; Kendrick et al. 2017), blueschist and eclogite (Debret et al. 2016; Pagé et al. 2016; Hughes et al. 2018), antigorite serpentinite (Pagé et al. 2018), and AOC estimates (Straub and Layne 2003; Van den Bleeken and Koga 2015; Barnes et al. 2018; Kendrick 2019a). MORB with Cl/K values in excess of 0.1 were screened out, due to possible seawater contamination after Shimizu and Saal (2016) and references therein. Peridotite mantle plots off the scale and would be 1.4–31 μg/g for F and from 0.14 to 0.38 μg/g for Cl (Urann et al. 2017). B. F/Nd and Cl/K ratios of Raspas samples (Nd and K from John et al. (2010)), MORB glasses from Le Voyer (2018), mean antigorite serpentinite halogen concentrations from Page et al. (2018) with DMM K (60 μg/g) and Nd (0.713 μg/g) values of Salters and Stracke (2004), and OIB MIs and glasses from the literature (Cabral et al. 2014; Jackson et al. 2015; Kendrick et al. 2017). We note that our eclogitized AOC samples indeed plot below the canonical F/Nd of 21, as posited by Rose-Koga et al. (2012) for deeply subducted oceanic crust.

Figure S1. Representative full-section photomicrographs of Raspas samples analyzed in this study. A. Prograde assemblage in SEC43-01 contains garnet porphyroblasts within a matrix of omphacite and lesser quartz and phengite with minor apatite and rutile. The sample shows no evidence for retrogression. B. SEC43-03 megacrystic garnet showing sector zoning with minor quartz. C. Amphibole veinlet in sample SEC46-02, outlined in white dashed line. Adjacent omphacite shows abundant fluid inclusions (dark patches).

Figure S2. Representative calibration slope used in this study. Calibration slope confidence intervals were calculated with a non-linear bootstrapping technique using 5,000 iterations.

Figure S3. SEC43-01 phengite EMP profile from rim to rim shows Na_2O and Al_2O_3 increases from core to rim, while K_2O, SiO_2, and MgO all decrease toward the grain boundary.

Figure S4. SEC43-01 garnet core to rim transect. Zero values represent rim, 750 μm spot location is the garnet core. Overall, OH and F show intragrain variability likely related to partitioning and re-equilibration during garnet growth. The combination of internal and propagated calibration slope uncertainty corresponds to the positive error bar on our analyses.

The negative error bars are larger for Cl because they incorporate the conservative uncertainty on the maximum background.

Figure S5. SEC43-01 omphacite core (~1300 µm) to rim (zero µm) profile for OH, F, and Cl. Significant variations occur on length scales of <100 µm, with apparent rim depletions in F and OH.

Figure S6. SEC43-01 phengite rim-to-rim transect. F shows depletions toward the grain boundaries, while Cl shows rim enrichments of approximately 40%.

Figure S7. Fluorine concentrations (black y-axis, yellow dots) and contributions to the bulk-rock (blue y-axis, blue dots) plotted against modal proportion of each phase for A. omphacite, B. amphibole, C. apatite, and D. phengite.

Figure S8. Fluorine and chlorine concentrations in each phase as a function of the modal proportion of nominally anhydrous minerals (omphacite plus garnet). As the modal proportion of NAMs increases, so does the halogen concentration in most phases.

Figure S9. Grain boundary transects using SIMS across amphibole (A.) and garnet (B.). While there are likely unaccounted for matrix effects with this approach, both measurements on the grain boundary qualitatively show pronounced spikes in Cl/Si ratios at near-constant constant Si counts, indicating Cl enrichment within the grain boundary (C. and D.). Also shown are raw ^{30}Si counts for comparison (panels E and F).

Acknowledgments

We thank two anonymous reviewers for their insights and suggestions, which improved the manuscript. This research was supported by NSF award EAR-P&G #1524311 and #1839128 to VLR. BMU acknowledges the support of the WHOI Ocean Venture Fund. This work was also supported by NSF-PIRE grant (OIA- 1545903) to JDB.

References Cited

Anderson, A.T., and Greenland, L.P. (1969) Phosphorus fractionation diagram as a quantitative indicator of crystallization differentiation of basaltic liquids. Geochimica et Cosmochimica Acta, 33, 493–505.

Armstrong, J.T. (1995) CITZAF—a package of correction programs for the quantitative electron microbeam X-ray analysis of thick polished materials, thin lms, and particles. Microbeam Anal, 177–200.

Barnes, J.D., and Cisneros, M. (2012) Mineralogical control on the chlorine isotope composition of altered oceanic crust. Chemical Geology, 326-327, 51–60.

Barnes, J.D., Manning, C.E., Scambelluri, M., and Selverstone, J. (2018) The Behavior of Halogens During Subduction-Zone Processes. In The Role of Halogens in Terrestrial and Extraterrestrial Geochemical Processes Vol. 263, pp. 545–590. Springer International Publishing, Cham.

Beinlich, A., Klemd, R., John, T., and Gao, J. (2010) Trace-element mobilization during Ca-metasomatism along a major fluid conduit: Eclogitization of blueschist as a consequence of fluid–rock interaction. Geochimica et Cosmochimica Acta, 74, 1892–1922.

Beyer, C., Klemme, S., Grützner, T., Ireland, T.R., Magee, C.W., and Frost, D.J. (2016) Fluorine partitioning between eclogitic garnet, clinopyroxene, and melt at upper mantle conditions. Chemical Geology, 437, 88–97.

Cabral, R.A., Jackson, M.G., Koga, K.T., Rose-Koga, E.F., Hauri, E.H., Whitehouse, M.J., Price, A.A., Day, J.M.D., Shimizu, N., and Kelley, K.A. (2014) Volatile cycling of H_2O, CO_2, F, and Cl in the HIMU mantle: A new window provided by melt inclusions from oceanic hot spot lavas at Mangaia, Cook Islands. Geochemistry, Geophysics, Geosystems, 15, 4445–4467.

Chase, C.G. (1981) Oceanic island Pb: Two-stage histories and mantle evolution. Earth and Planetary Science Letters, 52, 277–284.

Chavrit, D., Burgess, R., Sumino, H., Teagle, D.A.H., Droop, G., Shimizu, A., and Ballentine, C.J. (2016) The contribution of hydrothermally altered ocean crust to the mantle halogen and noble gas cycles. Geochimica et Cosmochimica Acta, 183, 106–124.

Dalou, C., Koga, K.T., Le Voyer, M., and Shimizu, N. (2014) Contrasting partition behavior of F and Cl during hydrous mantle melting: implications for Cl/F signature in arc magmas. Progress in Earth and Planetary Science, 1, 26.

Debret, B., Koga, K.T., Cattani, F., Nicollet, C., Van den Bleeken, G., and Schwartz, S. (2016) Volatile (Li, B, F and Cl) mobility during amphibole breakdown in subduction zones. LITHOS, 244, 165–181.

Feininger, T. (1980) Eclogite and Related High-Pressure Regional Metamorphic Rocks from the Andes of Ecuador. Journal of Petrology, 21, 107–140.

Feininger, T. (1987) Allochthonous terranes in the Andes of Ecuador and northwestern Peru. Canadian Journal of Earth Sciences, 24, 266–278.

Freundt, A., Grevemeyer, I., Rabbel, W., Hansteen, T.H., Hensen, C., Wehrmann, H., Kutterolf, S., Halama, R., and Frische, M. (2014) Volatile (H2O, CO2, Cl, S) budget of the Central American subduction zone. International Journal of Earth Sciences, 103, 2101–2127.

Gabriele, P. (2002) HP terranes exhumation in an active margin setting: geology, petrology and geochemistry of the Raspas Complex in SW Ecuador.

Gale, A., Dalton, C.A., Langmuir, C.H., Su, Y., and Schilling, J.G. (2013) The mean composition of ocean ridge basalts. Geochemistry, Geophysics, Geosystems, 14, 489–518.

Gao, J., and Klemd, R. (2001) Primary fluids entrapped at blueschist to eclogite transition: evidence from the Tianshan meta-subduction complex in northwestern China. Contributions to Mineralogy and Petrology, 142, 1–14.

Halama, R., John, T., Herms, P., Hauff, F., and Schenk, V. (2011) A stable (Li, O) and radiogenic (Sr, Nd) isotope perspective on metasomatic processes in a subducting slab. Chemical Geology, 281, 151–166.

Hanyu, T., Shimizu, K., Ushikubo, T., Kimura, J.-I., Chang, Q., Hamada, M., Ito, M., Iwamori, H., and Ishikawa, T. (2019) Tiny droplets of ocean island basalts unveil Earth's deep chlorine cycle. Nature Communications, 10, 222.

Herms, P., John, T., Bakker, R.J., and Schenk, V. (2012) Evidence for channelized external fluid flow and element transfer in subducting slabs (Raspas Complex, Ecuador). Chemical Geology, 310-311, 79–96.

Hofmann, A.W., and White, W.M. (1982) Mantle plumes from ancient oceanic crust. Earth and Planetary Science Letters, 57, 421–436.

Hughes, L., Burgess, R., Chavrit, D., Pawley, A., Tartèse, R., Droop, G., Ballentine, C.J., and Lyon, I. (2018) Halogen behaviour in subduction zones: Eclogite facies rocks from the Western and Central Alps. Geochimica et Cosmochimica Acta, 243, 1–23.

Imai, N., Terashima, S., Itoh, S., and Ando, A. (1995) 1994 Complilation of Analyitical Data for Minor and Trace Elements in Seventeen GSJ Geochemical Reference Samples, "Igneous Rock Series." Geostandards and Geoanalytical Research, 19, 135–213.

Ito, E., Harris, D.M., and Anderson, A.T. (1983) Alteration of oceanic crust and geologic cycling of chlorine and water. Geochimica et Cosmochimica Acta, 47, 1613–1624.

Jackson, M.G., Koga, K.T., Price, A., Konter, J.G., Koppers, A.A.P., Finlayson, V.A., Konrad, K., Hauri, E.H., Kylander-Clark, A., Kelley, K.A., and others (2015) Deeply dredged submarine HIMU glasses from the Tuvalu Islands, Polynesia: implications for volatile budgets of recycled oceanic crust. Wiley Online Library

.

Joachim, B., Pawley, A., Lyon, I.C., neé Hartmann, K.M., Henkel, T., Clay, P.L., Ruzié, L., Burgess, R., and Ballentine, C.J. (2015) Experimental partitioning of F and Cl between olivine, orthopyroxene and silicate melt at Earth's mantle conditions. Chemical Geology, 416, 65–78.

John, T., and Schenk, V. (2003) Partial eclogitisation of gabbroic rocks in a late Precambrian subduction zone (Zambia): prograde metamorphism triggered by fluid infiltration. Contributions to Mineralogy and Petrology, 146, 174–191.

DOI: https://doi.org/10.2138/am-2020-6994

John, T., Scambelluri, M., Frische, M., Barnes, J.D., and Bach, W. (2011) Dehydration of subducting serpentinite: Implications for halogen mobility in subduction zones and the deep halogen cycle. Earth and Planetary Science Letters, 308, 65–76.

John, T., Scherer, E.E., Schenk, V., Herms, P., Halama, R., and Garbe-Schönberg, D. (2010) Subducted seamounts in an eclogite-facies ophiolite sequence: the Andean Raspas Complex, SW Ecuador. Contributions to Mineralogy and Petrology, 159, 265–284.

Kendrick, M.A. (2018) Halogens in Seawater, Marine Sediments and the Altered Oceanic Lithosphere. In The Role of Halogens in Terrestrial and Extraterrestrial Geochemical Processes Vol. 87, pp. 591–648. Springer, Cham, Cham.

Kendrick, M.A. (2019a) Halogens in altered ocean crust from the East Pacific Rise (ODP/IODP Hole 1256D). Geochimica et Cosmochimica Acta, 261, 93–112.

Kendrick, M.A. (2019b) Halogens in Atlantis Bank gabbros, SW Indian Ridge: Implications for styles of seafloor alteration. Earth and Planetary Science Letters, 514, 96–107.

Kendrick, M.A., Hémond, C., Kamenetsky, V.S., Danyushevsky, L., Devey, C.W., Rodemann, T., Jackson, M.G., and Perfit, M.R. (2017) Seawater cycled throughout Earth's mantle in partially serpentinized lithosphere. Nature Geoscience, 10, 222–228.

Kendrick, M.A., Honda, M., and Vanko, D.A. (2015) Halogens and noble gases in Mathematician Ridge meta-gabbros, NE Pacific: implications for oceanic hydrothermal root zones and global volatile cycles. Contributions to Mineralogy and Petrology, 170, 173.

Kendrick, M.A., Jackson, M.G., Kent, A.J.R., Hauri, E.H., Wallace, P.J., and Woodhead, J. (2014) Contrasting behaviours of CO2, S, H2O and halogens (F, Cl, Br, and I) in enriched-mantle melts from Pitcairn and Society seamounts. Chemical Geology, 370, 69–81.

Konzett, J., and Frost, D.J. (2009) The High P–T Stability of Hydroxyl-apatite in Natural and Simplified MORB—an Experimental Study to 15 GPa with Implications for Transport and Storage of Phosphorus and Halogens in Subduction Zones. Journal of Petrology, 50, 2043–2062.

Kumamoto, K.M., Warren, J.M., and Hauri, E.H. (2017) New SIMS reference materials for measuring water in upper mantle minerals. American Mineralogist, 102, 537–547.

Kusebauch, C., John, T., Whitehouse, M.J., and Engvik, A.K. (2015) Apatite as probe for the halogen composition of metamorphic fluids (Bamble Sector, SE Norway). Contributions to Mineralogy and Petrology, 170, 271.

Le Voyer, M., Cottrell, E., Kelley, K.A., Brounce, M., and Hauri, E.H. (2015) The effect of primary versus secondary processes on the volatile content of MORB glasses: An example from the equatorial Mid-Atlantic Ridge (5°N–3°S). Journal of Geophysical Research: Solid Earth, 120, 125–144.

Le Voyer, M., Hauri, E.H., Cottrell, E., Kelley, K.A., Salters, V.J.M., Langmuir, C.H., Hilton, D.R., Barry, P.H., and Füri, E. (2018) Carbon fluxes and primary magma CO_2 contents along the global mid-ocean ridge system. Geochemistry, Geophysics, Geosystems.

Locock, A.J. (2014) An Excel spreadsheet to classify chemical analyses of amphiboles following the IMA 2012 recommendations. Computers & Geosciences, 62, 1–11.

Marschall, H.R., Altherr, R., Gméling, K., and Kasztovszky, Z. (2009) Lithium, boron and chlorine as tracers for metasomatism in high-pressure metamorphic rocks: a case study from Syros (Greece). Mineralogy and Petrology, 95, 291–302.

Maruyama, S., Liou, J.G., and Terabayashi, M. (1996) Blueschists and Eclogites of the World and Their Exhumation. International Geology Review, 38, 485–594.

Massonne, H.J. (2012) Formation of amphibole and clinozoisite–epidote in eclogite owing to fluid infiltration during exhumation in a subduction channel. Journal of Petrology, 53, 1969–1998.

Massonne, H.J., and Schreyer, W. (1987) Phengite geobarometry based on the limiting assemblage with K-feldspar, phlogopite, and quartz. Contributions to Mineralogy and Petrology, 96, 212–224.

Mather, T.A., Pyle, D.M., Tsanev, V.I., McGonigle, A.J.S., Oppenheimer, C., and Allen, A.G. (2006) A reassessment of current volcanic emissions from the Central American arc with specific examples from Nicaragua. Journal of Volcanology …, 149, 297–311.

Niu, Y., and O'Hara, M.J. (2003) Origin of ocean island basalts: A new perspective from petrology, geochemistry, and mineral physics considerations. Journal of Geophysical Research: Solid Earth, 108, 63.

Pagé, L., Hattori, K., and Guillot, S. (2018) Mantle wedge serpentinites: A transient reservoir of halogens, boron, and nitrogen for the deeper mantle. Geology, 46, 883–886.

Pagé, L., Hattori, K., de Hoog, J.C.M., and Okay, A.I. (2016) Halogen (F, Cl, Br, I) behaviour in subducting slabs: A study of lawsonite blueschists in western Turkey. Earth and Planetary Science Letters, 442, 133–142.

Philippot, P., Agrinier, P., and Scambelluri, M. (1998) Chlorine cycling during subduction of altered oceanic crust. Earth and Planetary Science Letters, 161, 33–44.

Philippot, P., and Selverstone, J. (1991) Trace-element-rich brines in eclogitic veins: implications for fluid composition and transport during subduction. Contributions to Mineralogy and Petrology, 106, 417–430.

Pyle, D.M., and Mather, T.A. (2009) Halogens in igneous processes and their fluxes to the atmosphere and oceans from volcanic activity: A review. Chemical Geology, 263, 110–121.

Rebay, G., Powell, R., and Diener, J.F.A. (2010) Calculated phase equilibria for a morb composition in a P-T range, 450-650 °C and 18-28 kbar: the stability of eclogite. Journal of Metamorphic Geology, 28, 635–645.

Rose-Koga, E.F., Koga, K.T., Moreira, M., Vlastelic, I., Jackson, M.G., Whitehouse, M.J., Shimizu, N., and Habib, N. (2017) Geochemical systematics of Pb isotopes, fluorine, and sulfur in melt inclusions from São Miguel, Azores. Chemical Geology.

Rose-Koga, E.F., Koga, K.T., Schiano, P., Le Voyer, M., Shimizu, N., Whitehouse, M.J., and Clocchiatti, R. (2012) Mantle source heterogeneity for South Tyrrhenian magmas revealed by Pb isotopes and halogen contents of olivine-hosted melt inclusions. Chemical Geology, 334, 266–279.

Sadofsky, S.J., Portnyagin, M., Hoernle, K., and van den Bogaard, P. (2008) Subduction cycling of volatiles and trace elements through the Central American volcanic arc: evidence from melt inclusions. Contributions to Mineralogy and Petrology, 155, 433–456.

Salters, V.J.M., and Stracke, A. (2004) Composition of the depleted mantle. Geochemistry, Geophysics, Geosystems, 5, n/a–n/a.

Scambelluri, M., and Philippot, P. (2001) Deep fluids in subduction zones. LITHOS, 55, 213–227.

Schmidt, M.W., and Poli, S. (1998) Experimentally based water budgets for dehydrating slabs and consequences for arc magma generation. Earth and Planetary Science Letters, 163, 361–379.

Schnetger, B., and Muramatsu, Y. (1996) Determination of halogens, with special reference to iodine, in geological and biological samples using pyrohydrolysis for preparation and inductively coupled plasma mass spectrometry and ion chromatography for measurement. The Analyst, 121, 1627.

Shimizu, K., Saal, A.E., Myers, C.E., Nagle, A.N., Hauri, E.H., Forsyth, D.W., Kamenetsky, V.S., and Niu, Y. (2016) Two-component mantle melting-mixing model for the generation of mid-ocean ridge basalts: Implications for the volatile content of the Pacific upper mantle. Geochimica et Cosmochimica Acta, 176, 44–80.

Shu, Y., Nielsen, S.G., Marschall, H.R., John, T., Blusztajn, J., and Auro, M. (2019) Closing the loop: Subducted eclogites match thallium isotope compositions of ocean island basalts. Geochimica et Cosmochimica Acta, 250, 130–148.

Stormer, J.C., and Pierson, M. (1993) Variation of F and Cl X-ray intensity due to anisotropic diffusion in apatite during electron microprobe analysis. pubs.geoscienceworld.org

.

Straub, S.M., and Layne, G.D. (2003) The systematics of chlorine, fluorine, and water in Izu arc front volcanic rocks: Implications for volatile recycling in subduction zones. Geochimica et Cosmochimica Acta, 67, 4179–4203.

Stroncik, N.A., and Haase, K.M. (2004) Chlorine in oceanic intraplate basalts: Constraints on mantle sources and recycling processes. Geology, 32, 945.

Svensen, H., Jamtveit, B., Banks, D.A., and Austrheim, H. (2001) Halogen contents of eclogite facies fluid inclusions and minerals: Caledonides, western Norway. Journal of Metamorphic Geology, 19, 165–178.

Turcotte, D.L., and Schubert, G. (2002) Geodynamics by Donald L. Turcotte, 2nd ed. Cambridge University Press, Cambridge.

Urann, B.M., Le Roux, V., Hammond, K., Marschall, H.R., Lee, C.T.A., and Monteleone, B.D. (2017) Fluorine and chlorine in mantle minerals and the halogen budget of the Earth's mantle. Contributions to Mineralogy and Petrology, 172, 324.

Van den Bleeken, G., and Koga, K.T. (2015) Experimentally determined distribution of fluorine and chlorine upon hydrous slab melting, and implications for F–Cl cycling through subduction zones. Geochimica et Cosmochimica Acta, 171, 353–373.

Watson, E. (1979) Apatite saturation in basic to intermediate magmas. Wiley Online Library

.

Zack, T., Rivers, T., and Foley, S. (2001) Cs–Rb–Ba systematics in phengite and amphibole: an assessment of fluid mobility at 2.0 GPa in eclogites from Trescolmen, Central Alps. Contributions to Mineralogy and Petrology, 140, 651–669.

Zindler, A., Jagoutz, E., and Goldstein, S. (1982) Nd, Sr and Pb isotopic systematics in a three-component mantle: a new perspective. Nature, 298, 519–523.

This is a preprint, the final version is subject to change, of the American Mineralogist (MSA)
Cite as Authors (Year) Title. American Mineralogist, in press.
DOI: https://doi.org/10.2138/am-2020-6994

Figure 1.

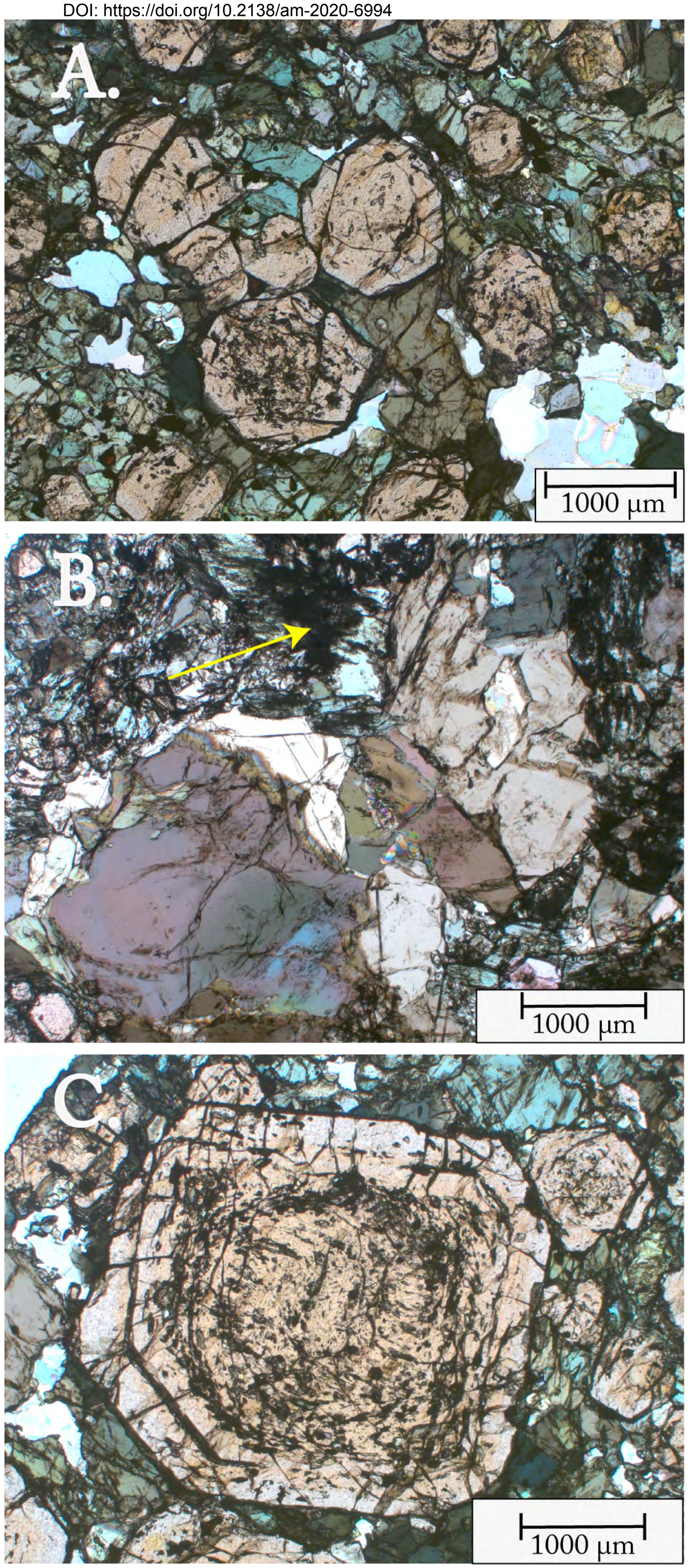

This is a preprint, the final version is subject to change, of the American Mineralogist (MSA)
Cite as Authors (Year) Title. American Mineralogist, in press.
DOI: https://doi.org/10.2138/am-2020-6994

Figure 2.

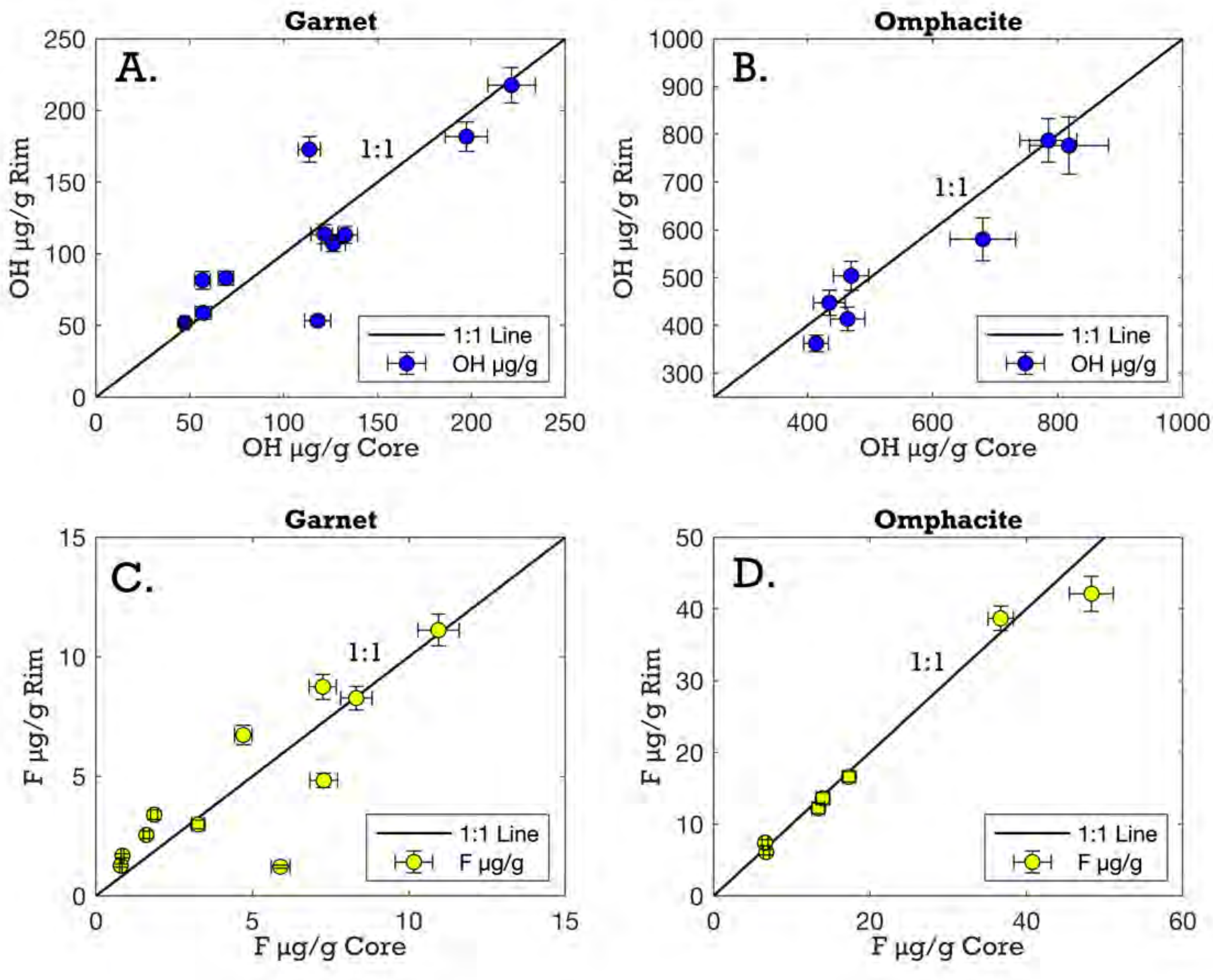

This is a preprint, the final version is subject to change, of the American Mineralogist (MSA)
Cite as Authors (Year) Title. American Mineralogist, in press.
DOI: https://doi.org/10.2138/am-2020-6994

Figure 3.

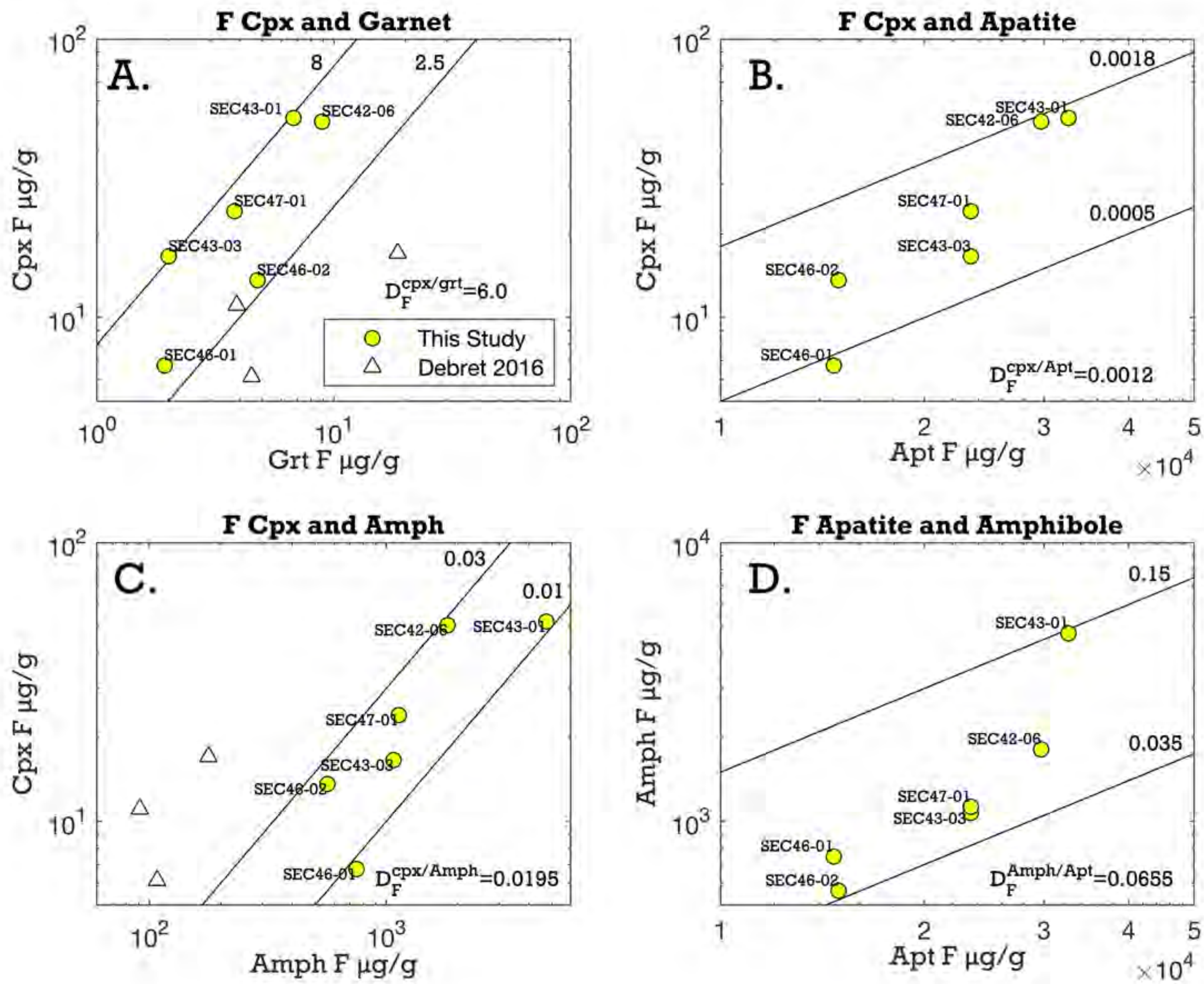

Figure 4.

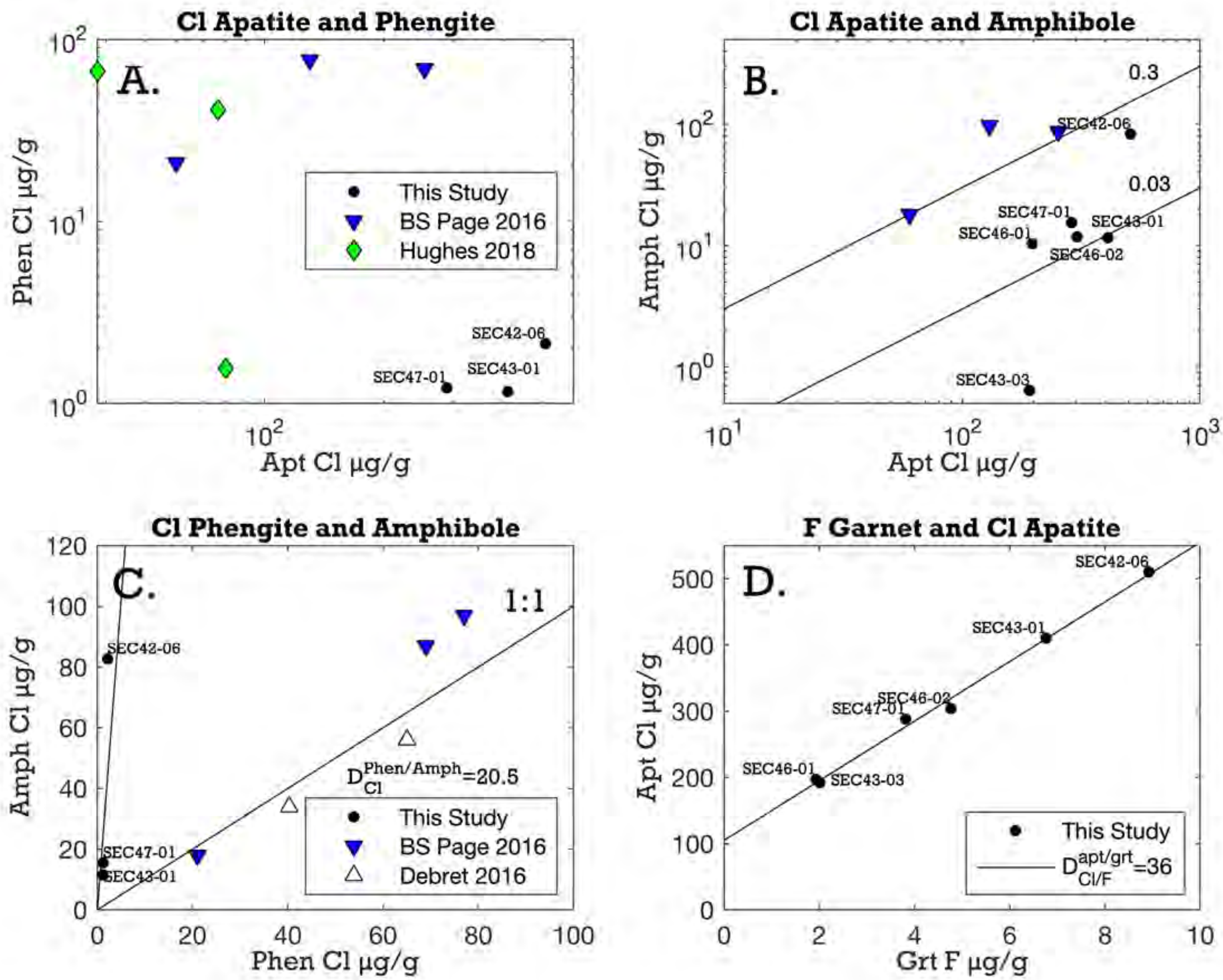
Cl Apatite and Phengite
A.
Phen Cl µg/g
Apt Cl µg/g
This Study
BS Page 2016
Hughes 2018
SEC42-06
SEC47-01
SEC43-01
Cl Apatite and Amphibole
B.
Amph Cl µg/g
Apt Cl µg/g
0.3
0.03
SEC42-06
SEC47-01
SEC46-01
SEC43-01
SEC46-02
SEC43-03
Cl Phengite and Amphibole
C.
Amph Cl µg/g
Phen Cl µg/g
1:1
SEC42-06
$D_{Cl}^{Phen/Amph}$=20.5
This Study
BS Page 2016
Debret 2016
SEC47-01
SEC43-01
F Garnet and Cl Apatite
D.
Apt Cl µg/g
Grt F µg/g
SEC42-06
SEC43-01
SEC46-02
SEC47-01
SEC46-01
SEC43-03
This Study
$D_{Cl/F}^{apt/grt}$=36

DOI: https://doi.org/10.2138/am-2020-6994

Figure 5.

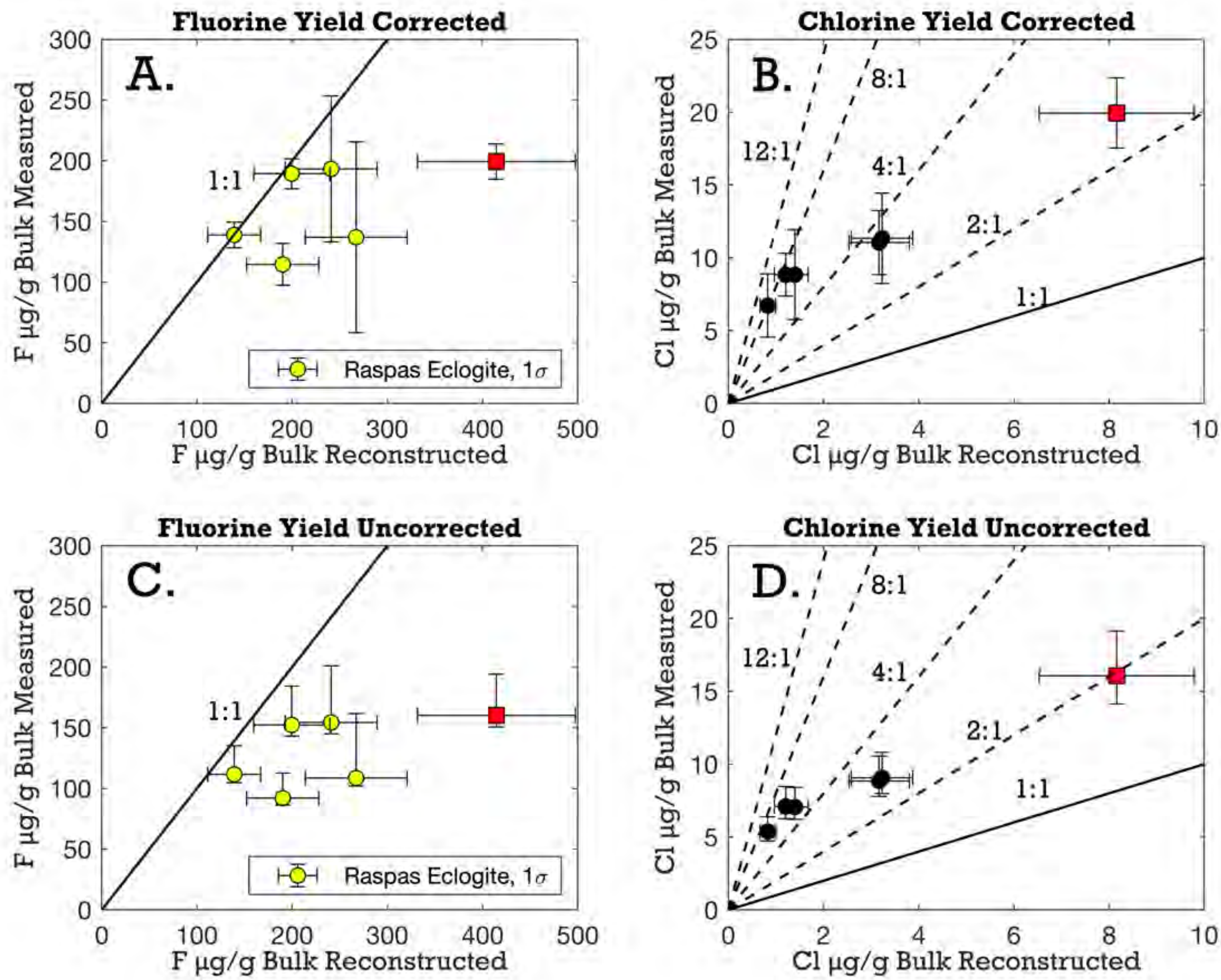

This is a preprint, the final version is subject to change, of the American Mineralogist (MSA)
Cite as Authors (Year) Title. American Mineralogist, in press.
DOI: https://doi.org/10.2138/am-2020-6994

Figure 6.

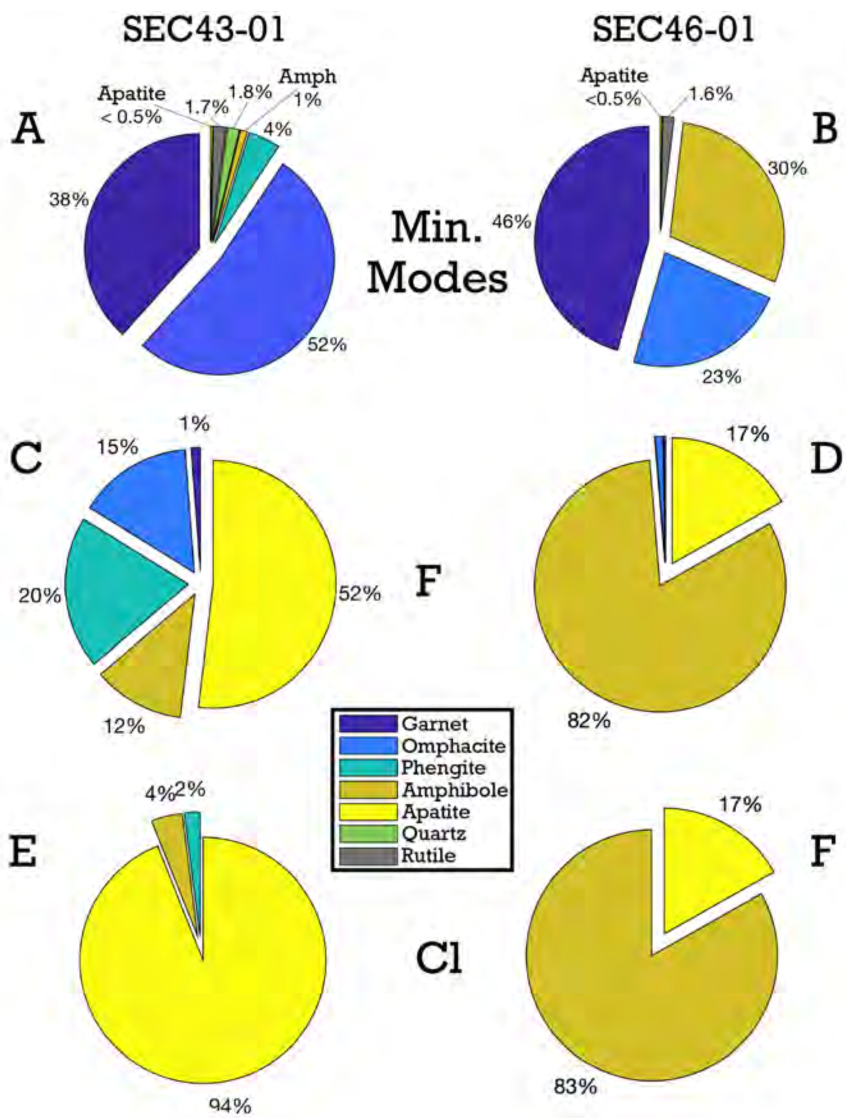

Figure 7.

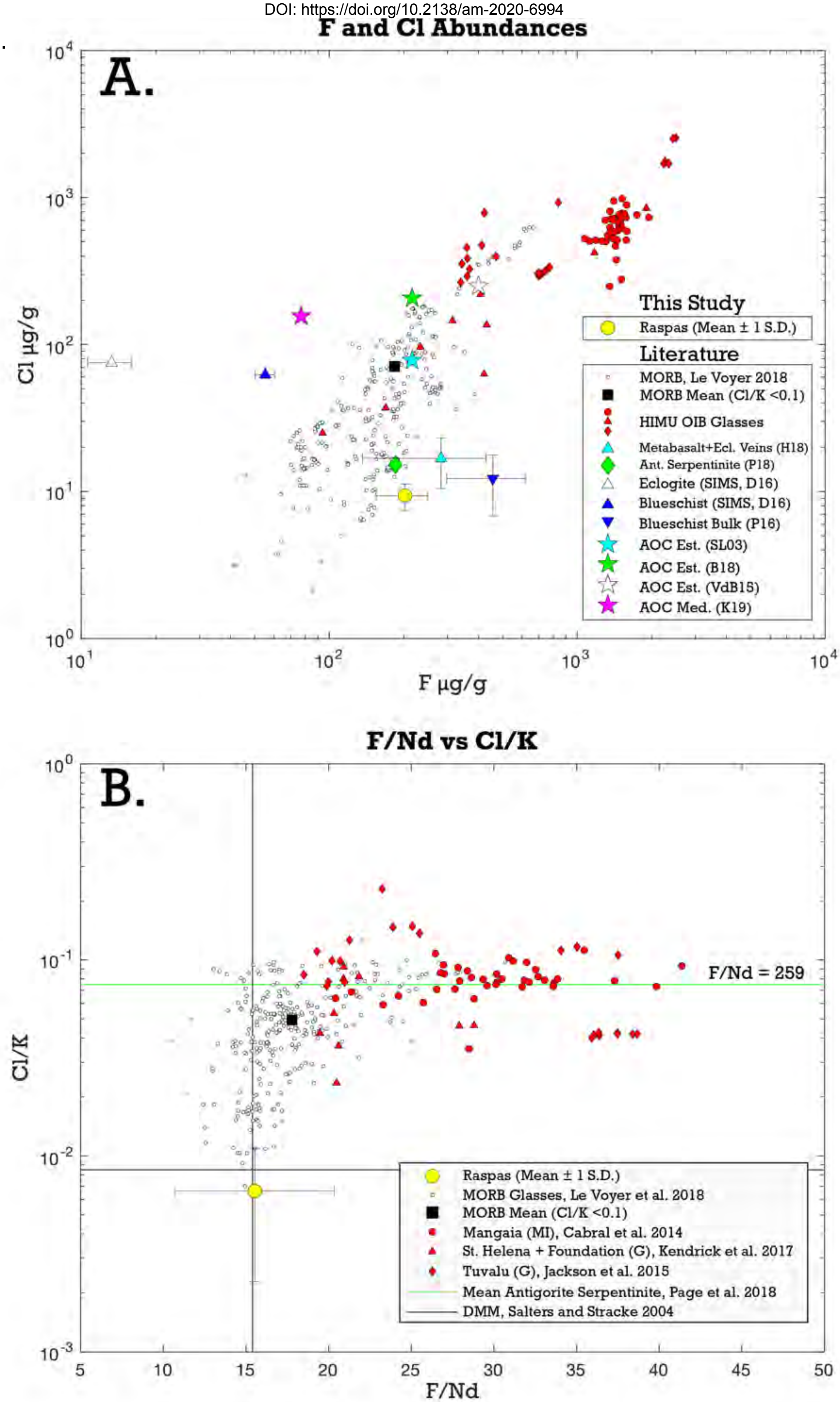
F and Cl Abundances
A.
Cl μg/g
F μg/g
This Study
Raspas (Mean ± 1 S.D.)
Literature
MORB, Le Voyer 2018
MORB Mean (Cl/K <0.1)
HIMU OIB Glasses
Metabasalt+Ecl. Veins (H18)
Ant. Serpentinite (P18)
Eclogite (SIMS, D16)
Blueschist (SIMS, D16)
Blueschist Bulk (P16)
AOC Est. (SL03)
AOC Est. (B18)
AOC Est. (VdB15)
AOC Med. (K19)
F/Nd vs Cl/K
B.
Cl/K
F/Nd
F/Nd = 259
Raspas (Mean ± 1 S.D.)
MORB Glasses, Le Voyer et al. 2018
MORB Mean (Cl/K <0.1)
Mangaia (MI), Cabral et al. 2014
St. Helena + Foundation (G), Kendrick et al. 2017
Tuvalu (G), Jackson et al. 2015
Mean Antigorite Serpentinite, Page et al. 2018
DMM, Salters and Stracke 2004

This is a preprint, the final version is subject to change, of the American Mineralogist (MSA)
Cite as Authors (Year) Title. American Mineralogist, in press.
DOI: https://doi.org/10.2138/am-2020-6994

Figure S1.

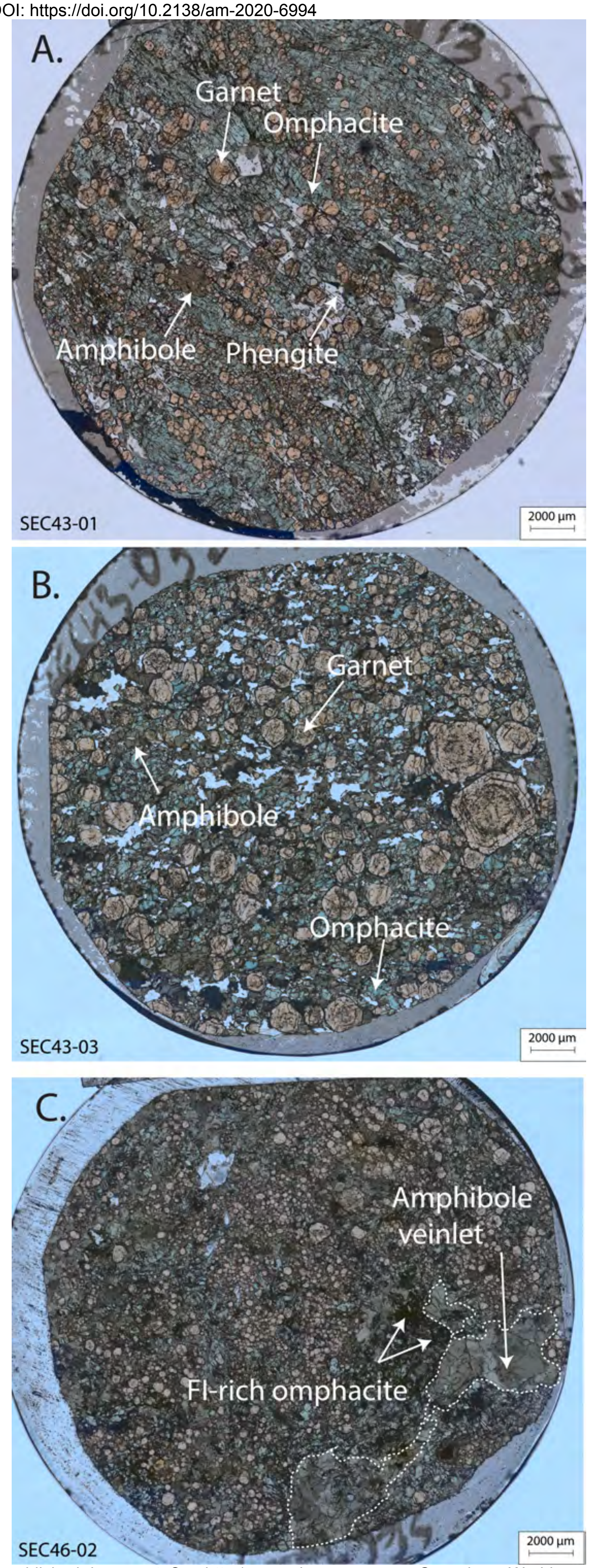

Figure S2.

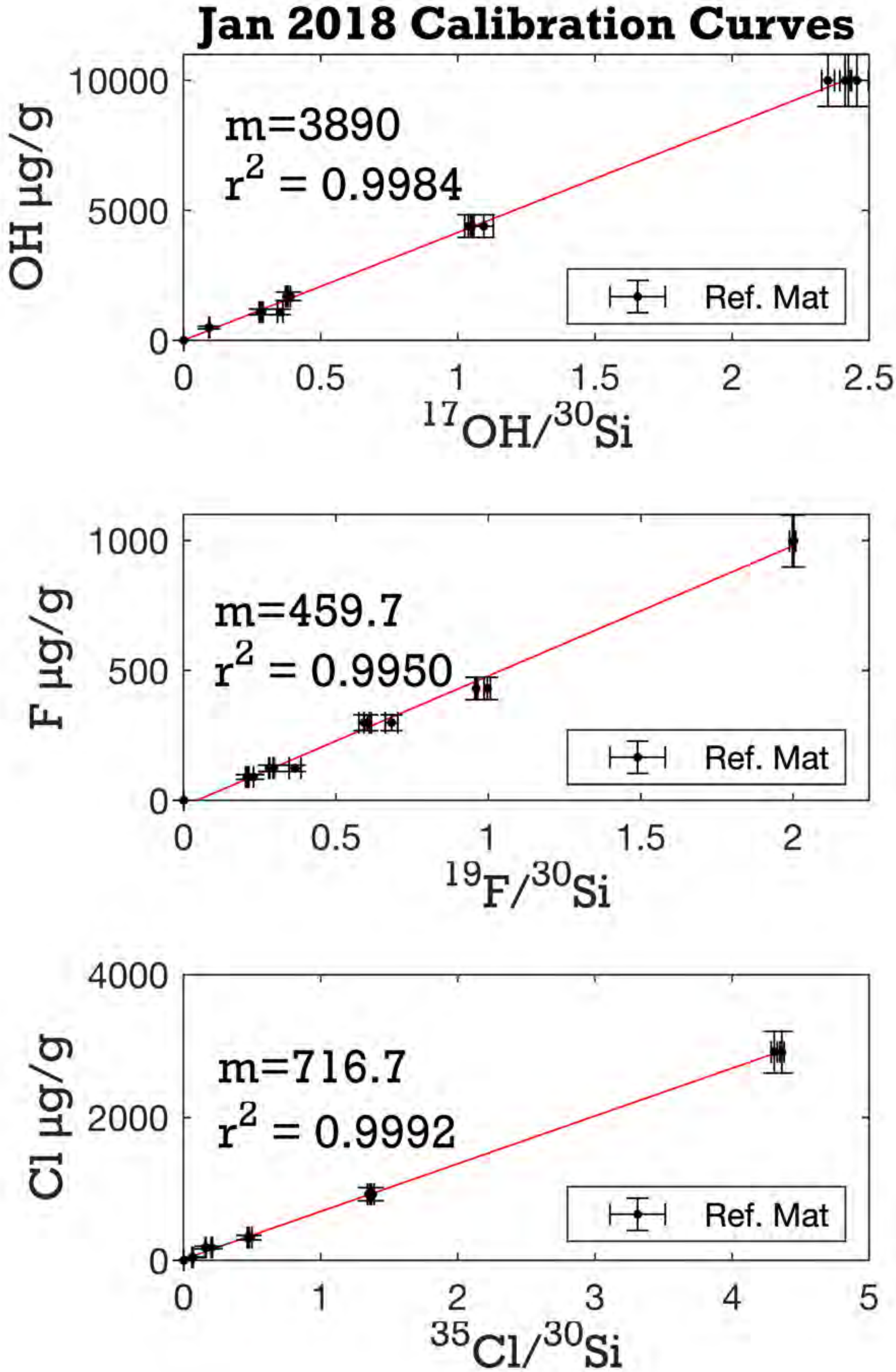
Jan 2018 Calibration Curves
m=3890
r^2 = 0.9984
Ref. Mat
OH µg/g
10000
5000
0
0
0.5
1
1.5
2
2.5
^{17}OH/^{30}Si
m=459.7
r^2 = 0.9950
Ref. Mat
F µg/g
1000
500
0
0
0.5
1
1.5
2
^{19}F/^{30}Si
m=716.7
r^2 = 0.9992
Ref. Mat
Cl µg/g
4000
2000
0
0
1
2
3
4
5
^{35}Cl/^{30}Si

This is a preprint, the final version is subject to change, of the American Mineralogist (MSA)
Cite as Authors (Year) Title. American Mineralogist, in press.
DOI: https://doi.org/10.2138/am-2020-6994

Figure S3.

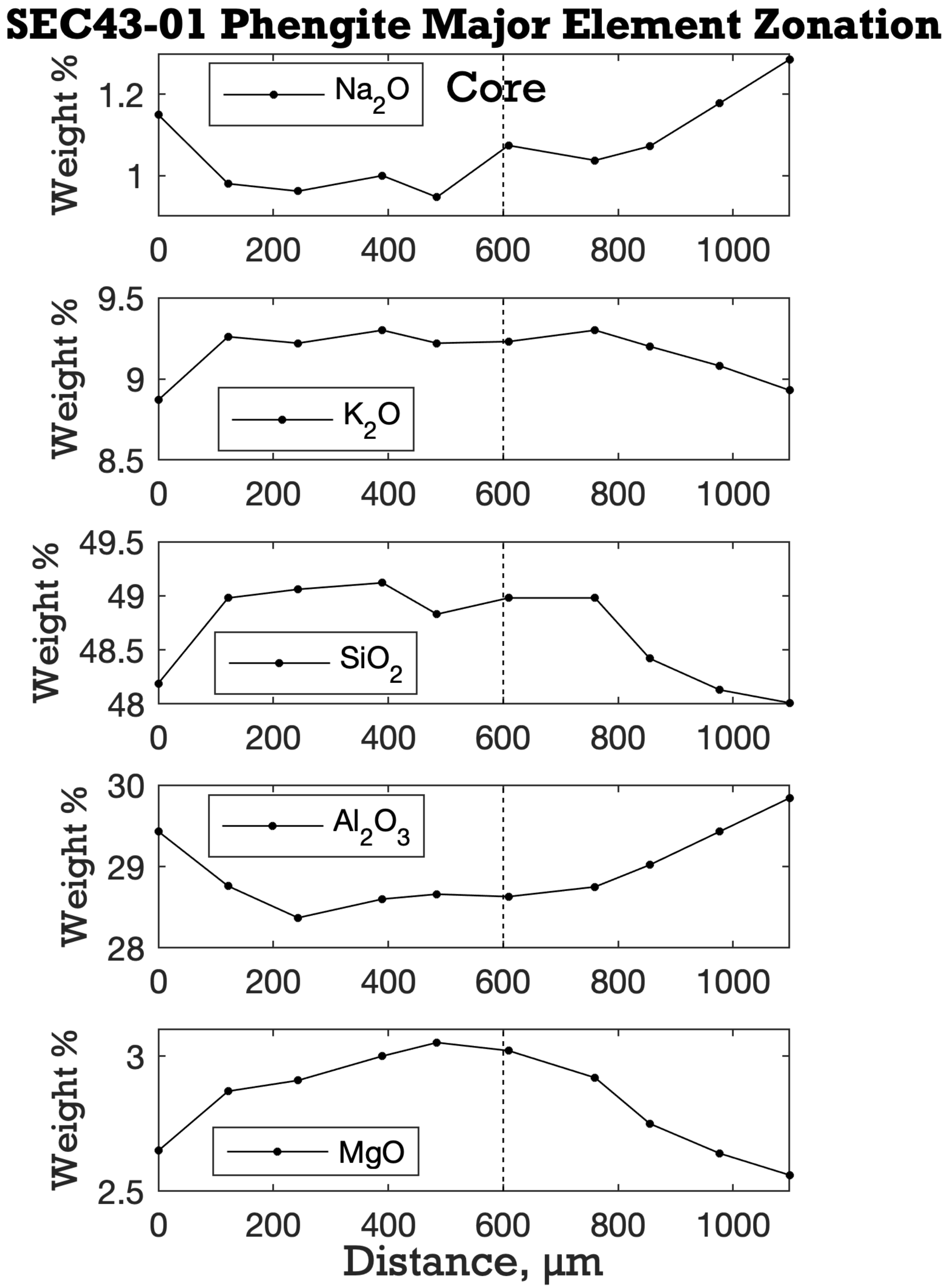

This is a preprint, the final version is subject to change, of the American Mineralogist (MSA)
Cite as Authors (Year) Title. American Mineralogist, in press.
DOI: https://doi.org/10.2138/am-2020-6994

Figure S4.

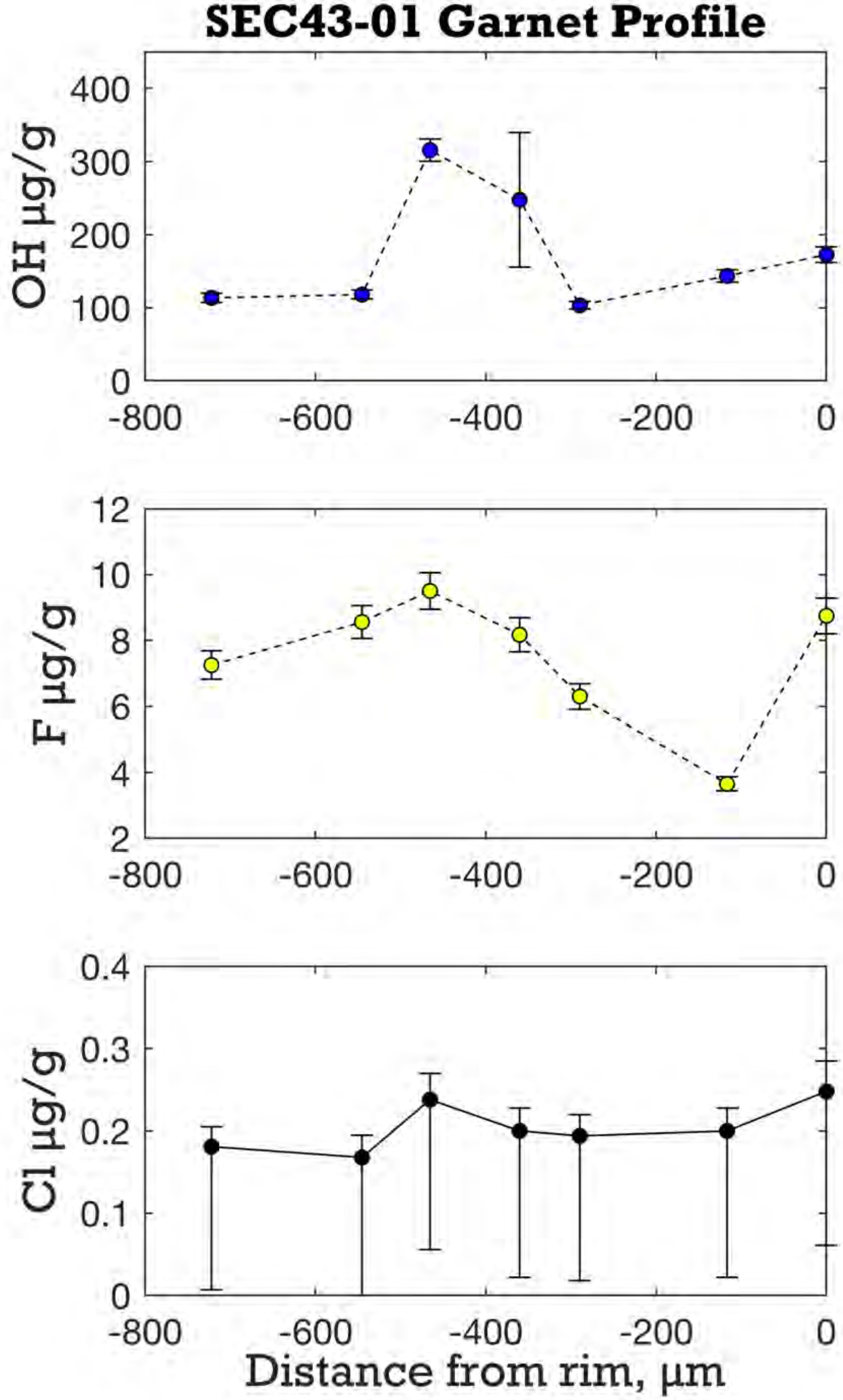

This is a preprint, the final version is subject to change, of the American Mineralogist (MSA)
Cite as Authors (Year) Title. American Mineralogist, in press.
DOI: https://doi.org/10.2138/am-2020-6994

Figure S5.

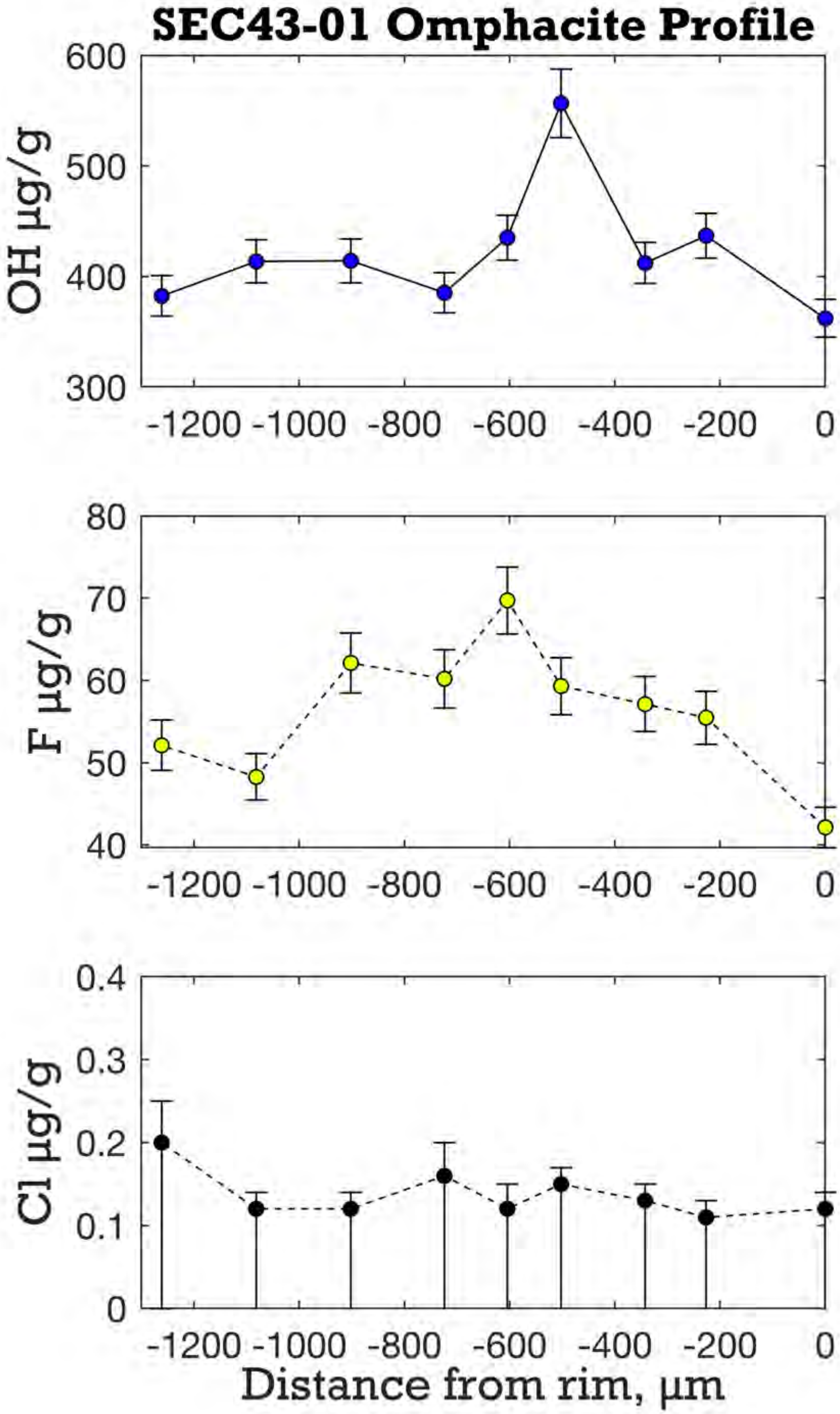

Figure S6.

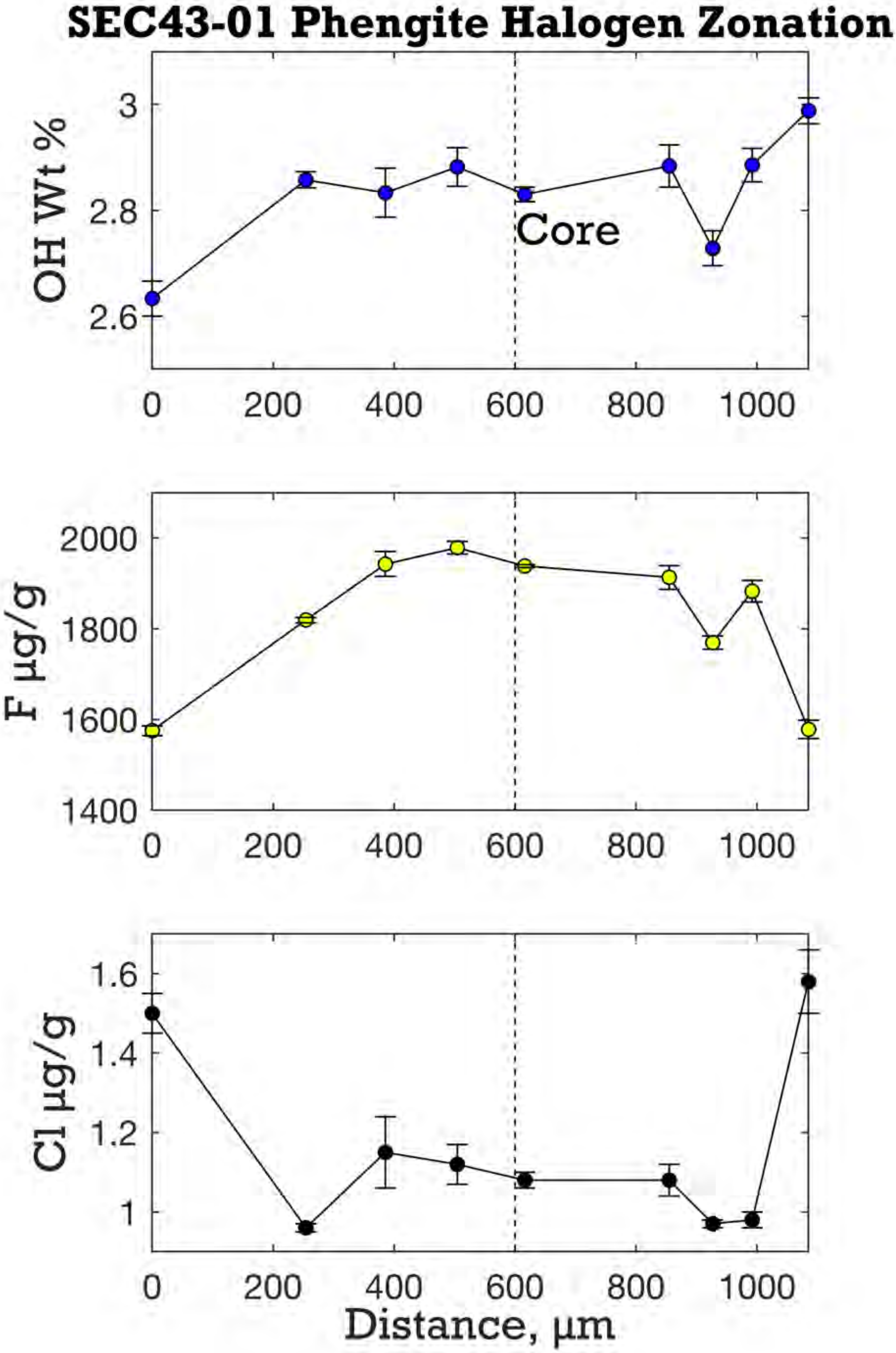
SEC43-01 Phengite Halogen Zonation
OH Wt %
3
2.8
2.6
Core
0
200
400
600
800
1000
F µg/g
2000
1800
1600
1400
Cl µg/g
1.6
1.4
1.2
1
Distance, µm

DOI: https://doi.org/10.2138/am-2020-6994

Figure S7.

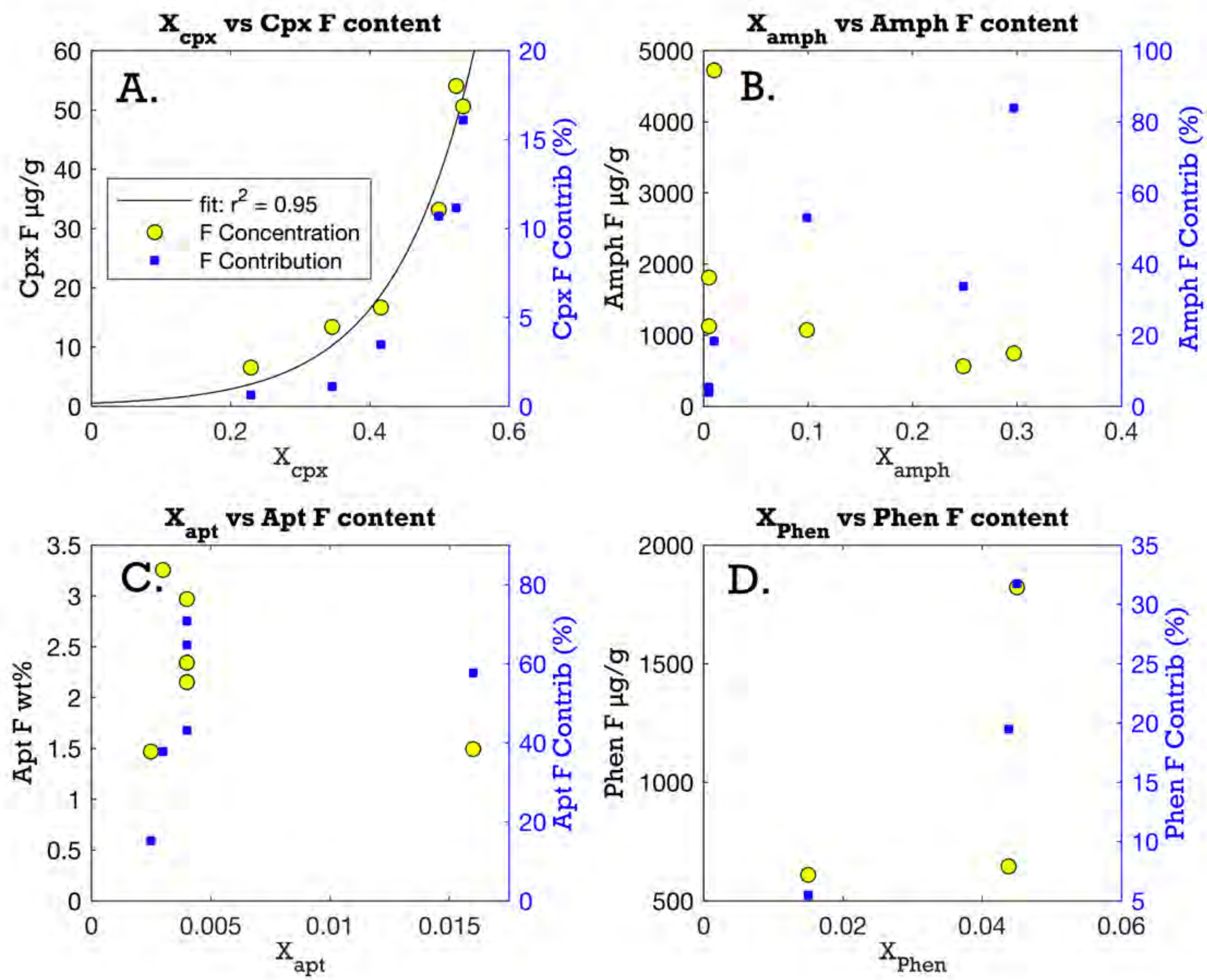

Figure S8.

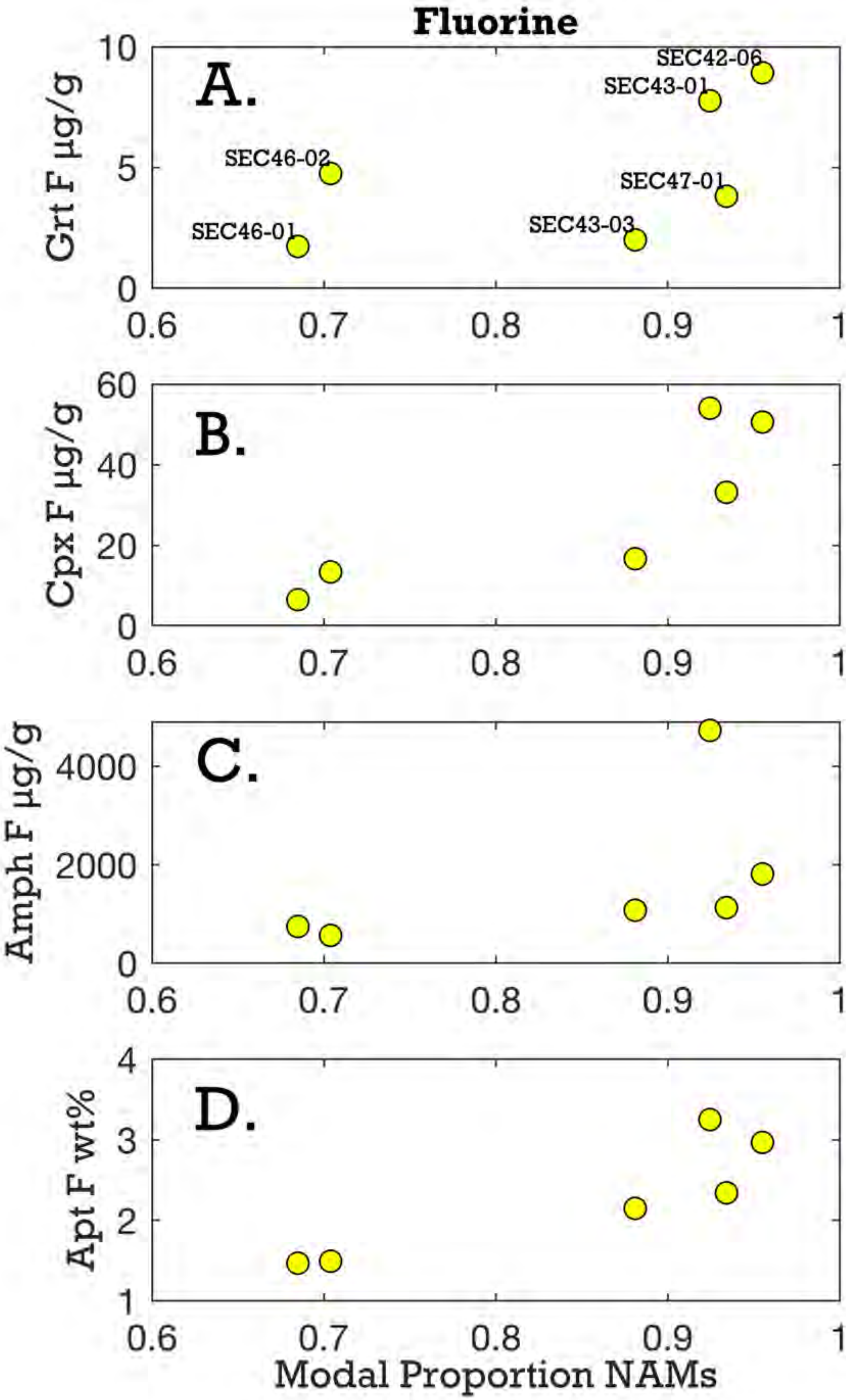
Fluorine
A.
Grt F µg/g
SEC42-06
SEC43-01
SEC46-02
SEC47-01
SEC43-03
SEC46-01
B.
Cpx F µg/g
C.
Amph F µg/g
D.
Apt F wt%
Modal Proportion NAMs

Figure S9.

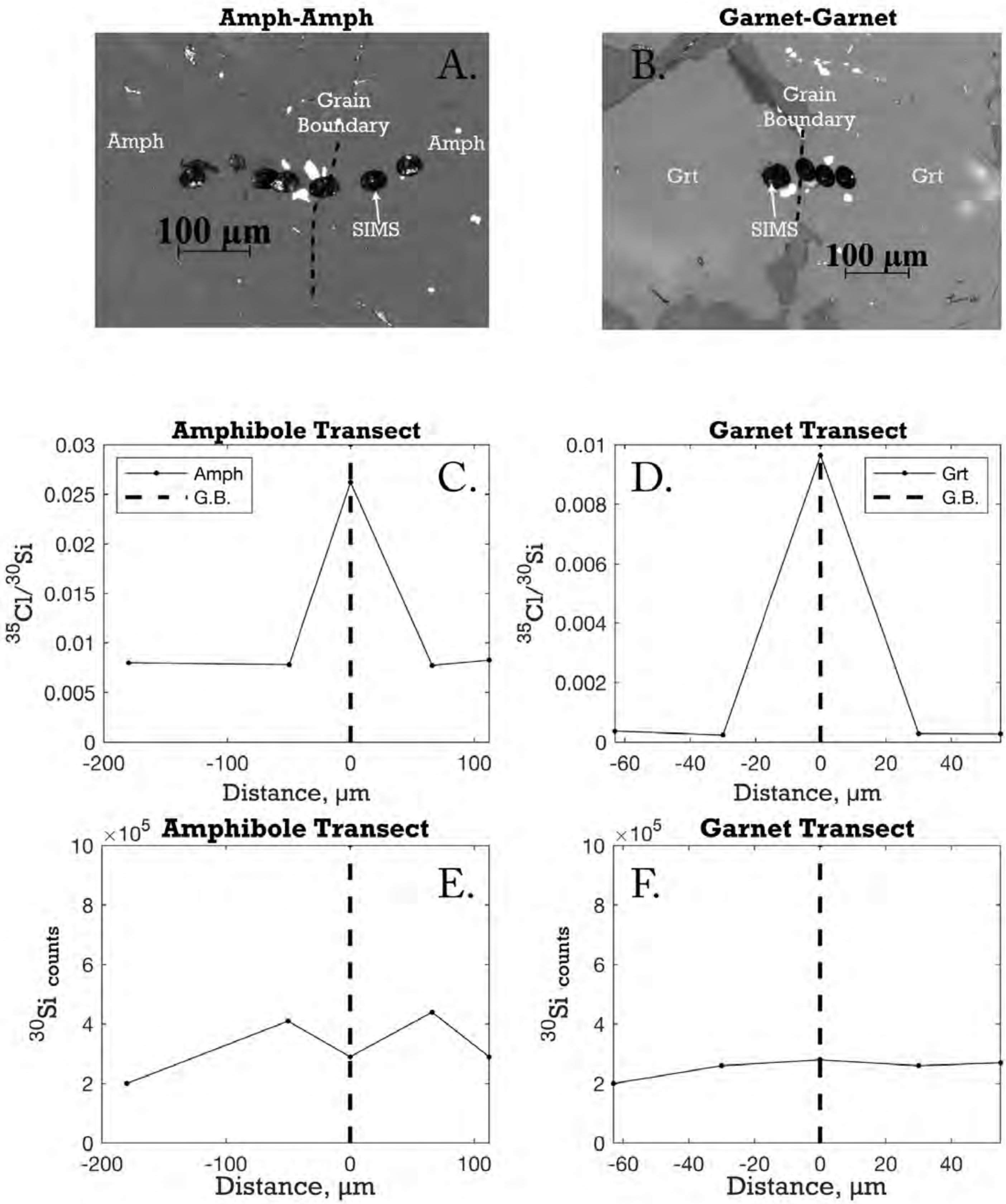
Amph-Amph
A.
Grain Boundary
Amph
Amph
100 μm
SIMS
Garnet-Garnet
B.
Grain Boundary
Grt
Grt
SIMS
100 μm
Amphibole Transect
C.
Amph
G.B.
$^{35}Cl/^{30}Si$
Distance, μm
Garnet Transect
D.
Grt
G.B.
$^{35}Cl/^{30}Si$
Distance, μm
Amphibole Transect
E.
^{30}Si counts
×10^5
Distance, μm
Garnet Transect
F.
^{30}Si counts
×10^5
Distance, μm

This is a preprint, the final version is subject to change, of the American Mineralogist (MSA)
Cite as Authors (Year) Title. American Mineralogist, in press.
DOI: https://doi.org/10.2138/am-2020-6994

Table 1. Halogen abundances by phase (SIMS)

Clinopyroxene

Sample	Description	No. grains analyzed	No. Analyses	F (μg/g)	F Error % (2SE Internal + Calibration Curve)	Cl (μg/g)	Cl background corrected (μg/g)	Cl Error % (2SE Internal + Calibration Curve)	OH (μg/g)	OH Error % (2SE Internal + Calibration Curve)	OH Error % (2SE Internal, Calibration, Background)	S (μg/g)	S Error % (2SE Internal + Calibration Curve)	Intra-sample Variability F, 1 sigma	OH, 1 sigma	Cl, 1 sigma
SEC 42-06	Eclogite	1	1	50.6	6.0%	0.18	0.03	15.7%	651	5.5%		<0.1	12.6%	-	-	-
SEC 43-01	Eclogite	1	6	54.1	5.8%	0.13	0.00	14.6%	433	4.8%		<0.1	15.5%	15%	13%	-
SEC 43-03	Eclogite	1	3	16.7	4.5%	0.08	0.00	11.2%	773	5.8%		<0.1	9.2%	3%	3%	-
SEC46-01	Eclogite	2	5	6.53	5.8%	0.11	0.03	10.5%	446	5.9%		<0.1	8.4%	4%	5%	-
SEC46-02	Eclogite	1	3	13.4	6.0%	1.17	1.05	9.7%	753	7.7%		<0.1	9.2%	5%	10%	25%
SEC47-01	Eclogite	3	7	33.2	4.4%	0.07	0.00	12.4%	445	6.0%		<0.1	13.4%	24%	14%	-

Garnet

Sample	Description	No. grains analyzed	No. Analyses	F (μg/g)	F Error % (2SE Internal + Calibration Curve)	Cl (μg/g)	Cl background corrected (μg/g)	Cl Error % (2SE Internal + Calibration Curve)	OH (μg/g)	OH Error % (2SE Internal + Calibration Curve)	OH Error μg/g (2SE Internal, Calibration, Background)	S (μg/g)	S Error % (2SE Internal + Calibration Curve)	F, 1 sigma	OH, 1 sigma	Cl, 1 sigma
SEC 42-06	Eclogite	2	5	8.92	6.0%	0.17	0.02	14.5%	113	5.1%	10.1	<0.1	11.4%	24%	16%	-
SEC 43-01	Eclogite	2	9	7.76	6.0%	0.18	0.03	14.0%	125	5.2%	10.8	<0.1	16.1%	29%	67%	-
SEC 43-03	Eclogite	2	6	2.01	6.1%	0.10	0.02	11.5%	201	5.7%	18.8	<0.1	9.2%	42%	10%	-
SEC46-01	Eclogite	2	7	1.73	5.1%	0.11	0.03	10.0%	85	5.9%	12.3	<0.1	11.5%	93%	27%	-
SEC46-02	Eclogite	2	6	4.76	6.1%	0.11	0.00	11.8%	60	7.6%	13.8	<0.1	10.5%	35%	22%	-
SEC47-01	Eclogite	3	3	3.81	5.3%	0.08	0.00	11.7%	80	6.2%	12.2	<0.1	10.4%	12%	7%	-

Phengite

Sample	Description	No. grains analyzed	No. Analyses	F (μg/g)	F Error % (2SE Internal + Calibration	Cl (μg/g)	Cl background corrected (μg/g)	Cl Error % (2SE Internal + Calibration	OH (μg/g)	OH Error % (2SE Internal + Calibration	OH Error % (2SE Internal, Calibration, Background)	S (μg/g)	S Error % (2SE Internal + Calibration	F, 1 sigma	OH, 1 sigma	Cl, 1 sigma
SEC 42-06	Eclogite	1	2	610	5.9%	2.13	1.98	12.7%	22452	4.6%		0.65	8.4%	6%	1%	4%
SEC 43-01	Eclogite	1	9	1822	5.9%	1.16	1.01	12.6%	28360	4.6%		0.54	7.6%	8%	4%	20%
SEC 43-03	Eclogite															
SEC46-01	Eclogite															
SEC46-02	Eclogite															
SEC47-01	Eclogite	2	6	645	4.4%	1.22	1.14	8.7%	26410	5.7%		0.48	5.7%	7%	9%	9%

Amphibole

Sample	Description	No. grains analyzed	No. Analyses	F (μg/g)	F Error % (2SE Internal + Calibration Curve)	Cl (μg/g)	Cl background corrected (μg/g)	Cl Error % (2SE Internal + Calibration Curve)	OH (μg/g)	OH Error % (2SE Internal + Calibration Curve)	OH Error % (2SE Internal, Calibration, Background)	S (μg/g)	S Error % (2SE Internal + Calibration Curve)	F, 1 sigma	OH, 1 sigma	Cl, 1 sigma
SEC 42-06	Eclogite	1	5	1812	4.7%	82.7	82.6	13.1%	18682	4.2%		27.9	11.0%	18%	5%	37%
SEC 43-01	Eclogite	1	3	4727	5.9%	11.6	11.5	12.2%	20187	4.6%		18.0	5.9%	3%	3%	24%
SEC 43-03	Eclogite	1	2	1073	4.6%	0.64	0.56	8.5%	17952	5.9%		27.0	4.4%			
SEC46-01	Eclogite	4	8	747	5.5%	10.3	10.3	8.7%	17292	5.9%		5.6	5.3%			
SEC46-02	Eclogite	2	6	563	6.2%	11.8	11.7	8.6%	23449	7.5%		5.9	6.1%			
SEC47-01	Eclogite	1	3	1127	5.0%	15.5	15.4	8.6%	15747	5.8%		3.0	5.2%			

Titanite

Sample	Description	No. grains analyzed	No. Analyses	F (μg/g)	F Error % (2SE Internal + Calibration Curve)	Cl (μg/g)	Cl background corrected (μg/g)	Cl Error % (2SE Internal + Calibration Curve)	OH (μg/g)	OH Error % (2SE Internal + Calibration Curve)	OH Error % (2SE Internal, Calibration, Background)	S (μg/g)	S Error % (2SE Internal + Calibration Curve)
SEC 46-02	Eclogite	1	3	1394	6.0%	0.11		9.7%	4010	7.4%		<0.1	9.3%

DOI: https://doi.org/10.2138/am-2020-6994

Table 2. Calculated mineral modes

	Phase Fraction									
Est. Modal Abundances	Garnet	Omphacite	Phengite	Amphibole	Quartz	Rutile	Titanite	Apatite	SUM	NAMs (Grt+Cpx+Qtz)
SEC 42-06	0.421(32)	0.534(32)	0.015(2)	0.0050(5)	0	0.021(2)	0	0.0040(4)	1	0.96
SEC 43-01	0.384(30)	0.524(31)	0.045(4)	0.010(1)	0.017(2)	0.018(2)	0	0.0030(3)	1	0.92
SEC 43-03	0.378(28)	0.416(28)	0	0.099(10)	0.087(2)	0.016(2)	0	0.0040(4)	1	0.88
SEC46-01	0.456(28)	0.229(21)	0	0.297(25)	0	0.016(2)	0	0.0025(3)	1	0.68
SEC46-02	0.358(27)	0.346(27)	0	0.248(22)	0	0.010(1)	0.02(1)	0.016(2)	1	0.70
SEC47-01	0.406(31)	0.499(31)	0.044(4)	0.0050(5)	0.024	0.018(2)	0	0.0040(4)	1	0.93
Average Mineral Modes	0.41	0.43	0.011	0.107	0.023	0.000	0.018	0.006	1.000	

Values in parenthesis represent 1 sigma uncertainty

This is a preprint, the final version is subject to change, of the American Mineralogist (MSA)
Cite as Authors (Year) Title. American Mineralogist, in press.
DOI: https://doi.org/10.2138/am-2020-6994

Table 3. Halogen bulk rock abundances, ratios

				Uncorrected for Yield		Corrected for Yield		Uncertainty (Yield Corrected)							
	Calculated Bulk (WHOI)			Pyrohydrolysis (UTA)		Pyrohydrolysis (UTA)		1SD Propogated		Calculated/Measured Bulk					Notes
Sample	OH µg/g	F µg/g	Cl µg/g	F µg/g	Cl µg/g	F µg/g	Cl µg/g	F (µg/g)	Cl (µg/g)	F %	Cl %	Cl/Nb**	Cl/K**	F/Nd**	
SEC42-06	901	168	2.5	92	8.9	115	11.0	15	2.2	146%	23%	3.03	0.0089	10.8	
SEC43-01	1783	258	1.4	109	7.1	137	8.9	68	3.1	189%	16%	4.34	0.0020	22.5	
SEC43-03	2342	200	0.8	152	5.4	189	6.7	11	2.2	105%	12%	2.80	0.0116	15.8	
SEC46-01	5123	241	3.2	154	9.1	193	11.3	52	3.1	125%	28%	5.18	0.0085	17.3	
SEC46-02	6836	415	8.2	160	16.1	199	19.9	12	2.4	208%	41%	4.68	0.0218	32.1	Evidence for fluid interaction, minor retrogression
SEC47-01	1663	145	1.3	112	7.1	139	8.8	9.1	1.5	104%	15%	4.23	0.0021	11.2	Table 1. Halogen abundances by phase (SIMS)
Average		237.7	2.9	129.8	8.9	162.0	11.1								
Standard Deviation		96.6	2.7	29.2	3.8	36.1	4.6								
Average*		202.3	1.85	123.7	7.5	154.5	9.4					3.9	0.0066	15.5	
Standard Deviation*		47.7	0.987	28.0	1.51	34.9	1.88					1.0	0.0043	4.8	
AOC (Barnes et al. 2018)		216	207												
Average Reycling Efficiency (to mantle)		93.7%	0.9%	57.3%	3.6%	71.5%	4.5%								

* Excludes SEC46-02 due to retrograde alteration

* Values used in bulk flux calculations

**Cl and F values from yield corrected pyrohydrolysis, K, Nb, Nd using bulk rock chemistry from John et al. 2010

DOI: https://doi.org/10.2138/am-2020-6994

DOI: https://doi.org/10.2138/am-2020-6994

Supplementary Table 1. Garnet major element compo

	Cumulative Distance (µm)	Dist to grain boundary (µm)	Weight % Oxide											Atoms per formula unit															
			Cr2O3	Al2O3	CaO	MnO	Na2O	TiO2	SiO2	K2O	FeO	MgO	Total	Cr	Al	Ca	Mn	Na	Ti	Si	K	Fe	Mg	Total	X Almandine	X Pyrope	X Grossular	X Spessartine	Fe/(Fe+Mg)
Line 1 SEC42-06_grt_profile	0	-1346	0.04	21.96	8.76	0.62	0.00	0.07	38.00	0.00	25.30	4.23	98.98	0.0024	2.039	0.739	0.0413	0	0.0044	2.993	0.0001	1.667	0.497	7.9833	0.57	0.17	0.25	0.01	0.77
Line 2 SEC42-06_grt_profile	144	-1202	0.02	22.07	7.48	0.52	0.02	0.03	37.75	0.00	26.38	4.58	98.86	0.0014	2.054	0.633	0.035	0.003	0.0018	2.981	0	1.742	0.539	7.9903	0.59	0.18	0.21	0.01	0.76
Line 3 SEC42-06_grt_profile	316	-1030	0.07	21.92	7.68	0.36	0.00	0.09	37.54	0.00	26.60	4.39	98.65	0.0043	2.048	0.652	0.0243	0	0.0054	2.976	0	1.763	0.518	7.9911	0.60	0.18	0.22	0.01	0.77
Line 4 SEC42-06_grt_profile	440	-907	0.05	21.81	8.22	0.44	0.03	0.12	37.29	0.00	26.56	4.20	98.72	0.0032	2.042	0.7	0.0298	0.0049	0.0069	2.962	0	1.765	0.497	8.0108	0.59	0.17	0.23	0.01	0.78
Line 5 SEC42-06_grt_profile	580	-766	0.04	21.48	8.54	0.35	0.00	0.15	36.81	0.00	26.95	3.56	97.87	0.0027	2.037	0.736	0.0237	0	0.0088	2.961	0	1.813	0.426	8.0082	0.60	0.14	0.25	0.01	0.81
Line 6 SEC42-06_grt_profile	724	-622	0.07	21.50	8.56	0.77	0.00	0.10	36.54	0.00	26.74	3.32	97.61	0.0047	2.048	0.741	0.0528	0	0.0064	2.953	0	1.807	0.4	8.0129	0.60	0.13	0.25	0.02	0.82
Line 7 SEC42-06_grt_profile	904	-442	0.05	21.58	8.90	0.80	0.00	0.07	36.82	0.00	25.48	4.04	97.73	0.0031	2.042	0.765	0.0541	0	0.0041	2.956	0	1.71	0.484	8.0183	0.57	0.16	0.25	0.02	0.78
Line 8 SEC42-06_grt_profile	1001	-345	0.10	21.53	8.89	0.54	0.06	0.07	36.85	0.00	25.25	4.39	97.67	0.006	2.034	0.764	0.0364	0.009	0.004	2.955	0	1.693	0.525	8.0264	0.56	0.17	0.25	0.01	0.76
Line 9 SEC42-06_grt_profile	1195	-151	0.13	21.15	9.04	0.72	0.00	0.10	36.09	0.00	26.14	3.54	96.91	0.0082	2.031	0.789	0.0495	0	0.0063	2.94	0.0003	1.781	0.43	8.0353	0.58	0.14	0.26	0.02	0.81
Line 10 SEC42-06_grt_profile	1346	0	0.03	22.07	8.02	0.49	0.00	0.03	38.43	0.00	26.23	4.78	100.08	0.002	2.026	0.669	0.0325	0.0004	0.0015	2.994	0.0001	1.709	0.555	7.9896	0.58	0.19	0.23	0.01	0.75
SEC42-06 Average			0.06	21.71	8.41	0.56	0.01	0.08	37.21	0.00	26.16	4.10	98.31	0.00	2.04	0.72	0.04	0.00	0.00	2.97	0.00	1.75	0.49	8.01	0.58	0.16	0.24	0.01	0.78
Line 1 43-01_grt_grt->phen	0	-555	0.03	21.84	8.81	0.91	0.04	0.11	38.30	0.00	26.11	3.90	100.06	0.0018	2.015	0.738	0.0603	0.0067	0.0067	2.998	0	1.709	0.455	7.9906	0.58	0.15	0.25	0.02	0.79
Line 2 43-01_grt_grt->phen	62	-493	0.14	21.96	8.74	0.81	0.04	0.10	38.05	0.01	25.88	4.27	100.00	0.0086	2.026	0.733	0.0538	0.0057	0.0059	2.978	0.0013	1.693	0.498	8.0033	0.57	0.17	0.25	0.02	0.77
Line 3 43-01_grt_grt->phen	124	-431	0.09	22.02	8.42	0.71	0.02	0.02	38.19	0.00	25.92	4.30	99.68	0.0054	2.034	0.707	0.0469	0.003	0.0011	2.992	0	1.698	0.502	7.9894	0.57	0.17	0.24	0.02	0.77
Line 4 43-01_grt_grt->phen	185	-370	0.06	21.92	7.77	0.60	0.00	0.08	38.23	0.00	26.48	4.56	99.70	0.0038	2.024	0.652	0.0399	0	0.0044	2.995	0	1.735	0.533	7.9872	0.59	0.18	0.22	0.01	0.76
Line 5 43-01_grt_grt->phen	247	-308	0.08	22.02	7.54	0.61	0.05	0.07	38.29	0.01	26.76	4.83	100.26	0.0048	2.024	0.63	0.0403	0.0077	0.0043	2.985	0.0008	1.745	0.561	8.0029	0.59	0.19	0.21	0.01	0.76
Line 6 43-01_grt_grt->phen	308	-247	0.04	22.00	6.93	0.59	0.12	0.05	38.53	0.01	26.71	5.03	100.01	0.0026	2.021	0.578	0.0387	0.018	0.0027	3.003	0.0014	1.741	0.585	7.9915	0.59	0.20	0.20	0.01	0.75
Line 7 43-01_grt_grt->phen	370	-185	0.07	22.21	7.18	0.49	0.00	0.01	38.50	0.00	26.45	5.11	100.02	0.0041	2.037	0.599	0.0323	0.0007	0.0004	2.996	0.0004	1.721	0.593	7.984	0.58	0.20	0.20	0.01	0.74
Line 8 43-01_grt_grt->phen	431	-124	0.02	22.49	7.74	0.44	0.01	0.01	38.70	0.00	25.45	5.26	100.13	0.0014	2.053	0.642	0.0289	0.0022	0.0005	2.996	0.0004	1.648	0.607	7.9795	0.56	0.21	0.22	0.01	0.73
Line 9 43-01_grt_grt->phen	493	-62	0.02	22.50	7.95	0.49	0.00	0.01	38.81	0.00	25.51	5.17	100.47	0.0015	2.047	0.658	0.0324	0.0004	0.0004	2.996	0.0001	1.647	0.595	7.9778	0.56	0.20	0.22	0.01	0.73
Line 10 43-01_grt_grt->phen	555	0	0.02	22.79	8.53	0.52	0.06	0.02	39.07	0.04	24.75	4.97	100.77	0.0009	2.063	0.702	0.034	0.0096	0.0011	3	0.0038	1.589	0.569	7.9725	0.55	0.20	0.24	0.01	0.74
Line 1 43-01_grt_grt->cpx1	0	-451	0.04	22.07	8.79	0.79	0.05	0.11	38.28	0.00	25.64	3.97	99.74	0.0023	2.037	0.737	0.0523	0.007	0.0068	2.997	0	1.679	0.463	7.9814	0.57	0.16	0.25	0.02	0.78
Line 2 43-01_grt_grt->cpx1	49	-402	0.06	22.13	8.60	0.68	0.00	0.10	38.41	0.00	25.69	4.40	100.06	0.0035	2.033	0.718	0.0447	0	0.0056	2.993	0	1.674	0.511	7.9829	0.57	0.17	0.24	0.02	0.77
Line 3 43-01_grt_grt->cpx1	97	-353	0.06	22.15	8.16	0.62	0.00	0.09	38.53	0.00	25.93	4.47	100.01	0.0036	2.034	0.681	0.0411	0	0.0051	3.001	0	1.689	0.519	7.9738	0.58	0.18	0.23	0.01	0.76
Line 4 43-01_grt_grt->cpx1	150	-301	0.09	22.25	8.58	0.59	0.00	0.03	38.22	0.00	25.56	4.48	99.80	0.0055	2.048	0.718	0.039	0	0.0019	2.984	0	1.669	0.522	7.9875	0.57	0.18	0.24	0.01	0.76
Line 5 43-01_grt_grt->cpx1	200	-251	0.02	22.10	7.25	0.55	0.00	0.05	38.33	0.00	27.12	4.69	100.12	0.0014	2.033	0.606	0.0366	0	0.0031	2.991	0	1.77	0.545	7.9861	0.60	0.18	0.20	0.01	0.76
Line 6 43-01_grt_grt->cpx1	250	-201	0.02	22.01	7.06	0.45	0.00	0.06	37.57	0.01	27.23	4.64	99.04	0.0012	2.051	0.598	0.0302	0	0.0033	2.97	0.0008	1.8	0.546	8.0005	0.61	0.18	0.20	0.01	0.77
Line 7 43-01_grt_grt->cpx1	299	-152	0.07	22.29	6.80	0.35	0.04	0.05	38.46	0.01	27.26	5.01	100.34	0.0043	2.042	0.567	0.0228	0.0055	0.0031	2.989	0.001	1.772	0.58	7.9868	0.60	0.20	0.19	0.01	0.75
Line 8 43-01_grt_grt->cpx1	329	-122	0.05	22.34	6.84	0.37	0.00	0.05	38.53	0.00	26.86	5.15	100.19	0.0033	2.046	0.569	0.0243	0	0.0027	2.993	0	1.745	0.596	7.9794	0.59	0.20	0.19	0.01	0.75
Line 9 43-01_grt_grt->cpx1	401	-50	0.04	22.44	7.43	0.47	0.00	0.05	38.84	0.00	24.89	5.69	99.85	0.0024	2.046	0.616	0.0305	0	0.0028	3.005	0.0003	1.61	0.656	7.969	0.55	0.23	0.21	0.01	0.71
Line 10 43-01_grt_grt->cpx1	451	0	0.04	22.27	8.06	0.53	0.00	0.02	38.48	0.00	25.30	4.86	99.57	0.0026	2.047	0.673	0.035	0	0.0014	3	0.0004	1.65	0.565	7.9745	0.56	0.19	0.23	0.01	0.74
Sec43-01 Average			0.05	22.19	7.86	0.58	0.02	0.05	38.42	0.01	26.08	4.74	99.99	0.00	2.04	0.66	0.04	0.00	0.00	2.99	0.00	1.70	0.55	7.99	0.58	0.19	0.22	0.01	0.76
Line 1 SEC43-03_Grt1	0	-502	0.00	22.21	9.32	1.13	0.01	0.07	38.46	0.01	24.72	4.96	100.90	0	2.022	0.772	0.0742	0.0014	0.0042	2.971	0.001	1.597	0.572	8.0148	0.53	0.19	0.26	0.02	0.74
Line 2 SEC43-03_GRT1	36	-465	0.00	22.14	9.95	1.17	0.05	0.12	38.44	0.00	24.18	4.82	100.87	0	2.016	0.824	0.0766	0.0072	0.0071	2.97	0	1.563	0.555	8.019	0.52	0.18	0.27	0.03	0.74
Line 3 SEC43-03 GRT1	72	-430	0.00	21.99	9.97	1.28	0.01	0.15	38.23	0.00	24.09	4.75	100.46	0	2.012	0.829	0.0841	0.0014	0.0085	2.968	0	1.564	0.55	8.017	0.52	0.18	0.27	0.03	0.74
Line 4 SEC43-03 GRT1	107	-395	0.00	21.76	10.41	1.30	0.04	0.64	38.00	0.00	23.27	4.55	99.97	0	1.999	0.869	0.086	0.0061	0.0377	2.961	0	1.517	0.529	8.0048	0.51	0.18	0.29	0.03	0.74
Line 5 SEC43-03 GRT1	143	-358	0.00	21.86	10.28	1.33	0.05	0.16	38.27	0.00	23.72	4.65	100.32	0.0002	2.002	0.856	0.088	0.0076	0.0092	2.975	0	1.542	0.539	8.019	0.51	0.18	0.28	0.03	0.74
Line 6 SEC43-03 GRT1	179	-323	0.00	21.87	10.71	1.67	0.08	0.19	38.18	0.00	23.33	4.27	100.30	0	2.007	0.893	0.11	0.0119	0.011	2.972	0	1.519	0.495	8.0189	0.50	0.16	0.30	0.04	0.75
Line 7 SEC43-03 GRT1	215	-287	0.00	21.48	10.98	2.43	0.05	0.12	37.65	0.00	24.00	3.32	100.03	0	1.995	0.927	0.162	0.0074	0.0073	2.965	0	1.581	0.389	8.0337	0.52	0.13	0.30	0.05	0.80
Line 8 SEC43-03 GRT1	251	-251	0.00	21.04	10.15	2.12	0.00	0.16	37.00	0.01	23.78	4.06	98.31	0	1.983	0.87	0.144	0	0.0093	2.959	0.0007	1.59	0.484	8.0401	0.51	0.16	0.28	0.05	0.77
Line 9 SEC43-03 GRT1	288	-214	0.02	22.36	11.27	2.24	0.03	0.11	38.89	0.00	24.06	2.63	101.60	0.0011	2.033	0.931	0.146	0.0043	0.0062	3.001	0	1.553	0.302	7.9777	0.53	0.10	0.32	0.05	0.84
Line 10 SEC43-03 GRT1	326	-176	0.00	21.64	11.42	1.62	0.02	0.10	37.50	0.00	23.91	3.62	99.84	0	2.008	0.963	0.108	0.0037	0.006	2.952	0.0002	1.574	0.425	8.0399	0.51	0.14	0.31	0.04	0.79
Line 11 SEC43-03 GRT1	362	-140	0.06	21.54	9.80	0.75	0.06	0.06	37.66	0.00	24.43	4.92	99.28	0.0037	1.997	0.826	0.0502	0.0084	0.0036	2.963	0	1.607	0.578	8.0369	0.52	0.19	0.27	0.02	0.74
Line 12 SEC43-03 GRT1	397	-105	0.00	21.41	10.31	0.72	0.02	0.05	37.40	0.00	24.36	4.80	99.07	0	1.994	0.873	0.048	0.0026	0.0032	2.953	0	1.609	0.565	8.0478	0.52	0.18	0.28	0.02	0.74
Line 13 SEC43-03 GRT1	434	-68	0.00	23.15	10.49	0.58	0.03	0.06	39.77	0.00	24.04	4.38	102.51	0	2.06	0.849	0.0373	0.0045	0.0035	3.003	0.0002	1.518	0.492	7.9676	0.52	0.17	0.29	0.01	0.76
Line 14 SEC43-03 GRT1	450	-52	0.00	21.88	10.47	0.64	0.07	0.01	37.66	0.00	23.43	5.09	99.26	0	2.022	0.88	0.0427	0.0105	0.0008	2.953	0	1.537	0.595	8.041	0.50	0.19	0.29	0.01	0.72
Line 15 SEC43-03 GRT1	502	0	0.00	21.60	7.47	0.79	0.03	0.03	37.02	0.00	26.40	5.37	98.71	0	2.022	0.635	0.0529	0.0045	0.002	2.941	0	1.754	0.636	8.0474	0.57	0.21	0.21	0.02	0.73
Line 1 SEC43-03_Grt2	0	-1245	0.04	22.12	10.35	2.17	0.06	0.17	38.53	0.00	23.64	4.15	101.23	0.0022	2.013	0.856	0.142	0.009	0.0098	2.975	0	1.527	0.478	8.012	0.51	0.16	0.29	0.05	0.76
Line 2 SEC43-03_Grt2	64	-1181	0.00	22.16	10.21	1.55	0.00	0.20	38.54	0.00	23.98	4.51	101.15	0.0002	2.014	0.843	0.101	0	0.0116	2.972	0	1.547	0.518	8.0068	0.51	0.17	0.28	0.03	0.75
Line 3 SEC43-03_Grt2	126	-1119	0.00	22.44	9.46	1.11	0.00	0.05	38.35	0.00	24.66	4.81	100.88	0	2.044	0.783	0.0724	0	0.0031	2.963	0.0001	1.593	0.554	8.0126	0.53	0.18	0.26	0.02	0.74
Line 4 SEC43-03_Grt2	190	-1055	0.00	22.08	10.12	0.86	0.01	0.09	38.23	0.01	24.46	4.73	100.59	0	2.019	0.841	0.0564	0.0018	0.0052	2.965	0.0012	1.587	0.547	8.0237	0.52	0.18	0.28	0.02	0.74
Line 5 SEC43-03_Grt2	254	-991	0.00	22.03	10.06	0.77	0.00	0.14	38.33	0.00	24.57	4.83	100.73	0	2.01	0.834	0.0506	0	0.008	2.968	0.0003	1.591	0.558	8.0199	0.52	0.18	0.27	0.02	0.74
Line 6 SEC43-03_Grt2	330	-915	0.00	21.89	10.22	0.73	0.02	0.14	38.46	0.00	24.13	4.82	100.40	0	2	0.849	0.0477	0.0036	0.0079	2.982	0	1.565	0.557	8.0122	0.52	0.18	0.28	0.02	0.74
Line 7 SEC43-03_Grt2	383	-862	0.00	21.94	9.55	0.71	0.05	0.12	38.54	0.00	24.84	5.05	100.80	0	1.999	0.791	0.0467	0.0068	0.007	2.98	0	1.606	0.582	8.0185	0.53	0.19	0.26	0.02	0.73
Line 8 SEC43-03_Grt2	447	-798	0.00	22.17	10.23	0.68	0.02	0.16	38.61	0.00	24.37	4.74	100.99	0	2.015	0.845	0.0445	0.0036	0.0094	2.976	0.0004	1.571	0.545	8.0099	0.52	0.18	0.28	0.01	0.74
Line 9 SEC43-03_Grt2	523	-722	0.00	22.26	9.92	0.68	0.00	0.13	38.64	0.00	24.43	4.87	100.94	0	2.021	0.819	0.0446	0.0004	0.0076	2.977	0	1.575	0.56	8.0047	0.53	0.19	0.27	0.01	0.74
Line 10 SEC43-03_Grt2	596	-649	0.00	22.05	10.29	0.69	0.01	0.19	38.51	0.00	24.23	4.70	100.68	0	2.01	0.852	0.0454	0.0021	0.0111	2.978	0	1.567	0.542	8.0076	0.52	0.18	0.28	0.02	0.74
Line 11 SEC43-03_Grt2	659	-586	0.00	22.20	9.88	0.66	0.02	0.12	38.54	0.00	24.70	4.87	100.98	0	2.018	0.817	0.0429	0.0025	0.007	2.973	0	1.593	0.56	8.0134	0.53	0.19	0.27	0.01	0.74
Line 12 SEC43-03_Grt2	741	-504	0.01	22.31	9.25	0.73	0.00	0.07	38.42	0.00	25.49	4.89	101.16	0.0005	2.029	0.765	0.0474	0	0.0041	2.964	0	1.645	0.563	8.018	0.54	0.19	0.25	0.02	0.75
Line 13 SEC43-03_Grt2	794	-451	0.00	22.40	10.21	0.68	0.00	0.03	38.65	0.00	24.43	4.64	101.04	0	2.033	0.843	0.0441	0	0.002	2.977	0	1.574	0.533	8.0061	0.53	0.18	0.28	0.01	0.75
Line 14 SEC43-03_Grt2	864	-381	0.02	22.20	10.17	0.65	0.00	0.06	38.36	0.01	24.88	4.78	101.13	0.001	2.02	0.841	0.0424	0	0.0036	2.961	0.0011	1.606	0.55	8.0261	0.53	0.18	0.28	0.01	0.74
Line 15 SEC43-03_Grt2	924	-321	0.01	22.35	10.14	0.59	0.00	0.02	38.43	0.00	24.30	4.87	100.71	0.0006	2.035	0.839	0.0387	0	0.0013	2.968	0	1.57	0.561	8.0136	0.52	0.19	0.28	0.01	0.74
Line 16 SEC43-03_Grt2	988	-257	0.07	22.17	9.90	0.65	0.00	0.00	38.42	0.01	24.61	4.84	100.67	0.0045	2.022	0.821	0.0428	0	0.0001	2.973	0.0005	1.593	0.558	8.0149	0.53	0.19	0.27	0.01	0.74
Line 17 SEC43-03_Grt2	1052	-193	0.01	22.53	10.11	0.44	0.00	0.02	38.41	0.00	24.54	4.72	100.77	0.0004	2.05	0.837	0.0287	0	0.001	2.965	0	1.584	0.543	8.0091	0.53	0.18	0.28	0.01	0.74
Line 18 SEC43-03_Grt2	1116	-130	0.00	22.52	7.04	0.58	0.00	0.02	38.23	0.00	26.45	5.97	100.81	0	2.05	0.583	0.0378	0	0.0013	2.952	0	1.709	0.688	8.0211	0.57	0.23	0.19	0.01	0.71
Line 19 SEC43-03_Grt2	1176	-70	0.03	22.64	7.06	0.62	0.00	0.00	38.45	0.00	26.27	5.85	100.91	0.0016	2.057	0.583	0.0404	0	0	2.963	0	1.693	0.672	8.01	0.57	0.22	0.20	0.01	0.72
Line 20 SEC43-03_Grt2	1245	0	0.02	22.32	8.09	0.60	0.00	0.00	38.32	0.00	25.84	5.63	100.82	0.0013	2.033	0.67	0.0392	0	0	2.961	0	1.67	0.649	8.0236	0.55	0.21	0.22	0.01	0.72
SEC43-03 Average			0.01	22.08	9.86	1.03	0.02	0.11	38.26	0.00	24.47	4.70	100.54	0.00	2.02	0.82	0.07	0.00	0.01	2.97	0.00	1.59	0.54	8.02	0.53	0.18	0.27	0.02	0.75
Line 1 SEC46-01_grt1	0	-557	0.02	22.26	7.96	1.83	0.02	0.17	38.59	0.00	24.07	5.67	100.59	0.0014	2.025	0.658	0.12	0.0032	0.0097	2.978	0	1.554	0.652	8.0013	0.52	0.22	0.22	0.04	0.70
Line 2 SEC46-01_grt1	20	-537	0.00	22.19	7.76	2.73	0.00	0.21	38.59	0.00	23.95	5.52	100.95	0	2.017	0.641	0.178	0	0.0121	2.976	0	1.545	0.634	8.0031	0.52	0.21	0.21	0.06	0.71
Line 3 SEC46-01_grt1	66	-491	0.00	22.57	7.84	1.61	0.04	0.21	38.75	0.00	24.37	5.83	101.22	0	2.039	0.643	0.105	0.0057	0.012	2.97	0	1.562	0.666	8.0028	0.52	0.22	0.22	0.04	0.70
Line 4 SEC46-01_grt1	87	-470	0.00	22.30	7.59	1.46	0.03	0.19	38.67	0.00	24.59	5.95	100.78	0	2.023	0.626	0.095	0.0039	0.0112	2.977	0	1.583	0.683	8.0021	0.53	0.23	0.21	0.03	0.70
Line 5 SEC46-01_grt1	116	-441	0.01	22.19	7.76	1.43	0.05	0.15	38.64	0.00	24.50	5.95	100.69	0.0007	2.016	0.641	0.093	0.0082	0.0089	2.978	0	1.579	0.684	8.0089	0.53	0.23	0.21	0.03	0.70
Line 6 SEC46-01_grt1	145	-412	0.00	22.33	8.18	1.29	0.00	0.16	38.70	0.00	24.25	5.74	100.66	0	2.027	0.675	0.084	0.0007	0.0095	2.98	0	1.562	0.659	7.9973	0.52	0.22	0.23	0.03	0.70
Line 7 SEC46-01_grt1	174	-384	0.00	22.28	8.09	1.19	0.00	0.15	38.31	0.00	24.25	5.90	100.17	0	2.033	0.672	0.0783	0	0.0085	2.966	0	1.57	0.681	8.0089	0.52	0.23	0.22	0.03	0.70
Line 8 SEC46-01_grt1	203	-355	0.00	22.37	8.09	1.09	0.02	0.12	38.42	0.00	24.49	5.95	100.55	0	2.034	0.669	0.0709	0.0029	0.0072	2.964	0	1.58	0.684	8.012	0.53	0.23	0.22	0.02	0.70
Line 9 SEC46-01_grt1	236	-321	0.01	22.45	7.95	1.01	0.04	0.08	38.72	0.00	24.57	5.97	100.81	0.0007	2.034	0.654	0.0657	0.0064	0.0049	2.976	0	1.58	0.684	8.0057	0.53	0.23	0.22	0.02	0.70
Line 10 SEC46-01_grt1	260	-297	0.00	22.50	7.63	1.03	0.08	0.08	38.54	0.00	24.85	6.12	100.82	0	2.04	0.629	0.0669	0.0114	0.0045	2.965	0	1.599	0.702	8.0178	0.53	0.23	0.21	0.02	0.69
Line 11 SEC46-01_grt1	284	-273	0.01	22.52	8.22	0.98	0.04	0.05	38.51	0.00	24.45	5.91	100.69	0.0007	2.044	0.678	0.064	0.006	0.003	2.965	0	1.574	0.678	8.0127	0.53	0.23	0.23	0.02	0.70
Line 12 SEC46-01_grt1	335	-222	0.03	22.72	7.75	0.91	0.00	0.04	38.75	0.00	24.73	6.08	101.01	0.0017	2.052	0.637	0.0588	0.0004	0.0026	2.969	0	1.585	0.695	8.0015	0.53	0.23	0.21	0.02	0.70
Line 13 SEC46-01_grt1	349	-208	0.00	22.47	7.13	0.97	0.02	0.03	38.53	0.00	25.15	6.38	100.68	0	2.039	0.588	0.0632	0.0036	0.0018	2.967	0	1.619	0.732	8.0136	0.54	0.24	0.20	0.02	0.69
Line 14 SEC46-01_grt1	373	-185	0.03	22.69	7.72	0.91	0.03	0.04	38.21	0.00	24.76	6.18	100.58	0.0021	2.062	0.638	0.0593	0.005	0.0026	2.946	0	1.597	0.711	8.0231	0.53	0.24	0.21	0.02	0.69
Line 15 SEC46-01_grt1	405	-152	0.03	22.67	8.04	0.74	0.01	0.02	38.42	0.00	24.70	6.00	100.63	0.0016	2.058	0.663	0.0483	0.0018	0.0014	2.958	0	1.591	0.688	8.0111	0.53	0.23	0.22	0.02	0.70
Line 16 SEC46-01_grt1	439	-118	0.00	22.51	9.40	0.68	0.01	0.04	38.42	0.00	23.67	5.57	100.29	0	2.048	0.778	0.0442	0.0011	0.0024	2.966	0.0001	1.528	0.641	8.0089	0.51	0.21	0.26	0.01	0.70
Line 17 SEC46-01_grt1	468	-89	0.00	22.54	8.72	0.64	0.00	0.05	38.64	0.00	24.32	5.87	100.78	0	2.041	0.718	0.0416	0	0.0027	2.969	0	1.563	0.672	8.0073	0.52	0.22	0.24	0.01	0.70
Line 18 SEC46-01_grt1	473	-85	0.00	22.64	8.53	0.59	0.00	0.05	38.37	0.00	24.45	5.90	100.54	0.0002	2.056	0.704	0.0387	0	0.003	2.957	0	1.576	0.677	8.0119	0.53	0.23	0.24	0.01	0.70
Line 19 SEC46-01_grt1	514	-43	0.00	22.68	7.61	0.58	0.00	0.04	38.38	0.00	25.00	6.15	100.44	0	2.061	0.629	0.0378	0	0.0024	2.959	0	1.612	0.707	8.0083	0.54	0.24	0.21	0.01	0.70
Line 20 SEC46-01_grt1	557	0	0.00	22.66	8.96	0.49	0.04	0.00	38.36	0.00	23.69	5.70	99.90	0	2.066	0.743	0.0323	0.0057	0.0001	2.967	0.0002	1.532	0.657	8.0033	0.52	0.22	0.25	0.01	0.70
Line 1 SEC46-1_grt3	0	**-227.6**	0.0305	22.35	6.92	1.69	0.0048	0.0552	37.97	0	25.41	5.87	100.3005	0.0019	2.047	0.576	0.111	0.0007	0.0032	2.95	0	1.651	0.68	8.0209	0.55	0.23	0.19	0.04	0.71
Line 2 SEC46-01_grt3	25.7	**-201.9**	0.1208	22.48	6.84	1.32	0.0024	0.0412	38.1	0	25.66	6.17	100.7343	0.0074	2.048	0.567	0.086	0.0004	0.0024	2.945	0	1.658	0.711	8.0252	0.55	0.24	0.19	0.03	0.70
Line 3 SEC46-01_grt3	51.2	**-176.4**	0.0217	22.52	6.94	0.9555	0	0.0322	38.04	0	25.85	6.19	100.5493	0.0013	2.054	0.575	0.0626	0	0.0019	2.944	0	1.673	0.714	8.0258	0.55	0.24	0.19	0.02	0.70
Line 4 SEC46-01_grt3	76.9	**-150.7**	0.0428	22.45	7.02	0.9969	0.0407	0.0136	38.1	0	25.49	6.28	100.4339	0.0026	2.048	0.583	0.0654	0.0061	0.0008	2.949	0	1.65	0.724	8.0289	0.55	0.24	0.19	0.02	0.70
Line 5 SEC46-01_grt3	102.6	**-125.0**	0.0214	22.45	9.63	0.6204	0.0378	0.0228	38.13	0	23.69	5.48	100.0824	0.0013	2.05	0.8	0.0407	0.0057	0.0013	2.954	0	1.535	0.633	8.021	0.51	0.21	0.27	0.01	0.71
Line 6 SEC46-01_grt3	128.1	**-99.5**	0.0876	22.5	10.08	0.5765	0.0024	0.0444	38.75	0	23.67	5.44	101.1508	0.0053	2.032	0.827	0.0374	0.0004	0.0026	2.969	0	1.516	0.621	8.0107	0.51	0.21	0.28	0.01	0.71
Line 7 SEC46-01_grt3	153.8	**-73.8**	0.0264	22.75	8.93	0.5603	0.0426	0.0199	39	0	24.57	5.81	101.7091	0.0016	2.042	0.729	0.0361	0.0063	0.0011	2.97	0	1.565	0.66	8.0112	0.52	0.22	0.24	0.01	0.70
Line 8 SEC46-01_grt3	179.5	**-48.1**	0.057	22.68	8.23	0.5325	0	0.0085	38.93	0	25.03	5.97	101.4379	0.0034	2.042	0.673	0.0344	0	0.0005	2.973	0	1.598	0.68	8.0043	0.54	0.23	0.23	0.01	0.70
Line 9 SEC46-01_grt3	205.0	**-22.6**	0.038	22.69	7.82	0.5725	0.0499	0.0073	38.66	0	25.19	6.22	101.2477	0.0023	2.048	0.641	0.0371	0.0074	0.0004	2.96	0	1.613	0.71	8.0192	0.54	0.24	0.21	0.01	0.69
Line 10 SEC46-01_grt3	227.6	**0.0**	0.0466	22.57	9.88	0.5333	0.0165	0	38.51	0	23.7	5.53	100.7863	0.0028	2.045	0.814	0.0347	0.0025	0	2.961	0	1.524	0.633	8.017	0.51	0.21	0.27	0.01	0.71
Line 1 SEC46-01_grt2	0	**-279.6**	0.0224	22.45	7.21	0.5875	0.0309	0.0142	38.56	0.0015	25.16	6.55	100.5864	0.0014	2.037	0.594	0.0383	0.0046	0.0008	2.968	0.0001	1.619	0.752	8.0153	0.54	0.25	0.20	0.01	0.68
Line 2 SEC46-01_grt2	20.4	**-259.2**	0.0191	22.38	7.02	0.5871	0.0571	0.0333	38.62	0	25.18	6.51	100.4065	0.0012	2.033	0.58	0.0383	0.0085	0.0019	2.976	0	1.623	0.747	8.0089	0.54	0.25	0.19	0.01	0.68
Line 3 SEC46-01_grt2	39.8	**-239.8**	0.0479	22.39	7.25	0.7083	0.0476	0.0503	38.46	0	25.07	6.44	100.4641	0.0029	2.035	0.599	0.0463	0.0071	0.0029	2.966	0	1.617	0.74	8.0162	0.54	0.25	0.20	0.02	0.69
Line 4 SEC46-01_grt2	60.2	**-219.4**	0.0163	22.61	7.1	0.7309	0.0572	0.0294	38.44	0	25.21	6.52	100.7137	0.001	2.05	0.585	0.0476	0.0085	0.0017	2.957	0	1.621	0.748	8.0198	0.54	0.25	0.19	0.02	0.68
Line 5 SEC46-01_grt2	80.6	**-199.0**	0.0185	22.43	7.14	0.6994	0.0262	0.0435	38.38	0	25.18	6.54	100.4576	0.0011	2.039	0.59	0.0457	0.0039	0.0025	2.96	0	1.624	0.752	8.0183	0.54	0.25	0.20	0.02	0.68
Line 6 SEC46-01_grt2	101.0	**-178.6**	0.0246	22.45	7.57	0.5824	0.0285	0.0312	38.54	0	24.93	6.22	100.3766	0.0015	2.041	0.625	0.038	0.0043	0.0018	2.972	0	1.608	0.715	8.0066	0.54	0.24	0.21	0.01	0.69
Line 7 SEC46-01_grt2	120.4	**-159.2**	0.038	22.5	7.77	0.533	0.0594	0.0277	38.65	0	24.92	6.34	100.8381	0.0023	2.036	0.639	0.0347	0.0088	0.0016	2.968	0	1.6	0.726	8.0164	0.53	0.24	0.21	0.01	0.69
Line 8 SEC46-01_grt2	140.8	**-138.8**	0.0453	22.51	8.06	0.5967	0.0475	0.0617	38.52	0	24.86	6.19	100.8912	0.0028	2.038	0.663	0.0388	0.0071	0.0036	2.959	0	1.597	0.709	8.0183	0.53	0.24	0.22	0.01	0.69
Line 9 SEC46-01_grt2	161.0	**-118.6**	0.0487	22.51	8.35	0.4907	0.0639	0.0397	38.74	0	24.44	6.13	100.813	0.003	2.036	0.686	0.0319	0.0095	0.0023	2.973	0	1.569	0.701	8.0118	0.53	0.23	0.23	0.01	0.69
Line 10 SEC46-01_grt2	181.4	**-98.2**	0.0619	22.49	7.29	0.5534	0.0309	0.039	38.87	0	25.23	6.46	101.0251	0.0037	2.03	0.598	0.0359	0.0046	0.0022	2.977	0	1.616	0.738	8.0055	0.54	0.25	0.20	0.01	0.69
Line 11 SEC46-01_grt2	201.8	**-77.8**	0.0328	22.4	10.53	0.5186	0.0188	0.0376	38.83	0.006	22.9	5.36	100.6337	0.002	2.028	0.866	0.0337	0.0028	0.0022	2.982	0.0006	1.471	0.613	8.0013	0.49	0.21	0.29	0.01	0.71
Line 12 SEC46-01_grt2	221.2	**-58.4**	0	22.78	9.5	0.5296	0.1128	0.0694	39.19	0	23.55	5.61	101.3417	0	2.045	0.775	0.0342	0.0167	0.004	2.985	0	1.5	0.637	7.997	0.51	0.22	0.26	0.01	0.70
Line 13 SEC46-01_grt2	239.5	**-40.1**	0.0203	22.62	8.96	0.5501	0.0686	0.0267	38.7	0	24.27	5.88	101.0956	0.0012	2.042	0.736	0.0357	0.0102	0.0015	2.965	0	1.555	0.671	8.0176	0.52	0.22	0.25	0.01	0.70
Line 14 SEC46-01_grt2	264.1	**-15.5**	0.0336	22.57	8.34	0.5595	0.0735	0.0107	38.66	0.0042	24.72	5.88	100.8514	0.002	2.043	0.686	0.0364	0.011	0.0006	2.97	0.0004	1.588	0.674	8.0114	0.53	0.23	0.23	0.01	0.70
Line 15 SEC46-01_grt2	279.6	**0.0**	0.0392	22.51	8.62	0.522	0.0831	0.0533	38.67	0	24.55	5.74	100.7875	0.0024	2.039	0.71	0.034	0.0124	0.0031	2.972	0	1.578	0.658	8.0089	0.53	0.22	0.24	0.01	0.71

SEC46-01 Average			0.02	22.50	8.09	0.87	0.03	0.06	38.55	0.00	24.61	5.99	100.72	0.00	2.04	0.67	0.06	0.00	0.00	2.97	0.00	1.58	0.69	8.01	0.53	0.23	0.22	0.02	0.70
Line 1 SEC46-02_grt1	0	-216	0.03	22.16	10.31	0.71	0.06	0.13	38.48	0.00	24.07	4.87	100.82	0.0018	2.016	0.853	0.0464	0.0093	0.0077	2.97	0	1.554	0.56	8.0182	0.52	0.19	0.28	0.02	0.74
Line 2 SEC46-02_grt1	54	-162	0.02	22.29	10.56	0.65	0.04	0.14	38.77	0.00	23.51	5.04	101.03	0.0013	2.017	0.869	0.0424	0.0067	0.0084	2.977	0	1.51	0.576	8.0078	0.50	0.19	0.29	0.01	0.72
Line 3 SEC46-02_grt1	108	-108	0.05	22.39	10.48	0.67	0.05	0.09	38.42	0.00	23.82	4.88	100.85	0.0028	2.034	0.866	0.0436	0.0078	0.0054	2.962	0	1.536	0.561	8.0186	0.51	0.19	0.29	0.01	0.73
Line 4 SEC46-02_grt1	163	-53	0.02	22.60	9.58	0.57	0.04	0.11	38.78	0.00	24.21	5.41	101.31	0.0011	2.039	0.785	0.0367	0.0056	0.0062	2.968	0	1.55	0.617	8.0086	0.52	0.21	0.26	0.01	0.72
Line 5 SEC46-02_grt1	216	0	0.00	22.44	8.17	0.65	0.05	0.06	38.69	0.00	25.31	5.70	101.07	0	2.032	0.672	0.0425	0.0068	0.0037	2.973	0	1.626	0.653	8.009	0.54	0.22	0.22	0.01	0.71
Line 1 SEC46-02_grt2	0	-222	0.01	22.44	11.06	0.62	0.03	0.07	38.73	0.00	22.83	4.96	100.73	0.0005	2.033	0.911	0.0401	0.0039	0.0038	2.977	0	1.467	0.568	8.0043	0.49	0.19	0.31	0.01	0.72
Line 2 SEC46-02_grt2	23	-198	0.06	22.47	10.01	0.58	0.06	0.05	38.68	0.00	24.89	4.66	101.45	0.0034	2.034	0.824	0.0374	0.0089	0.0028	2.97	0	1.599	0.534	8.0135	0.53	0.18	0.28	0.01	0.75
Line 3 SEC46-02_grt2	48	-174	0.00	22.56	10.55	0.60	0.09	0.04	38.54	0.00	23.75	4.94	101.07	0.0003	2.044	0.868	0.039	0.0127	0.0022	2.961	0	1.527	0.566	8.0202	0.51	0.19	0.29	0.01	0.73
Line 4 SEC46-02_grt2	72	-150	0.01	22.43	10.37	0.60	0.00	0.04	38.51	0.00	24.63	4.57	101.16	0.0008	2.037	0.856	0.039	0	0.0021	2.967	0	1.587	0.524	8.0129	0.53	0.17	0.28	0.01	0.75
Line 5 SEC46-02_grt2	95	-127	0.03	22.33	9.73	0.70	0.03	0.01	38.31	0.00	26.11	4.21	101.47	0.002	2.033	0.806	0.0457	0.0051	0.0008	2.96	0	1.687	0.485	8.0246	0.56	0.16	0.27	0.02	0.78
Line 6 SEC46-02_grt2	122	-100	0.03	22.48	9.50	0.66	0.06	0.10	38.84	0.00	24.54	5.40	101.62	0.0016	2.025	0.778	0.043	0.0095	0.0059	2.969	0	1.569	0.615	8.016	0.52	0.20	0.26	0.01	0.72
Line 7 SEC46-02_grt2	146	-76	0.01	22.53	9.86	0.63	0.01	0.13	38.69	0.00	24.00	5.49	101.36	0.0007	2.033	0.808	0.0405	0.0021	0.0078	2.961	0	1.536	0.626	8.0152	0.51	0.21	0.27	0.01	0.71
Line 8 SEC46-02_grt2	171	-51	0.02	22.60	9.72	0.56	0.05	0.12	38.80	0.00	24.15	5.30	101.31	0.001	2.039	0.797	0.0363	0.007	0.0067	2.97	0	1.546	0.604	8.007	0.52	0.20	0.27	0.01	0.72
Line 9 SEC46-02_grt2	194	-28	0.01	22.39	9.73	0.59	0.01	0.10	38.64	0.00	24.83	4.95	101.24	0.0004	2.029	0.801	0.0381	0.0018	0.0055	2.971	0	1.596	0.567	8.0098	0.53	0.19	0.27	0.01	0.74
Line 10 SEC46-02_grt2	222	0	0.06	22.63	8.32	0.59	0.04	0.02	38.98	0.00	24.64	5.98	101.26	0.0034	2.038	0.681	0.038	0.006	0.0012	2.979	0	1.575	0.681	8.0026	0.53	0.23	0.23	0.01	0.70
SEC46-02 Average			0.02	22.45	9.86	0.62	0.04	0.08	38.66	0.00	24.35	5.09	101.18	0.00	2.03	0.81	0.04	0.01	0.00	2.97	0.00	1.56	0.58	8.01	0.52	0.19	0.27	0.01	0.73
Line 1 SEC47-01_grt1	0	-146	0.00	22.07	9.78	1.01	0.08	0.12	38.40	0.00	25.80	4.20	101.46	0	2.011	0.81	0.0662	0.0116	0.0069	2.968	0	1.668	0.484	8.0258	0.55	0.16	0.27	0.02	0.78
Line 2 SEC47-01_grt1	37	-109	0.05	22.28	9.43	0.59	0.06	0.15	38.37	0.00	26.22	4.58	101.73	0.0032	2.022	0.778	0.0384	0.009	0.0087	2.955	0.0001	1.689	0.526	8.0294	0.56	0.17	0.26	0.01	0.76
Line 3 SEC47-01_grt1	73	-73	0.03	22.25	8.06	0.55	0.00	0.12	38.55	0.00	26.99	5.00	101.56	0.0021	2.02	0.665	0.0361	0	0.0068	2.969	0	1.739	0.574	8.012	0.58	0.19	0.22	0.01	0.75
Line 4 SEC47-01_grt1	110	-36	0.03	22.38	7.59	0.64	0.00	0.11	38.43	0.00	27.12	5.18	101.48	0.0021	2.033	0.626	0.0416	0	0.0065	2.962	0	1.748	0.595	8.0142	0.58	0.20	0.21	0.01	0.75
Line 5 SEC47-01_grt1	146	0	0.04	22.35	8.89	0.64	0.00	0.07	38.63	0.00	26.42	4.64	101.67	0.0022	2.026	0.733	0.0418	0	0.0038	2.971	0	1.7	0.532	8.0098	0.57	0.18	0.24	0.01	0.76
Line 1 SEC47-01_grt2	0	-112	0.01	22.17	9.72	0.64	0.09	0.14	38.41	0.00	26.12	4.26	101.55	0.0004	2.017	0.804	0.0417	0.013	0.0083	2.965	0	1.686	0.49	8.0254	0.56	0.16	0.27	0.01	0.77
Line 2 SEC47-01_grt2	28	-84	0.04	22.18	9.46	0.70	0.00	0.13	38.42	0.00	26.10	4.49	101.52	0.0022	2.017	0.782	0.0457	0.0004	0.0075	2.964	0	1.684	0.516	8.0188	0.56	0.17	0.26	0.02	0.77
Line 3 SEC47-01_grt2	56	-56	0.05	22.05	9.26	0.44	0.07	0.15	38.40	0.00	26.85	4.39	101.66	0.0031	2.007	0.766	0.0286	0.0098	0.009	2.965	0	1.733	0.505	8.0265	0.57	0.17	0.25	0.01	0.77
Line 4 SEC47-01_grt2	84	-28	0.02	22.42	8.13	0.41	0.07	0.08	38.47	0.00	27.12	4.85	101.57	0.0013	2.036	0.671	0.0268	0.0101	0.0045	2.964	0	1.748	0.556	8.0177	0.58	0.19	0.22	0.01	0.76
Line 5 SEC47-01_grt2	112	0	0.04	22.52	7.99	0.58	0.07	0.07	38.50	0.00	26.35	5.25	101.37	0.0027	2.043	0.659	0.0376	0.0097	0.0042	2.962	0	1.696	0.602	8.0162	0.57	0.20	0.22	0.01	0.74
Line 1 SEC47-01_grt3	0	-160	0.10	22.08	9.78	0.77	0.05	0.09	38.39	0.00	26.06	4.13	101.44	0.006	2.013	0.81	0.0502	0.0069	0.0052	2.968	0	1.685	0.476	8.0203	0.56	0.16	0.27	0.02	0.78
Line 2 SEC47-01_grt3	48	-112	0.16	22.10	9.75	0.63	0.06	0.12	38.50	0.00	25.85	4.48	101.66	0.01	2.007	0.804	0.041	0.009	0.0071	2.966	0	1.665	0.514	8.0231	0.55	0.17	0.27	0.01	0.76
Line 3 SEC47-01_grt3	86	-74	0.09	22.10	8.86	0.66	0.01	0.16	38.25	0.00	26.91	4.35	101.40	0.0058	2.017	0.735	0.0434	0.0022	0.0091	2.962	0	1.743	0.502	8.0195	0.58	0.17	0.24	0.01	0.78
Line 4 SEC47-01_grt3	123	-36	0.03	22.40	7.98	0.57	0.01	0.11	38.39	0.00	27.23	4.80	101.52	0.0017	2.037	0.66	0.0373	0.0022	0.0063	2.962	0	1.757	0.552	8.0155	0.58	0.18	0.22	0.01	0.76
Line 5 SEC47-01_grt3	160	0	0.02	22.47	8.11	0.62	0.04	0.07	38.75	0.00	25.83	5.59	101.50	0.0014	2.03	0.666	0.0404	0.0053	0.0038	2.971	0	1.656	0.639	8.0129	0.55	0.21	0.22	0.01	0.72
SEC47-01 Average			0.05	22.25	8.85	0.63	0.04	0.11	38.46	0.00	26.46	4.68	101.54	0.00	2.02	0.73	0.04	0.01	0.01	2.96	0.00	1.71	0.54	8.02	0.57	0.18	0.24	0.01	0.76

This is a preprint, the final version is subject to change, of the American Mineralogist (MSA)
Cite as Authors (Year) Title. American Mineralogist, in press.
DOI: https://doi.org/10.2138/am-2020-6994

Supplementary Table 2. Omphacite major element comp

			Weight Percent Oxide											Atoms per formula unit															
	Cumulative Distance (µm)	Dist to grain boundary (µm)	TiO2	SiO2	K2O	MnO	Na2O	Cr2O3	Al2O3	CaO	FeO	MgO	Total	Ti	Si	K	Mn	Na	Cr	Al	Ca	Fe	Fe3+	Mg	Total	XWo = Ca/(Ca+Mg+FeT)	XEn = Mg/(Ca+Mg+FeT)	XFs = FeT/(Ca+Mg+FeT)	Mg/(Mg+Fe)
Line 1 SEC42-06_cpx1	0	-314	0.17	54.41	0.01	0.05	6.17	0.05	10.07	13.56	6.70	8.14	99.33	0.0046	1.976	0.0007	0.0016	0.434	0.0014	0.431	0.527	0.203		0.441	4.0203	45.00	37.66	17.34	0.68
Line 2 SEC42-06_cpx1	32	-282	0.16	54.26	0.00	0.04	6.56	0.07	9.99	13.49	6.66	8.10	99.33	0.0044	1.973	0.0001	0.0013	0.462	0.0019	0.428	0.526	0.203		0.439	4.0388	45.03	37.59	17.38	0.68
Line 3 SEC42-06_cpx1	64	-250	0.17	54.47	0.00	0.04	6.33	0.04	10.06	13.66	6.73	8.13	99.63	0.0046	1.974	0	0.0013	0.445	0.001	0.43	0.53	0.204		0.439	4.029	45.18	37.43	17.39	0.68
Line 4 SEC42-06_cpx1	108	-206	0.20	54.46	0.00	0.04	6.56	0.05	10.27	13.48	6.63	7.97	99.66	0.0055	1.972	0	0.0011	0.46	0.0016	0.438	0.523	0.201		0.43	4.0322	45.32	37.26	17.42	0.68
Line 5 SEC42-06_cpx1	153	-161	0.17	54.36	0.00	0.02	6.37	0.07	9.90	13.54	6.65	8.09	99.17	0.0047	1.978	0.0001	0.0007	0.45	0.002	0.425	0.528	0.202		0.439	4.0296	45.17	37.55	17.28	0.68
Line 6 SEC42-06_cpx1	185	-129	0.16	54.77	0.00	0.02	6.35	0.06	10.07	13.40	6.88	8.03	99.74	0.0045	1.981	0	0.0007	0.445	0.0016	0.429	0.519	0.208		0.433	4.0219	44.74	37.33	17.93	0.68
Line 7 SEC42-06_cpx1	224	-89	0.12	54.63	0.00	0.05	6.42	0.06	10.26	13.32	6.86	8.07	99.79	0.0033	1.975	0	0.0014	0.45	0.0018	0.437	0.516	0.207		0.435	4.0266	44.56	37.56	17.88	0.68
Line 8 SEC42-06_cpx1	254	-60	0.14	54.56	0.00	0.02	6.68	0.02	10.42	13.15	6.70	7.95	99.63	0.0037	1.974	0	0.0007	0.469	0.0004	0.444	0.51	0.203		0.429	4.0339	44.66	37.57	17.78	0.68
Line 9 SEC42-06_cpx1	293	-21	0.13	54.78	0.01	0.04	6.34	0.02	9.87	13.64	6.89	8.19	99.92	0.0036	1.98	0.0003	0.0013	0.444	0.0007	0.42	0.528	0.208		0.441	4.027	44.86	37.47	17.67	0.68
Line 10 SEC42-06_cpx1	314	0	0.13	54.83	0.00	0.02	6.11	0.03	9.98	13.46	6.95	8.22	99.74	0.0035	1.982	0.0001	0.0006	0.428	0.0009	0.425	0.521	0.21		0.443	4.0142	44.38	37.73	17.89	0.68
Line 1 SEC42-06_cpx2_core->rim	0	-692	0.17	54.73	0.00	0.02	6.74	0.00	9.74	13.82	6.65	8.19	100.07	0.0047	1.977	0	0.0007	0.472	0.0001	0.415	0.535	0.201		0.441	4.0466	45.45	37.47	17.08	0.69
Line 2 SEC42-06_cpx2_core->rim	157	-535	0.14	54.55	0.00	0.00	6.29	0.03	10.05	13.67	6.74	8.01	99.47	0.0037	1.978	0	0	0.442	0.0007	0.43	0.531	0.205		0.433	4.0235	45.42	37.04	17.54	0.68
Line 3 SEC42-06_cpx2_core->rim	443	-249	0.19	54.61	0.00	0.03	6.57	0.01	10.20	13.75	6.69	7.96	100.01	0.0052	1.972	0	0.0009	0.46	0.0004	0.434	0.532	0.202		0.429	4.0356	45.74	36.89	17.37	0.68
Line 4 SEC42-06_cpx2_core->rim	565	-127	0.18	54.15	0.00	0.03	6.55	0.03	10.17	13.68	6.79	8.06	99.64	0.005	1.965	0	0.001	0.461	0.0008	0.435	0.532	0.206		0.436	4.0419	45.32	37.14	17.55	0.68
Line 5 SEC42-06_cpx2_core->rim	692	0	0.15	54.66	0.00	0.02	6.51	0.06	10.20	13.51	6.81	7.93	99.86	0.0041	1.976	0.0001	0.0007	0.456	0.0018	0.435	0.523	0.206		0.427	4.0297	45.24	36.94	17.82	0.67
SEC42-06 Average			0.16	54.55	0.00	0.03	6.44	0.04	10.08	13.54	6.76	8.07	99.67	0.00	1.98	0.00	0.00	0.45	0.00	0.43	0.53	0.20		0.44	4.03	45.07	37.37	17.55	0.68
Line 1 43-01_Cpx1	0	-1944	0.12	54.95	0.00	0.02	6.13	0.05	10.37	13.99	4.98	8.89	99.50	0.0033	1.976	0	0.0005	0.428	0.0015	0.439	0.539	0.15		0.476	4.0134	46.27	40.86	12.88	0.76
Line 2 43-01_Cpx1	211	-1734	0.15	54.82	0.00	0.02	6.09	0.12	10.22	14.16	5.04	8.73	99.34	0.004	1.977	0	0.0005	0.426	0.0033	0.435	0.547	0.152		0.469	4.0138	46.83	40.15	13.01	0.76
Line 3 43-01_Cpx1	442	-1502	0.13	54.97	0.00	0.01	5.94	0.09	10.04	14.39	4.92	9.26	99.74	0.0034	1.974	0	0.0003	0.414	0.0024	0.425	0.554	0.148		0.495	4.0161	46.28	41.35	12.36	0.77
Line 4 43-01_Cpx1	647	-1298	0.16	54.87	0.00	0.01	5.90	0.06	10.09	14.41	5.10	8.89	99.50	0.0044	1.976	0	0.0004	0.412	0.0018	0.428	0.556	0.154		0.477	4.0096	46.84	40.19	12.97	0.76
Line 5 43-01_Cpx1	862	-1082	0.12	54.82	0.00	0.01	6.23	0.04	10.14	14.22	5.02	8.88	99.49	0.0034	1.975	0	0.0004	0.435	0.0012	0.431	0.549	0.151		0.477	4.023	46.64	40.53	12.83	0.76
Line 6 43-01_Cpx1	1078	-866	0.11	55.44	0.00	0.00	6.22	0.06	10.02	14.41	4.88	8.89	100.03	0.0031	1.984	0	0	0.431	0.0016	0.423	0.553	0.146		0.474	4.0157	47.14	40.41	12.45	0.76
Line 7 43-01_Cpx1	1293	-651	0.13	55.36	0.00	0.03	6.29	0.06	10.06	14.40	4.88	8.87	100.07	0.0034	1.982	0	0.0008	0.436	0.0017	0.425	0.552	0.146		0.473	4.0199	47.14	40.39	12.47	0.76
Line 8 43-01_Cpx1	1532	-412	0.10	55.35	0.00	0.01	6.15	0.07	9.85	14.35	4.98	8.90	99.77	0.0027	1.987	0	0.0003	0.428	0.0021	0.417	0.552	0.15		0.476	4.0152	46.86	40.41	12.73	0.76
Line 9 43-01_Cpx1	1738	-207	0.14	55.43	0.00	0.01	6.07	0.06	10.19	14.18	4.97	8.57	99.61	0.0037	1.99	0	0.0002	0.422	0.0016	0.431	0.545	0.149		0.459	4.0016	47.27	39.81	12.92	0.75
Line 10 43-01_Cpx1	1944	0	0.14	55.32	0.00	0.01	6.20	0.07	10.28	14.28	5.04	8.61	99.95	0.0038	1.982	0	0.0003	0.43	0.0021	0.434	0.548	0.151		0.46	4.0113	47.28	39.69	13.03	0.75
SEC43-01 Average			0.13	55.13	0.00	0.01	6.12	0.07	10.13	14.28	4.98	8.85	99.70	0.00	1.98	0.00	0.00	0.43	0.00	0.43	0.55	0.15		0.47	4.01	46.86	40.38	12.77	0.76
Line 1 SEC43-03_omph1	0	-210	0.21	54.26	0.00	0.03	6.19	0.00	10.38	13.85	6.15	8.37	99.45	0.0059	1.965	0.0001	0.0009	0.434	0.0001	0.443	0.538	0.186		0.452	4.0251	45.75	38.44	15.82	0.71
Line 2 SEC43-03_omph1	23	-187	0.20	54.38	0.00	0.03	6.21	0.03	10.42	13.82	6.18	8.43	99.70	0.0053	1.964	0	0.001	0.435	0.0008	0.444	0.535	0.187		0.454	4.0262	45.49	38.61	15.90	0.71
Line 3 SEC43-03_omph1	47	-164	0.17	54.41	0.00	0.02	6.27	0.02	10.41	13.94	6.22	8.48	99.94	0.0045	1.962	0	0.0008	0.438	0.0004	0.442	0.539	0.188		0.456	4.0308	45.56	38.55	15.89	0.71
Line 4 SEC43-03_omph1	70	-141	0.21	54.35	0.00	0.04	6.08	0.02	10.46	13.96	6.18	8.43	99.74	0.0058	1.963	0.0002	0.0013	0.425	0.0007	0.445	0.54	0.187		0.454	4.0221	45.72	38.44	15.83	0.71
Line 5 SEC43-03_omph1	94	-117	0.21	54.36	0.00	0.02	5.94	0.04	10.35	13.95	6.23	8.52	99.62	0.0056	1.965	0	0.0007	0.416	0.001	0.441	0.54	0.188		0.459	4.0163	45.49	38.67	15.84	0.71
Line 6 SEC43-03_omph1	117	-94	0.19	54.22	0.00	0.03	6.29	0.06	10.30	13.94	6.17	8.41	99.61	0.0051	1.963	0	0.0011	0.441	0.0017	0.439	0.541	0.187		0.454	4.0329	45.77	38.41	15.82	0.71
ne 7 SEC43-03_omph1 pit @!	138	-73	0.24	54.20	0.00	0.03	6.04	0.03	10.46	13.93	6.27	8.53	99.73	0.0065	1.958	0	0.001	0.423	0.0009	0.445	0.539	0.189		0.459	4.0215	45.41	38.67	15.92	0.71
Line 8 SEC43-03_omph1	164	-47	0.19	54.21	0.00	0.01	6.24	0.03	10.47	14.09	6.23	8.56	100.03	0.0051	1.955	0	0.0004	0.436	0.0009	0.445	0.545	0.188		0.46	4.0354	45.68	38.56	15.76	0.71
Line 9 SEC43-03_omph1	187	-24	0.21	54.10	0.00	0.05	6.18	0.02	10.33	14.00	6.31	8.49	99.69	0.0057	1.958	0	0.0014	0.434	0.0006	0.441	0.543	0.191		0.458	4.0328	45.55	38.42	16.02	0.71
Line 10 SEC43-03_omph1	210	0	0.20	53.95	0.00	0.03	6.59	0.03	10.33	13.87	6.66	8.35	100.01	0.0056	1.953	0	0.0008	0.462	0.0009	0.441	0.538	0.202		0.45	4.0533	45.21	37.82	16.97	0.69
SEC43-03 Average			0.20	54.24	0.00	0.03	6.20	0.03	10.39	13.94	6.26	8.46	99.75	0.01	1.96	0.00	0.00	0.43	0.00	0.44	0.54	0.19		0.46	4.03	45.56	38.46	15.98	0.71
Line 1 SEC46-01_omph1	0	-364	0.25	54.11	0.01	0.04	4.17	0.03	7.54	17.63	4.48	11.20	99.46	0.0067	1.963	0.0003	0.0014	0.294	0.0009	0.322	0.685	0.136		0.606	4.0154	48.00	42.47	9.53	0.82
Line 2 SEC46-01_omph1	25	-339	0.18	54.07	0.00	0.03	4.39	0.00	8.13	17.04	4.49	10.79	99.12	0.0049	1.964	0	0.0011	0.309	0	0.348	0.663	0.136		0.584	4.01	47.94	42.23	9.83	0.81
Line 3 SEC46-01_omph1	50	-313	0.16	53.95	0.01	0.01	4.18	0.01	7.95	17.26	4.55	10.94	99.02	0.0044	1.963	0.0003	0.0002	0.295	0.0004	0.341	0.673	0.139		0.594	4.0104	47.87	42.25	9.89	0.81
Line 4 SEC46-01_omph1	76	-288	0.36	49.19	0.19	0.01	2.58	0.00	9.97	11.09	8.72	14.83	96.95	0.0102	1.839	0.0092	0.0004	0.187	0	0.439	0.444	0.273		0.827	4.0289	28.76	53.56	17.68	0.75
Line 5 SEC46-01_omph1	101	-262	0.13	54.04	0.00	0.01	4.45	0.01	7.99	17.21	4.62	10.83	99.29	0.0035	1.963	0	0.0003	0.314	0.0002	0.342	0.67	0.14		0.586	4.0191	47.99	41.98	10.03	0.81
Line 6 SEC46-01_omph1	126	-238	0.14	53.89	0.00	0.00	4.14	0.02	7.56	17.51	4.58	11.11	98.96	0.0039	1.965	0.0001	0.0001	0.293	0.0006	0.325	0.684	0.14		0.604	4.0158	47.90	42.30	9.80	0.81
Line 7 SEC46-01_omph1	147	-217	0.15	54.79	0.00	0.02	4.19	0.01	8.31	17.21	4.57	10.50	99.75	0.0041	1.974	0	0.0007	0.293	0.0002	0.353	0.665	0.138		0.564	3.9921	48.65	41.26	10.10	0.80
Line 8 SEC46-01_omph1	194	-170	0.20	53.91	0.01	0.02	4.18	0.02	7.47	17.65	4.60	11.18	99.24	0.0054	1.962	0.0002	0.0008	0.295	0.0007	0.321	0.688	0.14		0.606	4.0192	47.98	42.26	9.76	0.81
Line 9 SEC46-01_omph1	212	-152	0.35	53.85	0.00	0.03	4.08	0.02	7.56	17.66	4.56	11.21	99.32	0.0095	1.958	0	0.001	0.287	0.0005	0.324	0.688	0.139		0.607	4.0141	47.98	42.33	9.69	0.81
Line 10 SEC46-01_omph1	238	-126	0.14	53.79	0.00	0.01	4.04	0.04	7.34	17.75	4.64	11.33	99.08	0.0039	1.962	0.0001	0.0004	0.286	0.0011	0.316	0.693	0.141		0.616	4.0196	47.79	42.48	9.72	0.81
Line 11 SEC46-01_omph1	263	-101	0.11	54.20	0.00	0.04	4.28	0.10	7.48	17.28	4.53	11.05	99.08	0.0031	1.972	0	0.0014	0.302	0.0029	0.321	0.674	0.138		0.6	4.0145	47.73	42.49	9.77	0.81
Line 12 SEC46-01_omph1	289	-75	0.14	54.06	0.00	0.03	4.24	0.10	7.66	17.34	4.62	11.08	99.27	0.004	1.965	0	0.0009	0.298	0.0028	0.328	0.675	0.141		0.6	4.0148	47.67	42.37	9.96	0.81
Line 13 SEC46-01_omph1	314	-50	0.13	54.18	0.00	0.03	4.02	0.06	7.35	17.59	4.62	11.20	99.19	0.0036	1.971	0	0.001	0.284	0.0019	0.315	0.686	0.14		0.607	4.0096	47.87	42.36	9.77	0.81
Line 14 SEC46-01_omph1	340	-24	0.14	54.28	0.00	0.03	4.34	0.06	7.71	17.48	4.53	11.13	99.70	0.0038	1.964	0	0.0008	0.304	0.0018	0.329	0.678	0.137		0.6	4.0185	47.92	42.40	9.68	0.81
Line 15 SEC46-01_omph1	364	0	0.16	54.24	0.00	0.03	4.12	0.07	7.46	17.40	4.65	11.24	99.37	0.0045	1.969	0	0.0009	0.29	0.0019	0.319	0.677	0.141		0.608	4.0114	47.48	42.64	9.89	0.81
Line 1 SEC46-01_omph2	0	-310	0.12	53.56	0.00	0.03	4.01	0.07	7.72	17.46	4.71	10.95	98.63	0.0034	1.961	0.0002	0.0008	0.284	0.0019	0.333	0.685	0.144		0.598	4.0113	48.00	41.91	10.09	0.81
Line 2 SEC46-01_omph2	78	-232	0.15	53.03	0.01	0.03	4.17	0.08	7.84	17.52	4.70	10.99	98.52	0.0041	1.947	0.0003	0.0008	0.297	0.0025	0.339	0.689	0.144		0.602	4.0258	48.01	41.95	10.03	0.81
Line 3 SEC46-01_omph2	155	-155	0.12	53.60	0.00	0.03	3.99	0.05	7.40	17.72	4.74	11.15	98.80	0.0034	1.961	0	0.0008	0.283	0.0013	0.319	0.695	0.145		0.608	4.0166	48.00	41.99	10.01	0.81
Line 4 SEC46-01_omph2	233	-77	0.17	53.48	0.01	0.03	4.12	0.09	7.53	17.54	4.65	11.10	98.71	0.0046	1.958	0.0003	0.0008	0.292	0.0025	0.325	0.688	0.142		0.606	4.0193	47.91	42.20	9.89	0.81
SEC46-01 Average			0.17	53.70	0.01	0.02	4.09	0.04	7.79	17.12	4.82	11.25	99.02	0.00	1.96	0.00	0.00	0.29	0.00	0.33	0.67	0.15		0.61	4.02	46.92	42.81	10.27	0.81
Line 1 SEC46-02_omph1	0	-175	0.14	54.47	0.00	0.03	5.90	0.04	9.31	14.79	5.20	9.25	99.12	0.0037	1.976	0.0001	0.0008	0.415	0.001	0.398	0.575	0.158		0.5	4.0277	46.63	40.55	12.81	0.76
Line 2 SEC46-02_omph1	19	-156	0.11	54.37	0.01	0.01	5.79	0.04	9.33	14.91	5.23	9.26	99.06	0.0029	1.974	0.0004	0.0004	0.408	0.0011	0.4	0.58	0.159		0.501	4.0268	46.77	40.40	12.82	0.76
Line 3 SEC46-02_omph1	39	-136	0.10	54.30	0.01	0.02	5.69	0.00	9.49	14.80	5.26	9.13	98.80	0.0028	1.975	0.0004	0.0005	0.401	0.0001	0.407	0.577	0.16		0.495	4.0189	46.83	40.18	12.99	0.76
Line 4 SEC46-02_omph1	59	-116	0.13	54.26	0.01	0.02	5.90	0.02	9.27	14.98	5.36	9.24	99.19	0.0036	1.971	0.0005	0.0006	0.415	0.0007	0.397	0.583	0.163		0.5	4.0345	46.79	40.13	13.08	0.75
Line 5 SEC46-02_omph1	78	-97	0.12	54.09	0.00	0.01	5.65	0.04	9.28	14.97	5.39	9.09	98.63	0.0032	1.974	0.0002	0.0002	0.4	0.0011	0.399	0.585	0.165		0.495	4.0228	46.99	39.76	13.25	0.75
Line 6 SEC46-02_omph1	98	-77	0.12	54.26	0.00	0.02	5.78	0.02	9.20	14.89	5.39	9.29	98.98	0.0033	1.974	0.0002	0.0007	0.408	0.0006	0.395	0.58	0.164		0.504	4.0299	46.47	40.38	13.14	0.75
Line 7 SEC46-02_omph1	117	-58	0.09	54.29	0.01	0.02	5.95	0.02	9.23	14.77	5.22	9.31	98.91	0.0025	1.975	0.0004	0.0006	0.42	0.0006	0.396	0.576	0.159		0.505	4.0352	46.45	40.73	12.82	0.76
Line 8 SEC46-02_omph1	136	-39	0.12	54.35	0.01	0.02	5.54	0.03	9.35	14.82	5.17	9.17	98.59	0.0033	1.98	0.0004	0.0008	0.392	0.001	0.401	0.579	0.158		0.498	4.0135	46.88	40.32	12.79	0.76
Line 9 SEC46-02_omph1	156	-19	0.08	54.63	0.00	0.02	6.03	0.05	9.65	14.57	5.08	9.24	99.35	0.0022	1.974	0	0.0006	0.423	0.0015	0.411	0.564	0.154		0.498	4.0283	46.38	40.95	12.66	0.76
Line 10 SEC46-02_omph1	175	0	0.10	54.29	0.01	0.01	5.61	0.03	9.28	14.87	5.28	9.40	98.88	0.0028	1.974	0.0004	0.0004	0.396	0.0009	0.398	0.58	0.161		0.509	4.0225	46.40	40.72	12.88	0.76
Line 1 SEC46-02_omph2	0	-238	0.09	54.32	0.00	0.01	5.50	0.02	9.09	15.03	5.40	9.37	98.84	0.0025	1.978	0	0.0004	0.389	0.0006	0.39	0.586	0.165		0.508	4.0195	46.54	40.35	13.11	0.75
Line 2 SEC46-02_omph2	59	-178	0.09	54.23	0.00	0.01	5.69	0.04	9.25	14.95	5.38	9.34	98.98	0.0025	1.973	0	0.0004	0.401	0.0011	0.396	0.583	0.164		0.506	4.0271	46.53	40.38	13.09	0.76
Line 3 SEC46-02_omph2	119	-119	0.13	54.29	0.00	0.01	5.71	0.04	9.15	14.93	5.39	9.16	98.82	0.0035	1.978	0.0001	0.0003	0.404	0.0013	0.393	0.583	0.164		0.497	4.0243	46.86	39.95	13.18	0.75
Line 4 SEC46-02_omph2	178	-59	0.11	54.36	0.00	0.02	5.59	0.00	9.13	15.07	5.41	9.21	98.90	0.003	1.978	0	0.0008	0.394	0	0.392	0.588	0.165		0.5	4.0209	46.93	39.90	13.17	0.75
Line 5 SEC46-02_omph2	238	0	0.12	54.08	0.00	0.02	5.55	0.04	9.22	14.92	5.39	9.28	98.62	0.0032	1.974	0	0.0006	0.393	0.0012	0.397	0.583	0.165		0.505	4.022	46.53	40.30	13.17	0.75
SEC46-02 Average			0.11	54.31	0.00	0.02	5.73	0.03	9.28	14.88	5.30	9.25	98.91	0.00	1.98	0.00	0.00	0.40	0.00	0.40	0.58	0.16		0.50	4.02	46.67	40.33	13.00	0.76
Line 1 SEC47-01_omph1	0	-327	0.11	54.54	0.00	0.04	6.15	0.01	9.09	14.29	6.03	8.73	98.99	0.0029	1.987	0	0.0011	0.435	0.0004	0.39	0.558	0.184		0.474	4.0325	45.89	38.98	15.13	0.72
Line 2 SEC47-01_omph1	82	-245	0.11	54.24	0.00	0.03	6.03	0.03	9.30	14.15	5.90	8.61	98.41	0.0031	1.985	0	0.0011	0.428	0.0008	0.401	0.555	0.181		0.47	4.0251	46.02	38.97	15.01	0.72
Line 3 SEC47-01_omph1	164	-163	0.09	54.44	0.00	0.02	6.05	0.06	9.22	14.34	6.04	8.76	99.02	0.0024	1.983	0	0.0007	0.427	0.0016	0.396	0.56	0.184		0.475	4.0297	45.94	38.97	15.09	0.72
Line 4 SEC47-01_omph1	245	-82	0.11	54.33	0.00	0.01	6.34	0.06	9.64	13.90	6.33	8.39	99.12	0.0031	1.978	0.0001	0.0004	0.447	0.0017	0.414	0.542	0.193		0.455	4.0344	45.55	38.24	16.22	0.70
Line 5 SEC47-01_omph1	327	0	0.13	54.35	0.00	0.03	6.38	0.02	9.81	13.96	6.51	8.27	99.45	0.0035	1.974	0	0.0008	0.449	0.0005	0.42	0.543	0.198		0.448	4.0368	45.67	37.68	16.65	0.69
Line 1 SEC47-01_omph2	0	-96	0.10	54.53	0.00	0.00	6.24	0.03	9.50	13.73	5.95	8.65	98.74	0.0027	1.987	0.0002	0.0001	0.441	0.0008	0.408	0.536	0.181		0.47	4.0268	45.16	39.60	15.25	0.72
Line 2 SEC47-01_omph2	24	-72	0.09	54.31	0.00	0.00	6.02	0.01	9.41	13.77	5.89	8.57	98.08	0.0024	1.991	0.0002	0.0001	0.428	0.0004	0.406	0.541	0.181		0.468	4.0182	45.46	39.33	15.21	0.72
Line 3 SEC47-01_omph2	49	-47	0.12	54.42	0.00	0.01	6.20	0.02	9.57	13.82	5.95	8.53	98.64	0.0032	1.985	0	0.0004	0.439	0.0006	0.412	0.54	0.182		0.464	4.0262	45.53	39.12	15.35	0.72
Line 4 SEC47-01_omph2	73	-23	0.10	54.08	0.01	0.01	6.03	0.03	9.62	13.75	6.19	8.43	98.26	0.0028	1.982	0.0004	0.0005	0.428	0.001	0.416	0.54	0.19		0.461	4.0217	45.34	38.71	15.95	0.71
Line 5 SEC47-01_omph2	96	0	0.12	54.38	0.01	0.01	6.03	0.03	9.80	13.75	6.17	8.22	98.52	0.0032	1.986	0.0005	0.0003	0.427	0.0009	0.422	0.538	0.189		0.448	4.015	45.79	38.13	16.09	0.70
SEC47-01 Average			0.11	54.36	0.00	0.02	6.15	0.03	9.50	13.95	6.10	8.52	98.72	0.00	1.98	0.00	0.00	0.43	0.00	0.41	0.55	0.19		0.46	4.03	45.63	38.77	15.59	0.71

Supplementary Table 3. Phengite major

			Weight %															
	Cumulative Dist µm	Dist to grain boundary (µm)	TiO2	F	Cl	MnO	Na2O	Cr2O3	SiO2	K2O	FeO	MgO	Al2O3	CaO	Total	H2O (100 minus sum)	F µg/g	Cl µg/g
Line 1 SEC42-06_Phen1	0	-123	1.04	0.00	0.00	0.00	1.27	0.00	47.68	8.89	2.60	2.45	29.31	0.01	93.26	6.74	-	-
Line 2 SEC42-06_Phen1	31	-92	0.97	0.00	0.00	0.00	1.08	0.03	47.59	8.87	2.54	2.44	29.35	0.00	92.88	7.12	-	-
Line 3 SEC42-06_Phen1	61	-62	1.05	0.00	0.01	0.00	1.23	0.05	47.54	8.95	2.53	2.39	29.45	0.00	93.19	6.81	-	-
Line 4 SEC42-06_Phen1	91	-32	0.99	0.00	0.01	0.00	1.18	0.02	47.87	8.87	2.50	2.47	29.56	0.00	93.47	6.53	-	82
Line 5 SEC42-06_Phen1	123	0	0.92	0.00	0.01	0.00	1.43	0.03	47.98	8.77	2.51	2.40	29.42	0.02	93.49	6.51	-	106
SEC42-06 Average			0.99	0.00	0.01	0.00	1.24	0.03	47.73	8.87	2.54	2.43	29.42	0.01	93.26	6.74		
																	-	-
Line 1 43-01_Phen1	0	-1098	0.92	0.00	0.01	0.01	1.15	0.06	48.19	8.87	1.72	2.65	29.43	0.01	93.02	6.98	-	71
Line 2 43-01_Phen1	121	-977	0.76	0.06	0.01	0.01	0.98	0.07	48.98	9.26	1.86	2.87	28.76	0.00	93.61	6.39	648	-
Line 3 43-01_Phen1	243	-855	0.74	0.02	0.00	0.00	0.96	0.05	49.06	9.22	1.87	2.91	28.37	0.00	93.20	6.80	-	-
Line 4 43-01_Phen1	390	-708	0.78	0.02	0.00	0.02	1.00	0.07	49.12	9.30	1.98	3.00	28.60	0.00	93.90	6.10	-	-
Line 5 43-01_Phen1	485	-613	0.68	0.07	0.01	0.00	0.95	0.11	48.83	9.22	1.87	3.05	28.66	0.00	93.45	6.55	668	102
Line 6 43-01_Phen1	609	-489	0.62	0.01	0.01	0.01	1.07	0.08	48.98	9.23	1.87	3.02	28.63	0.00	93.53	6.47	-	125
Line 7 43-01_Phen1	760	-338	0.81	0.00	0.01	0.01	1.04	0.04	48.98	9.30	1.99	2.92	28.75	0.01	93.84	6.16	-	63
Line 8 43-01_Phen1	855	-243	0.90	0.00	0.01	0.00	1.07	0.06	48.42	9.20	1.89	2.75	29.02	0.00	93.33	6.67	-	114
Line 9 43-01_Phen1	977	-121	0.96	0.04	0.00	0.00	1.18	0.05	48.13	9.08	1.90	2.64	29.43	0.00	93.41	6.59	-	-
Line 10 43-01_Phen1	1098	0	0.88	0.00	0.01	0.00	1.29	0.02	48.01	8.93	1.77	2.56	29.84	0.00	93.30	6.70	-	71
SEC43-01 Average			0.80	0.02	0.01	0.01	1.07	0.06	48.67	9.16	1.87	2.84	28.95	0.00	93.46			
Line 1 SEC47-01 phen1	0	-1108	0.75	0.05	0.00	0.00	1.20	0.06	48.42	9.09	2.32	2.83	29.1	0	93.86	6.14	519	-
Line 2 sec47-01 phen1	277	-831	0.73	0.00	0.00	0.00	1.06	0.05	48.4	9.18	2.36	2.92	28.9	0	93.58	6.42	-	-
Line 3 sec47-01 phen1	553	-555	0.69	0.04	0.00	0.01	1.01	0.03	48.77	9.13	2.28	2.85	29.0	0.0054	93.78	6.22	434	-
Line 4 sec47-01 phen1	863	-244	0.75	0.00	0.00	0.00	1.12	0.01	48.76	9.15	2.36	2.76	29.3	0.0107	94.25	5.75	-	-
Line 5 sec47-01 phen1	1108	0	0.69	0.00	0.00	0.00	1.09	0.07	48.66	9.21	2.24	2.73	29.3	0	93.96	6.04	-	-
Line 1 SEC47-01 phen2	0	-305	0.64	0.00	0.00	0.00	1.14	0.07	48.3	9.18	2.37	2.92	28.5	0	93.15	6.85	-	-
Line 2 SEC47-01 phen2	29	-275	0.58	0.00	0.00	0.01	0.97	0.06	49.13	9.28	2.42	3.05	28.2	0.0061	93.67	6.33	-	-
Line 3 SEC47-01 phen2	68	-237	0.62	0.00	0.00	0.00	1.03	0.05	48.94	9.34	2.46	3.11	28.1	0	93.59	6.41	-	-
Line 4 SEC47-01 phen2	101	-204	0.63	0.00	0.00	0.01	1.04	0.04	49.08	9.32	2.31	3.01	28.4	0.0097	93.84	6.16	-	-
Line 5 SEC47-01 phen2	136	-169	0.53	0.00	0.00	0.00	1.00	0.03	48.98	9.13	2.47	3.36	27.9	0.0286	93.44	6.56	-	-
Line 6 SEC47-01 phen2	169	-135	0.57	0.00	0.00	0.01	0.94	0.06	49.15	9.41	2.47	3.04	28.3	0	93.91	6.09	-	-
Line 7 SEC47-01 phen2	203	-102	0.59	0.00	0.00	0.00	0.89	0.06	49.15	9.38	2.43	3.05	28.3	0	93.81	6.19	-	-
Line 8 SEC47-01 phen2	237	-68	0.58	0.00	0.00	0.00	0.94	0.06	49.23	9.47	2.53	2.98	28.1	0	93.89	6.11	-	-
Line 9 SEC47-01 phen2	270	-34	0.53	0.00	0.00	0.02	1.02	0.07	48.15	8.98	3.94	2.74	28.3	0.04	93.82	6.18	-	-
Line 10 SEC47-01 phen2	305	0	0.63	0.00	0.00	0.00	1.05	0.06	48.01	9.01	2.65	2.44	29.8	0.0097	93.64	6.36	-	-
SEC47-01 Average			0.63	0.01	0.00	0.00	1.03	0.05	48.74	9.22	2.51	2.92	28.62	0.01	93.75			

Supplementary Table 4. Amphibole major element composition

			Weight %														Atoms per formula unit															Calculated using Locock 2014 Workbook
	Cumulative Dist pos.	[illegible]	TiO2	F	Cl	MnO	Na2O	Cr2O3	SiO2	K2O	FeO	MgO	Al2O3	CaO	Total	H2O	Ti	F	Cl	Mn	Na	Cr	Si	K	Fe	Mg	Al	Ca	Total	Subgroup	Species	Formula
Line 1 SEC42-06_amph1	0	-370	0.69	0.18	0.00	0.08	4.13	0.04	44.17	0.70	13.73	10.06	14.82	8.72	97.33	2.67	0.076	0.086	0.001	0.010	1.180	0.005	6.513	0.132	1.693	2.212	2.577	1.377	15.86			
Line 2 SEC42-06_amph1	112	-258	0.72	0.14	0.00	0.06	3.94	0.03	45.16	0.69	13.30	10.79	13.69	8.96	97.48	2.52	0.079	0.066	0.001	0.007	1.121	0.003	6.626	0.129	1.632	2.359	2.368	1.409	15.80			
Line 3 SEC42-06_amph1	172	-197	0.60	0.12	0.01	0.04	4.28	0.03	44.28	0.61	12.70	10.30	14.36	8.43	95.75	4.25	0.067	0.054	0.004	0.005	1.236	0.003	6.593	0.115	1.582	2.287	2.521	1.345	15.81			
Line 4 SEC42-06_amph1	173	-196	0.64	0.13	0.01	0.05	4.10	0.00	43.52	0.60	12.21	10.23	14.20	8.20	93.89	6.11	0.073	0.061	0.002	0.006	1.205	0.000	6.596	0.117	1.547	2.311	2.536	1.331	15.79			
Line 5 SEC42-06_amph1	180	-190	0.65	0.17	0.01	0.07	4.17	0.03	44.58	0.63	13.22	10.38	14.55	8.62	97.09	2.91	0.072	0.079	0.004	0.009	1.192	0.004	6.565	0.118	1.628	2.278	2.526	1.360	15.83			
Line 6 SEC42-06_amph1	218	-151	0.67	0.09	0.01	0.07	4.16	0.02	44.94	0.65	13.11	10.68	14.39	8.55	97.34	2.66	0.074	0.040	0.002	0.008	1.184	0.003	6.587	0.122	1.607	2.334	2.486	1.342	15.79			
Line 7 SEC42-06_amph1	264	-106	0.71	0.10	0.01	0.04	4.33	0.04	44.57	0.67	13.06	10.34	15.03	8.51	97.41	2.59	0.078	0.047	0.002	0.005	1.230	0.005	6.532	0.126	1.601	2.259	2.596	1.337	15.82			
Line 8 SEC42-06_amph1	312	-58	0.71	0.11	0.01	0.06	4.15	0.02	44.64	0.67	12.95	10.28	14.99	8.40	96.99	3.01	0.078	0.049	0.002	0.008	1.182	0.003	6.560	0.126	1.592	2.252	2.595	1.322	15.77			
Line 9 SEC42-06_amph1	339	-31	0.67	0.11	-	0.06	4.33	0.04	45.05	0.63	13.08	10.40	14.43	8.34	97.14	2.86	0.074	0.051	0.000	0.007	1.233	0.005	6.612	0.118	1.605	2.275	2.497	1.312	15.79			
Line 10 SEC42-06_amph1	370	0	0.33	0.10	0.00	0.04	4.24	0.05	47.93	0.34	12.82	11.43	11.94	8.19	97.43	2.57	0.037	0.044	0.001	0.005	1.194	0.006	6.957	0.064	1.556	2.473	2.044	1.274	15.66			
SEC42-06 Average			0.64	0.12	0.01	0.06	4.18	0.03	44.88	0.62	13.02	10.49	14.24	8.49	96.78	3.22	0.071	0.058	0.002	0.007	1.196	0.004	6.614	0.117	1.604	2.304	2.475	1.341	15.79	Na-Ca	katophorite	[illegible]
Line 1 43-01_Amph1	0	-456	0.59	0.28	-	0.04	3.98	0.01	45.32	0.63	11.29	10.86	15.39	8.89	97.28	2.72	0.065	0.131	0.000	0.005	1.120	0.002	6.588	0.116	1.373	2.354	2.637	1.385	15.77			
Line 2 43-01_Amph1	51	-405	0.60	0.23	0.00	0.05	4.06	0.05	44.60	0.64	11.33	11.24	15.18	8.66	96.64	3.36	0.066	0.108	0.001	0.006	1.155	0.006	6.538	0.119	1.389	2.456	2.623	1.361	15.83			
Line 3 43-01_Amph1	102	-354	0.68	0.20	-	0.04	4.10	0.02	44.66	0.71	11.39	11.11	15.56	8.77	97.24	2.76	0.074	0.090	0.000	0.005	1.157	0.002	6.508	0.132	1.388	2.414	2.674	1.370	15.82			
Line 4 43-01_Amph1	152	-304	0.66	0.13	0.00	0.04	4.13	0.06	44.62	0.69	11.23	11.12	15.55	8.63	96.87	3.13	0.072	0.060	0.001	0.005	1.170	0.007	6.517	0.129	1.371	2.420	2.677	1.350	15.78			
Line 5 43-01_Amph1	203	-253	0.65	0.09	-	0.05	4.03	0.04	44.58	0.72	11.00	11.13	15.50	8.66	96.44	3.56	0.072	0.040	0.000	0.006	1.144	0.004	6.528	0.134	1.347	2.430	2.676	1.359	15.74			
Line 6 43-01_Amph1	253	-202	0.69	0.18	-	0.05	4.10	0.04	44.24	0.72	10.95	11.12	15.53	8.67	96.30	3.70	0.077	0.086	0.000	0.006	1.167	0.005	6.500	0.135	1.345	2.435	2.691	1.365	15.81			
Line 7 43-01_Amph1	304	-152	0.69	0.11	-	0.03	4.06	0.05	44.39	0.69	10.85	11.16	15.53	8.78	96.34	3.66	0.077	0.049	0.000	0.004	1.154	0.006	6.509	0.129	1.330	2.438	2.684	1.380	15.76			
Line 8 43-01_Amph1	355	-101	0.67	0.20	0.00	0.05	4.26	0.00	44.55	0.71	11.09	11.20	15.36	8.66	96.77	3.23	0.074	0.094	0.001	0.007	1.208	0.001	6.521	0.133	1.357	2.443	2.650	1.358	15.85			
Line 9 43-01_Amph1	405	-51	0.59	0.13	0.01	0.05	4.17	0.01	44.51	0.63	11.03	11.38	15.02	8.68	96.20	3.80	0.065	0.060	0.002	0.007	1.190	0.001	6.544	0.118	1.356	2.494	2.602	1.368	15.81			
Line 10 43-01_Amph1	456	0	0.61	0.13	0.00	0.04	4.44	0.04	44.48	0.60	11.06	11.53	14.80	8.74	96.47	3.53	0.067	0.060	0.000	0.006	1.265	0.005	6.532	0.112	1.358	2.524	2.561	1.376	15.87			
SEC43-01 Average			0.64	0.17	0.00	0.04	4.13	0.03	44.60	0.67	11.12	11.19	15.34	8.71	96.65	3.35	0.071	0.078	0.000	0.006	1.173	0.004	6.529	0.126	1.361	2.441	2.648	1.367	15.80	Na-Ca	katophorite	[illegible]
Line 1 SEC43-03_amph1	0	-640	0.58	0.12	-	0.02	4.39	0.02	45.88	0.28	10.94	12.49	14.29	8.61	97.61	2.39	0.063	0.054	0.000	0.002	1.229	0.002	6.622	0.052	1.320	2.687	2.430	1.332	15.7929			
Line 2 SEC43-03_amph1	35	-605	0.69	0.08	-	0.03	4.27	-	45.01	0.28	11.5	12.06	15.4	8.64	97.96	2.04	0.075	0.035	0.000	0.004	1.194	0.000	6.491	0.052	1.386	2.594	2.617	1.335	15.7826			
Line 3 SEC43-03_amph1	91	-549	0.70	0.06	-	0.02	4.47	0.03	45.33	0.31	11.39	11.86	15.22	8.41	97.80	2.20	0.076	0.027	0.000	0.003	1.250	0.003	6.540	0.058	1.374	2.550	2.589	1.300	15.7695			
Line 4 SEC43-03_amph1	137	-503	0.74	0.04	-	0.06	4.34	0.02	45.28	0.31	11.16	12.03	15.22	8.46	97.65	2.35	0.080	0.020	0.000	0.007	1.215	0.002	6.534	0.056	1.347	2.588	2.589	1.308	15.746			
Line 5 SEC43-03_amph1	182	-458	0.61	0.08	-	0.06	3.61	0.03	46.67	0.31	11.42	12.72	13.12	9.15	97.78	2.22	0.066	0.035	0.000	0.007	1.009	0.004	6.728	0.057	1.377	2.733	2.229	1.413	15.6579			
Line 6 SEC43-03_amph1	227	-412	0.69	0.11	-	0.02	4.27	0.01	44.97	0.34	11.48	12.07	15.31	8.49	97.76	2.24	0.075	0.049	0.000	0.003	1.196	0.002	6.500	0.062	1.387	2.600	2.608	1.316	15.7979			
Line 7 SEC43-03_amph1	272	-367	0.72	0.08	-	0.05	4.52	0.00	45.18	0.37	11.3	12.09	15.21	8.49	97.99	2.01	0.078	0.035	0.000	0.006	1.264	0.000	6.513	0.067	1.362	2.597	2.585	1.312	15.8183			
Line 8 SEC43-03_amph1	320	-320	0.63	0.16	-	0.01	4.32	0.01	44.76	0.36	11.64	11.7	15.67	8.64	97.90	2.10	0.069	0.072	0.000	0.002	1.211	0.001	6.473	0.067	1.408	2.523	2.671	1.339	15.8351			
Line 9 SEC43-03_amph1	366	-274	0.75	0.05	-	0.03	4.38	-	44.97	0.36	11.79	12.08	15.2	8.47	98.08	1.92	0.082	0.025	0.000	0.003	1.226	0.000	6.489	0.066	1.423	2.599	2.586	1.309	15.8074			
Line 10 SEC43-03_amph1	411	-229	0.72	0.16	-	0.03	4.46	0.00	44.75	0.34	11.71	11.91	15.49	8.52	98.09	1.91	0.079	0.073	0.000	0.004	1.249	0.000	6.464	0.062	1.414	2.566	2.638	1.319	15.8678			
Line 11 SEC43-03_amph1	466	-174	0.64	0.01	0.00	0.06	4.35	0.00	43.87	0.37	12.21	11.54	15.81	8.6	97.46	2.54	0.070	0.006	0.000	0.008	1.230	0.000	6.395	0.069	1.489	2.507	2.716	1.343	15.8325			
Line 12 SEC43-03_amph1	506	-134	0.71	0.02	0.01	0.03	4.42	0.01	44.49	0.34	12.04	11.58	15.51	8.64	97.80	2.20	0.078	0.010	0.001	0.004	1.244	0.001	6.451	0.062	1.460	2.504	2.651	1.342	15.809			
Line 13 SEC43-03_amph1	551	-89	0.69	0.09	0.00	0.05	4.24	0.03	44.25	0.34	12.44	11.42	15.79	8.54	97.88	2.12	0.075	0.042	0.001	0.007	1.193	0.003	6.424	0.064	1.510	2.472	2.702	1.328	15.8198			
Line 14 SEC43-03_amph1	596	-43	0.64	0.05	0.01	0.05	4.46	0.03	44.14	0.30	12.37	11.57	15.49	8.56	97.66	2.34	0.070	0.022	0.001	0.006	1.258	0.004	6.426	0.056	1.506	2.511	2.658	1.336	15.8534			
Line 15 SEC43-03_amph1	640	0	0.50	0.06	0.00	0.07	4.43	0.05	41.03	0.41	13.04	10.42	18.08	9.18	97.28	2.72	0.056	0.027	0.001	0.009	1.269	0.006	6.060	0.078	1.610	2.295	3.147	1.453	16.0102			
SEC43-03 Average			0.67	0.08	0.00	0.04	4.33	0.02	44.71	0.33	11.76	11.84	15.39	8.63	97.78	2.22	0.073	0.035	0.000	0.005	1.216	0.002	6.474	0.062	1.425	2.555	2.628	1.339	15.81	Na-Ca	katophorite	[illegible]
Line 1 SEC46-01_amph3	0	-324	0.52	0.01	0.01	0.05	3.1	0.04	46.85	0.41	8.68	14.99	11.48	9.9	96.03	3.97	0.057	0.005	0.002	0.007	0.872	0.004	6.805	0.075	1.054	3.246	1.966	1.541	15.6339			
Line 2 SEC46-01_amph3	35	-290	0.49	0.00	0.01	0.02	2.94	0.06	46.66	0.39	8.55	15.07	11.46	9.99	95.66	4.34	0.054	0.002	0.002	0.003	0.830	0.007	6.799	0.073	1.042	3.274	1.968	1.560	15.615			
Line 3 SEC46-01_amph3	62	-263	0.50	-	0.01	0.03	2.91	0.05	46.66	0.41	8.63	15.15	11.34	9.93	95.62	4.38	0.055	0.000	0.003	0.003	0.822	0.006	6.804	0.076	1.052	3.294	1.949	1.552	15.6156			
Line 4 SEC46-01_amph3	120	-205	0.48	-	-	0.03	3.05	0.08	46.4	0.38	8.66	15.05	11.32	9.86	95.31	4.69	0.053	0.000	0.000	0.004	0.866	0.009	6.793	0.072	1.061	3.285	1.953	1.546	15.6414			
Line 5 SEC46-01_amph3	151	-173	0.46	-	-	0.05	3.03	0.03	47.08	0.41	8.42	15.49	11.15	9.92	96.04	3.96	0.050	0.000	0.000	0.006	0.851	0.004	6.827	0.076	1.022	3.349	1.905	1.542	15.632			
Line 6 SEC46-01_amph3	193	-131	0.45	-	-	0.04	3.05	0.10	48.24	0.38	8.45	15.47	11.08	9.95	97.22	2.78	0.049	0.000	0.000	0.005	0.845	0.012	6.897	0.069	1.010	3.296	1.866	1.524	15.5724			
Line 7 SEC46-01_amph3	221	-103	0.44	-	-	0.07	2.89	0.07	48.35	0.38	8.44	15.32	11.06	9.95	96.97	3.03	0.048	0.000	0.000	0.008	0.801	0.008	6.922	0.069	1.011	3.270	1.866	1.527	15.5293			
Line 8 SEC46-01_amph3	256	-69	0.45	-	-	0.04	2.91	0.08	48.07	0.39	8.54	15.05	11.26	10.03	96.83	3.17	0.049	0.000	0.000	0.004	0.809	0.010	6.899	0.072	1.025	3.220	1.904	1.543	15.5351			
Line 9 SEC46-01_amph3	290	-35	0.49	0.01	-	0.05	2.95	0.12	47.97	0.37	8.58	15.09	11.63	10.04	97.31	2.69	0.053	0.005	0.000	0.006	0.817	0.014	6.855	0.067	1.026	3.215	1.959	1.537	15.5538			
Line 10 SEC46-01_amph3	324	0	0.41	-	-	0.03	2.73	0.12	48.5	0.33	8.58	15.25	10.73	10.33	97.01	2.99	0.044	0.000	0.000	0.004	0.758	0.014	6.946	0.060	1.027	3.255	1.811	1.586	15.5051			
Line 1 SEC46-01_amph1	0	-224	0.49	-	-	0.03	2.72	0.08	47.49	0.38	8.6	15.47	11.38	10.02	96.66	3.34	0.053	0.000	0.000	0.004	0.759	0.010	6.834	0.069	1.035	3.318	1.931	1.544	15.5565			
Line 2 SEC46-01_amph1	24	-200	0.52	-	-	0.03	2.91	0.06	47.54	0.38	8.57	15.3	11.4	10	96.70	3.30	0.056	0.000	0.000	0.003	0.812	0.006	6.839	0.069	1.032	3.280	1.934	1.542	15.5739			
Line 3 SEC46-01_amph1	50	-174	0.47	-	-	0.03	2.89	0.09	47.69	0.41	8.67	15.32	11.29	10.03	96.89	3.11	0.051	0.000	0.000	0.003	0.806	0.011	6.853	0.075	1.042	3.281	1.912	1.544	15.5778			
Line 4 SEC46-01_amph1	74	-150	0.47	0.03	-	0.03	2.76	0.08	47.6	0.37	8.63	15.49	11.1	10.01	96.58	3.42	0.051	0.016	0.000	0.004	0.772	0.009	6.860	0.069	1.040	3.328	1.885	1.546	15.5792			
Line 5 SEC46-01_amph1	100	-124	0.49	0.01	-	0.05	2.88	0.08	47.34	0.40	8.73	15.22	11.5	10.04	96.74	3.26	0.053	0.005	0.000	0.006	0.805	0.010	6.818	0.073	1.051	3.268	1.953	1.549	15.5909			
Line 6 SEC46-01_amph1	124	-100	0.50	0.19	0.01	0.01	2.93	0.03	48.08	0.41	8.71	15.36	11.43	10.06	97.72	2.28	0.053	0.086	0.003	0.001	0.811	0.004	6.859	0.075	1.039	3.266	1.922	1.538	15.6565			
Line 7 SEC46-01_amph1	149	-75	0.51	0.04	0.01	0.00	2.84	0.07	48.13	0.41	8.57	15.18	11.47	10	97.25	2.75	0.055	0.020	0.003	0.001	0.786	0.008	6.879	0.075	1.024	3.234	1.933	1.531	15.5491			
Line 8 SEC46-01_amph1	174	-50	0.51	0.04	0.01	0.02	2.9	0.04	47.83	0.39	8.66	15.33	11.52	10.09	97.34	2.66	0.055	0.018	0.003	0.002	0.805	0.004	6.840	0.072	1.036	3.268	1.942	1.546	15.5912			
Line 9 SEC46-01_amph1	193	-32	0.51	0.14	0.01	0.02	2.76	0.05	48.51	0.40	8.55	14.92	11.65	10.05	97.57	2.43	0.054	0.065	0.002	0.002	0.762	0.006	6.906	0.073	1.018	3.166	1.955	1.534	15.5427			
Line 10 SEC46-01_amph1	224	0	0.39	0.10	0.01	0.03	2.79	0.04	48.69	0.34	8.11	15.72	10.63	10.11	96.96	3.04	0.042	0.048	0.002	0.003	0.773	0.005	6.964	0.062	0.970	3.352	1.792	1.549	15.5611			
SEC46-01 Average			0.48	0.03	0.00	0.03	2.90	0.07	47.68	0.39	8.57	15.26	11.29	10.02	96.72	3.28	0.052	0.013	0.001	0.004	0.808	0.008	6.860	0.071	1.031	3.273	1.915	1.544	15.58	Ca	pargasite	[illegible]
Line 1 SEC46-02_Amph2	0	-436	0.47	0.04	0.01	0.05	3.35	0.05	47.63	0.36	10.15	13.55	12.11	9.72	97.48	2.52	0.051	0.018	0.002	0.007	0.933	0.006	6.844	0.066	1.219	2.903	2.052	1.496	15.5946			
Line 2 SEC46-02_Amph2	109	-327	0.46	0.02	0.00	0.02	3.09	0.07	47.06	0.32	10.19	13.61	11.86	9.88	96.59	3.41	0.050	0.010	0.001	0.003	0.870	0.008	6.830	0.060	1.237	2.944	2.030	1.536	15.5786			
Line 3 SEC46-02_Amph2	218	-218	0.44	0.01	0.01	-	3.31	0.03	47.4	0.34	10.2	13.73	12.22	9.88	97.56	2.44	0.048	0.005	0.002	0.000	0.923	0.003	6.809	0.062	1.225	2.940	2.070	1.520	15.6061			
Line 4 SEC46-02_Amph2	327	-109	0.46	0.02	0.00	0.00	3.09	0.04	47.34	0.34	10.24	13.55	11.98	9.89	96.96	3.04	0.050	0.007	0.001	0.000	0.866	0.004	6.840	0.064	1.238	2.918	2.041	1.531	15.561			
Line 5 SEC46-02_Amph2	436	0	0.44	0.07	0.01	0.03	3.15	0.08	47.39	0.33	10.07	13.5	12.09	9.92	97.08	2.92	0.048	0.032	0.002	0.004	0.881	0.009	6.839	0.061	1.216	2.904	2.056	1.534	15.5848			
Line 1 SEC46-02_amph3	0	-608	0.47	-	-	0.03	3.26	0.04	47.15	0.36	10.48	13.58	12.04	9.96	97.36	2.64	0.051	0.000	0.000	0.003	0.913	0.005	6.802	0.066	1.264	2.921	2.047	1.539	15.6105			
Line 2 SEC46-02_amph3	153	-455	0.43	0.05	0.00	0.05	3.33	0.03	47.02	0.35	10.37	13.47	12.21	9.83	97.15	2.85	0.047	0.022	0.000	0.006	0.933	0.004	6.798	0.065	1.253	2.902	2.081	1.522	15.6328			
Line 3 SEC46-02_amph3	304	-304	0.45	0.00	0.00	0.02	3.25	0.01	46.76	0.35	10.6	13.23	12.52	9.89	97.09	2.91	0.049	0.002	0.001	0.003	0.911	0.001	6.767	0.065	1.284	2.855	2.136	1.534	15.6075			
Line 4 SEC46-02_amph3	456	-152	0.46	0.07	-	0.03	3.22	0.04	46.95	0.39	10.34	13.23	12.57	9.78	97.07	2.93	0.050	0.030	0.000	0.003	0.904	0.005	6.787	0.071	1.250	2.851	2.142	1.514	15.6076			
Line 5 SEC46-02_amph3	608	0	0.43	0.00	0.00	0.05	3.34	0.03	47.38	0.35	10.63	13.24	12.33	9.63	97.41	2.59	0.046	0.000	0.001	0.006	0.934	0.004	6.824	0.065	1.280	2.842	2.094	1.486	15.5812			
SEC46-02 Average			0.45	0.03	0.00	0.03	3.24	0.04	47.21	0.35	10.33	13.47	12.19	9.84	97.17	2.83	0.049	0.013	0.001	0.003	0.907	0.005	6.814	0.064	1.247	2.898	2.075	1.521	15.60	Ca	pargasite	[illegible]
Line 1 SEC47-01 Amph1	0	-128	0.29	0.18	0.01	0.09	4.21	0.04	48.45	0.28	14.01	11.21	11.1	7.46	97.33	2.67	0.032	0.082	0.002	0.012	1.191	0.005	7.063	0.052	1.707	2.435	1.907	1.166	15.6531			
Line 2 SEC47-01 Amph1	32	-95	0.30	0.22	0.00	0.09	4.04	0.06	48.49	0.24	13.35	11.63	10.89	7.91	97.22	2.78	0.033	0.102	0.000	0.011	1.141	0.006	7.064	0.045	1.627	2.527	1.870	1.234	15.6607			
Line 3 SEC47-01 Amph1	64	-64	0.26	0.22	0.00	0.10	3.92	0.07	49.3	0.22	13.33	12.28	10.1	7.91	97.71	2.29	0.028	0.103	0.000	0.012	1.101	0.008	7.137	0.041	1.613	2.651	1.724	1.226	15.6435			
Line 4 SEC47-01 Amph1	96	-32	0.22	0.27	0.00	0.09	4.21	0.06	49.11	0.28	13.64	11.59	10.9	7.49	97.86	2.14	0.024	0.122	0.001	0.011	1.180	0.007	7.107	0.052	1.650	2.501	1.859	1.161	15.6742			
Line 5 SEC47-01 Amph1	128	0	0.31	0.27	0.00	0.10	4.35	0.07	48.84	0.25	13.52	11.49	10.67	7.33	97.19	2.81	0.034	0.125	0.000	0.012	1.228	0.008	7.117	0.046	1.648	2.496	1.833	1.144	15.6905			
SEC47-01 Average			0.28	0.23	0.00	0.09	4.15	0.06	48.84	0.25	13.57	11.64	10.73	7.62	97.46	2.54	0.030	0.107	0.001	0.012	1.168	0.007	7.098	0.047	1.649	2.522	1.839	1.186	15.66	Na-Ca	winchite	[illegible]

Supplementary Table 5. Apatite Compositions (EMPA)

			Weight %									
	# grains	# measurements	P2O5	1 s.d. (%)	F	1 s.d. (%)	CaO	1 s.d. (%)	Cl	1 s.d. (%)	Total	OH
SEC 42-06	5	23	40.94	0.8%	2.97	7.7%	53.94	0.8%	0.051	16%	97.89	2.11
SEC 43-01	5	27	41.62	1.5%	3.25	3.2%	53.52	1.1%	0.041	75%	98.44	1.56
SEC 43-03	3	10	41.93	0.6%	2.15	4.4%	52.46	1.2%	0.019	54%	96.56	3.44
SEC46-01	3	9	42.02	0.6%	1.47	5.6%	52.19	0.5%	0.020	14%	95.70	4.30
SEC46-02	3	9	42.00	0.5%	1.49	6.6%	52.39	0.3%	0.030	13%	95.91	4.09
SEC47-01	3	9	41.92	0.7%	2.34	5.7%	51.64	0.3%	0.029	18%	95.93	4.07

DOI: https://doi.org/10.2138/am-2020-6994

Supplementary Table 6. Titanite major elem								Weight %					
Comment	No.	TiO2	F	K2O	Cl	Na2O	Cr2O3	SiO2	CaO	MnO	MgO	Al2O3	FeO
Line 1 SEC46-02_titanite	46	36.97	0	0.012	0.0092	0.012	0.11	29.65	28.38	0.0454	0.01	1.84	0.20
Line 2 SEC46-02_titanite	47	36.78	0	0.014	0.0124	0.021	0.10	29.91	28.23	0.0285	0.00	1.85	0.22
Line 3 SEC46-02_titanite	48	36.48	0	0.014	0.0038	0.097	0.08	29.83	28.3	0.0310	0.00	2.07	0.20
Line 4 SEC46-02_titanite	49	36.96	0	0.012	0.0065	0.044	0.07	29.89	28.26	0.0060	0.00	1.79	0.21
Line 5 SEC46-02_titanite	50	36.91	0	0.015	0.0086	0.025	0.07	29.73	28.18	0.0320	0.00	1.78	0.28
Average		36.82	0	0.013	0.0081	0.040	0.09	29.802	28.27	0.0286	0.00	1.87	0.22

Total
97.24
97.17
97.11
97.25
97.03
97.16

This is a preprint, the final version is subject to change, of the American Mineralogist (MSA)
Cite as Authors (Year) Title. American Mineralogist, in press.
DOI: https://doi.org/10.2138/am-2020-6994

Supplementary Table 7. Halogen intra-grain profiles (SIMS)

SEC43-01

Garnet	SEC43-01_grt_1@44	SEC43-01_grt_07@50	SEC43-01_grt_3@46	SEC43-01_grt_06@49	SEC43-01_grt_04@47	SEC43-01_grt_5@48	SEC43-01_grt_2@45			Grain Mean	Grain S.D. (%)
OH µg/g	114	118	316	248	104	144	173			174	46%
OH Error % (2SE Int+Calib)	5.4%	5.0%	4.8%	37.1%	5.1%	5.8%	6.2%				
F µg/g	7.25	8.56	9.51	8.17	6.29	3.66	8.74			7.45	26%
F Error % (2SE Int+Calib)	6.0%	5.8%	5.9%	6.3%	6.2%	5.9%	6.1%				
S µg/g	-	0.04	0.06	0.05	0.05	0.07	-				
C Error % (2SE Int+Calib)	-	13.8%	17.7%	17.1%	12.9%	16.0%	-				
Cl µg/g	0.18	0.17	0.24	0.20	0.19	0.20	0.25			0.20	14%
Cl Error % (2SE Int+Calib)	13.0%	16.1%	13.4%	13.8%	13.5%	13.8%	14.8%				
Distance (µm)	722	546	465	360	290	117	0				
	Core						Rim				

Omphacite	SEC43-01_omph_1@70	SEC43-01_omph_3@72	SEC43-01_omph_5@74	SEC43-01_omph_7@76	SEC43-01_omph_8@77	SEC43-01_omph_9@78	SEC43-01_omph_6@75	SEC43-01_omph_4@73	SEC43-01_omph_2@71		
OH µg/g	362	437	412	557	435	385	414	414	383	422	13%
OH Error % (2SE Int+Calib)	4.7%	4.6%	4.6%	5.6%	4.7%	4.7%	4.8%	4.7%	4.8%		
F µg/g	42.1	55.5	57.1	59.3	69.7	60.2	62.1	48.3	52.1	56.3	14%
F Error % (2SE Int+Calib)	5.8%	5.8%	5.8%	5.8%	5.8%	5.9%	5.9%	5.8%	5.9%		
S µg/g	0.03	0.03	-	0.03	0.02	-	0.04	-	-		
C Error % (2SE Int+Calib)	13.4%	16.0%	-	17.4%	13.7%	-	12.2%	-	-		
Cl µg/g	0.12	0.11	0.13	0.15	-	-	0.12	0.12	-	0.13	11%
Cl Error % (2SE Int+Calib)	16.2%	15.1%	12.2%	14.7%	-	-	13.8%	13.5%	-		
Distance (µm)	0	227	343	502	604	724	902	1082	1262		
	Rim								Core		

Phengite	SEC43-01_phen_2@52	SEC43-01_phen_3@53	SEC43-01_phen_5@55	SEC43-01_phen_4@54	SEC43-01_phen_1@51	SEC43-01_phen_9@63	SEC43-01_phen_8@62	SEC43-01_phen_7@61	SEC43-01_phen_6@60		
OH µg/g	26335	28580	28337	28820	28304	28840	27286	28857	29884	28360	4%
OH Error % (2SE Int+Calib)	4.6%	4.5%	4.7%	4.6%	4.5%	4.7%	4.6%	4.6%	4.6%		
F µg/g	1575	1819	1943	1979	1938	1913	1769	1883	1578	1822	8%
F Error % (2SE Int+Calib)	5.8%	5.8%	6.0%	5.9%	5.8%	5.9%	5.9%	5.9%	5.9%		
S µg/g	0.90	0.53	0.42	0.43	0.45	0.58	0.52	0.50	0.51		
C Error % (2SE Int+Calib)	7.4%	7.4%	10.0%	6.9%	8.3%	6.7%	8.1%	7.0%	6.7%		
Cl µg/g	1.50	0.96	1.15	1.12	1.08	1.08	0.97	0.98	1.58	1.16	20%
Cl Error % (2SE Int+Calib)	12.5%	12.1%	13.9%	12.6%	12.2%	12.6%	12.2%	12.2%	12.8%		
Distance (µm)	0	254	386	505	616	855	927	992	1086		
	Rim, to grt grain boundary				Core				Rim, to omphacite grain boundary		

DOI: https://doi.org/10.2138/am-2020-6994

Supplementary Table 8. Intermineral partition coefficients

	Cpx			Grt			Phen				Amph				Apatite			
Sample	F (µg/g)	Cl (µg/g)	OH (µg/g)	F (µg/g)	Cl (µg/g)	OH (µg/g)	F (µg/g)	Cl (µg/g)	OH (µg/g)	F/Cl	F (µg/g)	Cl (µg/g)	OH (µg/g)	F/Cl	F (µg/g)	Cl (µg/g)	OH (µg/g)	F/Cl
SEC 42-06	50.6	0.18	651	8.92	0.17	113	610	2.13	22452	286	1812	82.7	18682	22	29700	510	18800	58
SEC 43-01	54.1	0.13	433	7.76	0.18	125	1822	1.16	28360	1571	4727	11.6	20187	407	32541	410	15560	79
SEC 43-03	16.7	0.08	773	2.01	0.10	201					1073	0.64	17952	1676	21510	192	32819	112
SEC46-01	6.53	0.11	446	1.73	0.11	85					747	10.3	17292	72	14689	197	41670	75
SEC46-02	13.5	1.17	770	4.76	0.11	60					563	11.8	23449	48	14933	304	40213	49
SEC47-01	33.2	0.07	445	3.81	0.08	80	645	1.22	26410	529	1127	15.5	15747	73	23422	288	39719	81
Mean																		
1SD																		
Literature																		
Debret et al. 2016																		
Gala.1	11.07	117		3.89	64													
QE29d.4	17.05	71.85		18.61	9.4		326.5	40.25		8.1								
Gala.4	6.13	110.4		4.5	14.9													
QE29d.3				8.2	53		428	65		6.6								
Hughes et al. 2018																		
DC58G							1880	1.56		1205					9260	80		116
DC50B							1333	66.75		20					29480	38		776
DC58L							190	43.2		4.4					17680	76.5		231
Page et al. 2016																		
TUR12											218	46		4.7	30600	-		
TUR14A							503	77		6.5	335	97		3.5	30590	130		235
TUR23															32790	163		201
TUR30							572	21		27	390	18		21.7	29560	60		493
TUR31															35070	108		325
TUR32											256	46		5.6	31800	113		281
TUR33							372	69		5.4	84	87		1.0	28770	253		114

	Intermineral Partition Coefficients (cpx-grt)			Intermineral Partition Coefficients (cpx-amph)			Intermineral Partition Coefficients (grt-amph)			Intermineral Partition Coefficients (amph-phen)			Intermineral Partition Coefficients (Cpx-Apt)			Intermineral Partition Coefficients (Amph-Apt)			Intermineral Partition Coefficients (Cpx-Phen)			Intermineral Partition Coefficients (Phen-Apt)		
Sample	DF Cpx-Grt	DCl Cpx-Grt	DOH Cpx-Grt	DF Cpx-Amph	DCl Cpx-Amph	DOH Cpx-Amph	DF Grt-Amph	DCl Grt-Amph	DOH Grt-Amph	D F Amph-Phen	DCl Amph-Phen	D OH Amph-Phen	DF Cpx-Apt	DCl Cpx-Apt	DOH Cpx-Apt	DF Amph-Apt	DCl Amph-Apt	DOH Amph-Apt	DF Cpx/Phen	DCl Cpx/Phen	DOH Cpx/Phen	DF Phen/Apt	DCl Phen/Apt	DOH Phen/Apt
SEC 42-06	5.7		5.74	0.028		0.035	0.005		0.006	3.0	38.8		0.0017		0.0346	0.0610	0.1621	0.9937	0.0829	0.0845	0.0290	0.0205	0.0042	1.1942
SEC 43-01	7.0		3.47	0.011		0.021	0.002		0.006	2.6	10.0		0.0017		0.0278	0.1453	0.0283	1.2974	0.0297	0.1121	0.0153	0.0560	0.0028	1.8227
SEC 43-03	8.3		3.84	0.016		0.043	0.002		0.011				0.0008		0.0236	0.0499	0.0033	0.5470						
SEC46-01	3.8		5.24	0.009		0.026	0.002		0.005				0.0004		0.0107	0.0509	0.0526	0.4150						
SEC46-02	2.8		12.8	0.024		0.033	0.008		0.003				0.0009		0.0191	0.0377	0.0387	0.5831						
SEC47-01	8.7		5.58	0.029		0.028	0.003		0.005	1.7	12.7		0.0014		0.0112	0.0481	0.0536	0.3965	0.0514	0.0574	0.0168	0.0275	0.0042	0.6649
Mean	6.0		6.1	0.0195		0.0310	0.0038		0.0060	2.44	20.5		0.0012		0.0212	0.0655	0.0565	0.7054	0.0547	0.0847	0.0204	0.0347	0.0037	1.2273
1SD	2.4		3.4	0.0088		0.0076	0.0026		0.0029	0.63	15.9		0.0005		0.0094	0.0398	0.0550	0.3615	0.0268	0.0273	0.0075	0.0188	0.0008	0.5796
	40%		56%	45%		25%	69%		48%	26%	78%		45%		44%	61%	97%	51%	49%	32%	37%	54%	21%	47%
Literature																								
Debret et al. 2016																								
Gala.1	2.8																							
QE29d.4	0.9																							
Gala.4	1.4																							
QE29d.3																								
Hughes et al. 2018																								
DC58G																						0.203	0.020	
DC50B																						0.045	1.757	
DC58L																						0.011	0.565	
Page et al. 2016																								
TUR12																0.0071								
TUR14A										0.67	1.26					0.0110	0.7462					0.016	0.592	
TUR23																								
TUR30										0.68	0.86					0.0132	0.3000					0.019	0.350	
TUR31																								
TUR32																0.0081	0.4071							
TUR33										0.23	1.26					0.0029	0.3439					0.013	0.273	

DOI: https://doi.org/10.2138/am-2020-6994

Supplementary Table 9. Pyrohydrolysis raw data and reference material replicates

		Uncorrected for Yield					Corrected for Yield					
	Analysis #	F (µg/g)	Cl (µg/g)		F (µg/g)	Cl (µg/g)	F (µg/g)	Cl (µg/g)		F (µg/g)	Cl (µg/g)	Yield Corrected to Batch #
SEC42-6	2	99.74	10.00	Average	**91.94**	**8.85**	**130.98**	**13.13**	Average	**114.56**	**11.04**	1
SEC42-6'	3	84.72	8.35	Std. Dev.	7.53	1.00	**102.35**	**10.09**	Std. Dev.	14.77	1.81	2
	4	91.34	8.20	Stdev%	8%	11%	**110.35**	**9.90**	Stdev%	12.89%	16%	2
SEC43-1	2	163.91	9.27	Average	**108.51**	**7.05**	**215.24**	**12.17**	Average	**136.83**	**8.85**	1
SEC43-1'	3	77.69	6.40	Std. Dev.	48.08	1.97	**93.86**	**7.73**	Std. Dev.	68.01	2.93	2
	4	83.92	5.49	Stdev%	44%	28%	**101.39**	**6.64**	Stdev%	49.71%	33.12%	2
SEC43-3	2	151.98	6.73	Average	**152.25**	**5.37**	**199.58**	**8.84**	Average	**189.25**	**6.73**	1
SEC43-3'	3	148.65	5.44	Std. Dev.	3.74	1.40	**179.58**	**6.57**	Std. Dev.	10.02	2.04	2
	4	156.12	3.94	Stdev%	2%	26%	**188.61**	**4.76**	Stdev%	5.3%	30.4%	2
SEC46-1	2	192.26	11.03	Average	**154.37**	**9.06**	**252.47**	**14.49**	Average	**193.23**	**11.34**	1
SEC46-1'	3	128.56	7.56	Std. Dev.	33.52	1.78	**155.31**	**9.14**	Std. Dev.	51.97	2.80	2
	4	142.30	8.59	Stdev%	22%	20%	**171.91**	**10.38**	Stdev%	26.9%	24.7%	2
SEC46-2	2	162.16	15.16	Average	**160.25**	**16.06**	**212.95**	**19.90**	Average	**199.28**	**19.94**	1
SEC46-2'	3	156.39	16.95	Std. Dev.	3.35	0.90	**188.93**	**20.47**	Std. Dev.	12.35	0.52	2
	4	162.22	16.09	Stdev%	2%	6%	**195.98**	**19.44**	Stdev%	6%	3%	2
SEC47-1	2	113.07	7.62	Average	**111.60**	**7.10**	**148.48**	**10.01**	Average	**138.78**	**8.84**	1
SEC47-1'	3	108.15	7.03	Std. Dev.	3.00	0.49	**130.65**	**8.49**	Std. Dev.	9.02	1.04	2
	4	113.58	6.65	Stdev%	3%	7%	**137.22**	**8.03**	Stdev%	6%	12%	2

*apostrophe (') indicates a duplicated sample

	Uncorrected for Yield				Corrected for Yield by Batch							
			1SD Pos (yield uncert)				1SD		1SD Propogated		1SD Propogated	
Sample	F (µg/g)	Cl (µg/g)	F (%)	Cl (%)	F (µg/g)	Cl (µg/g)	F (µg/g)	Cl (µg/g)	F %	Cl %	F (µg/g)	Cl (µg/g)
SEC42-06	**91.94**	**8.85**	22.5%	23.0%	**114.56**	**11.04**	14.77	1.81	13.05%	19.91%	14.95	2.20
SEC43-01	**108.51**	**7.05**	49.0%	34.4%	**136.83**	**8.85**	68.01	2.93	49.75%	34.98%	68.07	3.09
SEC43-03	**152.25**	**5.37**	21.1%	32.8%	**189.25**	**6.73**	10.02	2.04	5.66%	32.39%	10.71	2.18
SEC46-01	**154.37**	**9.06**	30.2%	28.1%	**193.23**	**11.34**	51.97	2.80	26.91%	27.38%	52.00	3.10
SEC46-02	**160.25**	**16.06**	21.1%	20.8%	**199.28**	**19.94**	12.35	0.52	6.27%	12.08%	12.49	2.41
SEC47-01	**111.60**	**7.10**	21.1%	21.2%	**138.78**	**8.84**	9.02	1.04	6.57%	16.65%	9.11	1.47
SEC50-01												

Standards			
	F ppm	**Cl ppm**	
JB-2-1	76.65	268.22	pyrohydrolysis group (SEC42-6, 43-1, 43-3, 46-1, 46-2, 47-1)
JB-2-2	73.70	215.25	
JB-2-3	74.67	233.68	
Batch 1 Mean	**75.01**	**239.05**	
Batch 1 Std	**1.50**	**26.89**	
Yield Batch 1	**76.1%**	**85.1%**	
Yield Std (%)	2.0%	11.3%	
JB-2-9	80.64	191.80	hydrolysis, duplicate group (SEC42-6', 43-1', 43-3', 46-1', 46-2', 47-1')
JB-2-11	82.04	208.73	
JB-2-12	81.93	241.47	
Batch 2 Mean	**81.53**	**214.00**	
Batch 2 Std	**0.78**	**25.25**	
Yield Batch 2	**82.8%**	**76.2%**	
Yield Std (%)	1.0%	11.8%	
Average (all)	78.27	226.53	
Std. Dev. (all)	3.73	27.07	
JB-2**	98.50	281.00	
Yield (min)*	75%	68%	
Yield (max)*	83%	95%	
Yield (average)	79%	81%	
STD ALL (average)	4%	5%	

igneous.html) reports the F and Cl concentration of JB-2 as 98.5ppm and 281ppm, respectively.

This is a preprint, the final version is subject to change, of the American Mineralogist (MSA)
Cite as Authors (Year) Title. American Mineralogist, in press.
DOI: https://doi.org/10.2138/am-2020-6994

Supplementary Table 10. Grain Boundary Calculations

Grain boundary calculations with sims spot size of 3.8μm^2

3.8μm

	Area (μm)	Ratio	CL GB meas	Calc Cl GB
3nm	0.019	0.00131579	17.65	13414
3.8 μm	14.44		6.5	4940
5nmx3.8μm	0.019	0.00131579	17.65	13414

Turcotte and Schubert, Geodynamics 1982

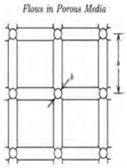

696 *Flows in Porous Media*

Figure 9.1 An idealized model of a porous medium. Circular tubes of diameter δ form a cubical matrix with dimensions b.

cube on each of these edges. Thus the equivalent of three tubes of diameter δ and length b lie within the cube. The porosity is therefore given by

$$\phi = 3\pi\left(\frac{\delta}{2}\right)^2\frac{b}{b^3} = \frac{3\pi}{4}\frac{\delta^2}{b^2}. \qquad (9.6)$$

Turcotte and Schuber 2002

delta	1.00E-03	
b	500	μm
Phi	9.42E-12	
		%
Cl GB contribution (%)		#REF!

Method 1		Sims Spot Size (μm)				Dolomite									
Est Phi, GB		14.44			Phi	5.00E-04	5.00E-05	5.00E-06	5.00E-07	5.00E-08	5.00E-09	5.00E-10	5.00E-11	5.00E-12	5.00E-13
Width								Increments of 10x							
	Grain bound:	Area (μm)	Ratio	CL GB meas	Calc Cl GB	Cl GB μg/g	Cl GB μg/g	Cl GB μg/g	Cl GB μg/g	Cl GB μg/g	Cl GB μg/g	Cl GB μg/g	Cl GB μg/g	Cl GB μg/g	
	1.00E-03	0.0038	0.00026316	17.65	67070	33.54	3.35	0.34	0.03	0.00	0.00	0.00	0.00	0.00	
	5.00E-03	0.019	0.00131579	17.65	13414	6.71	0.67	0.07	0.01	0.00	0.00	0.00	0.00	0.00	
	2.50E-02	0.095	0.00657895	17.65	2682.8	1.34	0.13	0.01	0.00	0.00	0.00	0.00	0.00	0.00	
Increments of 5x	1.25E-01	0.475	0.03289474	17.65	536.56	0.27	0.03	0.00	0.00	0.00	0.00	0.00	0.00	0.00	
	6.25E-01	2.375	0.16447368	17.65	107.312	0.05	0.01	0.00	0.00	0.00	0.00	0.00	0.00	0.00	
	3.80E+00	14.44	1	17.65	17.65	0.01	0.00	0.00	0.00	0.00	0.00	0.00	0.00	0.00	
	1.90E+01	72.2	5	17.65	3.53	0.00	0.00	0.00	0.00	0.00	0.00	0.00	0.00	0.00	
	9.50E+01	361	25	17.65	0.706	0.00	0.00	0.00	0.00	0.00	0.00	0.00	0.00	0.00	
	4.75E+02	1805	125	17.65	0.1412	0.00	0.00	0.00	0.00	0.00	0.00	0.00	0.00	0.00	
	Grain Size μm	500		CL GB meas	17.65										

		Delta μm	Phi	GB Cl contribution μg/g
Method 2	1nm	0.001	9.42E-12	0.00000
Calc Phi	5nm	0.005	2.36E-10	0.00000
from GB	25nm	0.025	5.89E-09	0.00002
	125nm	0.125	1.47E-07	0.00008
	625nm	0.625	3.68E-06	0.00039
	3.125μm	3.125	9.20E-05	0.00162
	15.625μm	15.625	2.30E-03	0.00812
	78.125μm	78.125	5.75E-02	0.04059
	390.625μm	390.625	1.44E+00	0.20296